Remote sensing approaches for district-level irrigation monitoring = Approcci di telerilevamento per il monitoraggio dell'irrigazione a livello distrettuale

Politecnico di Bari

LIBERATORIA PER L'ARCHIVIAZIONE DELLA TESI DI DOTTORATO

Al Magnifico Rettore
del Politecnico di Bari

Il sottoscritto Qotada ALALI nato a HASAKA (SIRIA) il 07/09/1990 residente a Valenzano (BA) 70010 in via Ceglie 9 e-mail qotada.alali@poliba.it iscritto al 3° anno di Corso di Dottorato di Ricerca in RISCHIO, SVILUPPO AMBIENTALE, TERRITORIALE ED EDILIZIO ciclo ed essendo stato ammesso a sostenere l'esame finale con la prevista discussione della tesi dal titolo:

Remote Sensing Approaches for District-Level Irrigation Monitoring

DICHIARA

1) di essere consapevole che, ai sensi del D.P.R. n. 445 del 28.12.2000, le dichiarazioni mendaci, la falsità negli atti e l'uso di atti falsi sono puniti ai sensi del codice penale e delle Leggi speciali in materia, e che nel caso ricorressero dette ipotesi, decade fin dall'inizio e senza necessità di nessuna formalità dai benefici conseguenti al provvedimento emanato sulla base di tali dichiarazioni;
2) di essere iscritto al Corso di Dottorato di ricerca RISCHIO, SVILUPPO AMBIENTALE, TERRITORIALE ED EDILIZIO ciclo XXXV, corso attivato ai sensi del "*Regolamento dei Corsi di Dottorato di ricerca del Politecnico di Bari"*, emanato con D.R. n.286 del 01.07.2013;
3) di essere pienamente a conoscenza delle disposizioni contenute nel predetto Regolamento in merito alla procedura di deposito, pubblicazione e autoarchiviazione della tesi di dottorato nell'Archivio Istituzionale ad accesso aperto alla letteratura scientifica;
4) di essere consapevole che attraverso l'autoarchiviazione delle tesi nell'Archivio Istituzionale ad accesso aperto alla letteratura scientifica del Politecnico di Bari (IRIS-POLIBA), l'Ateneo archivierà e renderà consultabile in rete (nel rispetto della Policy di Ateneo di cui al D.R. 642 del 13.11.2015) il testo completo della tesi di dottorato, fatta salva la possibilità di sottoscrizione di apposite licenze per le relative condizioni di utilizzo (di cui al sito http://www.creativecommons.it/Licenze), e fatte salve, altresì, le eventuali esigenze di "embargo", legate a strette considerazioni sulla tutelabilità e sfruttamento industriale/commerciale dei contenuti della tesi, da rappresentarsi mediante compilazione e sottoscrizione del modulo in calce (Richiesta di embargo);
5) che la tesi da depositare in IRIS-POLIBA, in formato digitale (PDF/A) sarà del tutto identica a quelle **consegnate**/inviate/da inviarsi ai componenti della commissione per l'esame finale e a qualsiasi altra copia depositata presso gli Uffici del Politecnico di Bari in forma cartacea o digitale, ovvero a quella da discutere in sede di esame finale, a quella da depositare, a cura dell'Ateneo, presso le Biblioteche Nazionali Centrali di Roma e Firenze e presso tutti gli Uffici competenti per legge al momento del deposito stesso, e che di conseguenza va esclusa qualsiasi responsabilità del Politecnico di Bari per quanto riguarda eventuali errori, imprecisioni o omissioni nei contenuti della tesi;
6) che il contenuto e l'organizzazione della tesi è opera originale realizzata dal sottoscritto e non compromette in alcun modo i diritti di terzi, ivi compresi quelli relativi alla sicurezza dei dati personali; che pertanto il Politecnico di Bari ed i suoi funzionari sono in ogni caso esenti da responsabilità di qualsivoglia natura: civile, amministrativa e penale e saranno dal sottoscritto tenuti indenni da qualsiasi richiesta o rivendicazione da parte di terzi;
7) che il contenuto della tesi non infrange in alcun modo il diritto d'Autore né gli obblighi connessi alla salvaguardia di diritti morali od economici di altri autori o di altri aventi diritto, sia per testi, immagini, foto, tabelle, o altre parti di cui la tesi è composta.

Luogo e data Bari 03/01/2024 Firma Qotada Alali

Il/La sottoscritto, con l'autoarchiviazione della propria tesi di dottorato nell'Archivio Istituzionale ad accesso aperto del Politecnico di Bari (POLIBA-IRIS), pur mantenendo su di essa tutti i diritti d'autore, morali ed economici, ai sensi della normativa vigente (Legge 633/1941 e ss.mm.ii.),

CONCEDE

- al Politecnico di Bari il permesso di trasferire l'opera su qualsiasi supporto e di convertirla in qualsiasi formato al fine di una corretta conservazione nel tempo. Il Politecnico di Bari garantisce che non verrà effettuata alcuna modifica al contenuto e alla struttura dell'opera.
- al Politecnico di Bari la possibilità di riprodurre l'opera in più di una copia per fini di sicurezza, back-up e conservazione.

Luogo e data Bari 03/01/2024 Firma Qotada Alali

D.R.R.S

POLITECNICO DI BARI

02

2023

Doctor of Philosophy in Environmental and Building Risk and Development

Coordinator: Prof. Michele Mossa

XXXV CYCLE
Curriculum: ICAR/02

DICATECh
Department of Civil, Environmental, Building Engineering and Chemistry

Remote Sensing Approaches for District-Level Irrigation Monitoring

Prof. Eng. Umberto FRATINO
DICATECh
Polytechnic University of Bari

Dr. Eng. Nicola LAMADDALENA
CIHEAM Bari

Nicola Lamaddalena

Qotada ALALI

D.R.R.S

POLITECNICO DI BARI

02

2023

Dottorato di Ricerca in Rischio e Sviluppo ambientale, territoriale ed edilizio

Coordinatore: Prof. Michele Mossa

XXXV CICLO
Curriculum: ICAR/02

DICATECh
Dipartimento di Ingegneria Civile, Ambientale, del Territorio, Edile e di Chimica

Approcci di telerilevamento per il monitoraggio dell'irrigazione a livello distrettuale

Prof. Eng. Umberto FRATINO
DICATECh
Politecnico di Bari

Dr. Eng. Nicola LAMADDALENA
CIHEAM Bari

Nicola Lamaddalena

Qotada ALALI

EXTENDED ABSTRACT (Eng)

The largest consumer of freshwater resources is the agricultural sector, globally around 70% of all freshwater withdrawals are used for food production. However, less than 60% of all the water used for irrigation is effectively consumed by crops.

One form of sustainable intensification of food production is irrigation. Irrigated agricultural food production systems use 70% of global annual water consumption, and whilst irrigated land use comprises only 16% of global cropland, irrigated landscapes produce around 44% of the total food production.

Climatic variability and change have implications not only for crop water use and water availability for agriculture but also for crop development. the Mediterranean region is particularly vulnerable to climate change, with forecasts indicating greater warming and increased precipitation variability. These changes are expected to have significant repercussions for irrigation, affecting water availability for agriculture and potentially amplifying conflicts among users dependent on these critical water resources.

Lack of proper water allocation practices has also made water resources management challenging. water allocation procedures must meet the expectations of all stakeholders at the same time ensuring sustainability of the resources.

Earth Observation (EO) methods have demonstrated their capability to serve as a source of unbiased, precise, economical, and current data pertaining to various influential factors, particularly those influencing extensive regions characterized by significant temporal variability, such as irrigation agriculture. EO techniques can be effectively utilized to achieve a dual-purpose:

- Mapping actual irrigated area, often missing or untrustworthy dataset.
- Estimating irrigation requirements.

In the present study, Remote Sensing (RS) methodologies were applied to estimate evapotranspiration and irrigation water requirement for subsequent

comparison with registered volumes recorded by flowmeters installed upstream at the district level.

The initial step involved the detection of irrigated areas using unsupervised classification, distinguishing those under irrigation from non-irrigated areas. This initial stage is of fundamental importance as it forms the basis for evaluating the effectiveness of the estimation methods.

To estimate the irrigation volumes, a one-step Penman Monteith (P-M) approach was employed, integrating surface parameters (leaf area index and hemispherical shortwave albedo) and resistance values derived from optical satellite Sentinel-2 data, complemented by in-situ agro-meteorological data. The estimates obtained using the P-M method, with adjustments for leaf resistance in perennial crops and considering evapotranspiration and transpiration (sparse canopy coverage), demonstrated an agreement with the registered volumes in the district.

To further validate the findings, an assessment of actual evapotranspiration and estimated irrigation requirements was conducted using a combination of the P-M and Shuttleworth and Wallace (S-W) approaches. This was further enhanced by integrating the physical Optical Trapezoid Model (OPTRAM) to dynamically adjust leaf and soil resistance with the Short-Wave Infrared (SWIR) band in Sentinel-2, representing soil and canopy water statues.

The use of these integrated methods produced positive outcomes, enabling the evaluation of the irrigation techniques used by farmers and the analysis of stress conditions. This, in turn, contributes to the enhancement of water allocation and irrigation management practices in the Mediterranean region.

Key words Water allocation; Remote sensing; Penman Monteith; Shuttleworth and Wallace; Evapotranspiration; Irrigation requirement; Irrigation management

EXTENDED ABSTRACT (Ita)

Il settore agricolo è il principale consumatore di acqua dolce, rappresentando globalmente circa il 70% di tutti i prelievi di questo tipo di risorsa per la produzione alimentare. Tuttavia, meno del 60% dell'acqua impiegata per l'irrigazione viene effettivamente utilizzata dalle coltivazioni.

Una forma di intensificazione sostenibile della produzione alimentare è l'irrigazione. I sistemi di produzione agro-alimentari irrigui utilizzano il 70% del consumo globale annuo di acqua e, mentre l'uso dei terreni irrigati comprende solo il 16% delle terre coltivate globali, le superfici irrigate producono circa il 44% della produzione alimentare totale.

La variabilità e il cambiamento climatico hanno implicazioni non solo sull'uso e sulla disponibilità di acqua per l'agricoltura, ma anche sullo sviluppo delle colture. La regione mediterranea è particolarmente vulnerabile ai cambiamenti climatici, con previsioni che indicano un maggiore riscaldamento e una maggiore variabilità delle precipitazioni. Si prevede che questi cambiamenti avranno ripercussioni significative sull'irrigazione, influenzando la disponibilità di acqua per l'agricoltura e potenzialmente amplificando i conflitti tra gli utenti che dipendono da queste risorse idriche critiche.

Anche la mancanza di adeguate pratiche di allocazione dell'acqua ha reso difficile la gestione delle risorse idriche. Le procedure di allocazione dell'acqua devono soddisfare le aspettative di tutte le parti interessate garantendo allo stesso tempo la sostenibilità delle risorse.

I metodi di osservazione della Terra (OT) hanno dimostrato la loro capacità di servire come fonte di dati imparziali, precisi, economici e attuali relativi a vari fattori influenti, in particolare quelli che influenzano vaste regioni caratterizzate da una significativa variabilità temporale, come l'agricoltura irrigua. Le tecniche OT possono essere utilizzate efficacemente per raggiungere un duplice scopo:

- Mappatura dell'effettiva area irrigata, spesso con dati mancanti o inaffidabili.

- Stima del fabbisogno irriguo.

Nel presente studio, le metodologie di Telerilevamento sono state applicate per stimare l'evapotraspirazione e i fabbisogni irrigui, per poi procedere al successivo confronto con i volumi registrati dai flussimetri installati a monte a livello distrettuale.

Il passo iniziale prevedeva la mappatura delle aree irrigate mediante classificazione non supervisionata, distinguendo quelle irrigate da quelle non irrigate. Questa fase iniziale è di fondamentale importanza, in quanto costituisce la base per valutare l'efficacia dei metodi di stima.

Per stimare i volumi di irrigazione, è stato utilizzato l'approccio Penman-Monteith (P-M) "one-step", integrando parametri di superficie (indice di area fogliare e albedo emisferico a onde corte) e valori di resistenza derivati dai dati del satellite multispettrale Sentinel-2 (S2), integrati da dati meteorologici acquisiti in-situ.

Le stime ottenute mediante il metodo P-M, con correzioni per la resistenza fogliare nelle coltivazioni arboree, considerando l'evapotraspirazione (ET) e/o la traspirazione (T) (nel caso di una copertura parziale della chioma), hanno dimostrato un buon accordo con i volumi registrati nel distretto.

Per convalidare ulteriormente i risultati, è stata condotta una valutazione dell'evapotraspirazione effettiva (ETa) e dei fabbisogni irrigui stimati, utilizzando una combinazione degli approcci P-M e Shuttleworth e Wallace (S-W). Ciò è stato ulteriormente migliorato integrando il modello OPTRAM (OPtical TRapezoid Model) per modulare dinamicamente la resistenza fogliare e del suolo, mediante l'utilizzo della banda dell'infrarosso a onde corte (SWIR) del S2, sensibile al contenuto idrico nel sistema suolo-pianta.

L'utilizzo di questi metodi integrati ha prodotto risultati positivi, consentendo la valutazione delle tecniche di irrigazione utilizzate dagli agricoltori e l'analisi delle condizioni di stress. Ciò, a sua volta, contribuisce al miglioramento delle pratiche di allocazione dell'acqua e di gestione dell'irrigazione nella regione del Mediterraneo.

Parole chiave Allocazione dell'acqua; Telerilevamento; Penman Monteith; Shuttleworth and Wallace; Evapotraspirazione; Fabbisogni irrigui; Gestione dell'irrigazione

Table Of contents

List of figures

List of tables

Chapter 1: Introduction

1.1 General background

Water is a scarce resource. Forty percent of the world's population today face shortages regardless of whether they live in dry areas or in areas where rainfall is abundant (Molden, 2013). The largest consumer of freshwater resources is the agricultural sector, globally around 70% of all freshwater withdrawals are used for food production. However, less than 60% of all the water used for irrigation is effectively consumed by crops (FAO, 2010b).

Over the past century there has been a dramatic increase in water scarcity and drought in arid territories on the southern hemisphere, that nowadays have become a topic of increasing research attention also in European Union (EU)

One form of sustainable intensification of food production is irrigation. Irrigated agricultural food production systems use 70% of global annual water consumption, and whilst irrigated land use comprises only 16% of global cropland, irrigated landscapes produce around 44% of the total food production (FAO, 2010a; Alexandratos and Bruinsma, 2012; Moreno-Pérez and Roldán-Cañas, 2013).

Climatic variability and change have implications not only for crop water use and water availability for agriculture but also for crop development (Alcamo *et al.*, 2007). In addition, consequences of climate change could produce negative impacts on the available water resources, adding pressure to the most stressed EU regions like Mediterranean regions (Pachauri and Reisinger, 2007).

Given the constraint of limited water resources, it is imperative to consider the significance of water usage efficiency and irrigation water requirement (IWR)(Johansson, 2005). the enhancement of water use efficiency is crucial in arid and semiarid areas characterized by limited water resources.

In spite of the relevance of this topic, accurate data concerning the actual extension of irrigated areas and the volumes of water applied are not easily available. In most cases information is based on statistics, in an irregular distribution in time and

space. This type of data can be very variable from one year to another, especially in water scarce conditions, with farmers facing limited access to irrigation. In addition to this, the quantification of water volumes used for irrigation is hindered by the lack of metering devices either at farm level either for collective distribution systems. This is due in most cases to the lack of regular maintenance of installed devices, which requires skilled operators dedicated to this activity. On the other hand, indirect estimation methods of the above-mentioned data have been developed in the context of research studies, by means of different methods. All these methods are based on the estimation of water balance terms, among which Evapotranspiration (ET).

ET plays a crucial role in maintaining water balance in arid and semi-arid regions, making it essential for the efficient management of water resources (Bastiaanssen, 2000; Moussa, Chahinian and Bocquillon, 2007).

The utilization of remote sensing has the potential for accurate measurement of actual evapotranspiration (ETa) and its spatial distribution across large-scale land use. Additionally, this approach enables the assessment of spatiotemporal variations in ET within a given area (Teixeira, Bastiaanssen and Bassoi, 2007). The utilization of remote sensing technology has facilitated the precise and replicable determination of actual evapotranspiration (ETa).

Earth Observation (EO) techniques have proven to be a source of objective, reliable, accurate, cost-effective, and up-to-date information on several of these factors, especially those affecting large areas and with high variability in time such irrigation agriculture. In particular, EO can be applied with a twofold objective:

- Mapping actual irrigated areas, which is an information very often missing or unreliable.
- Estimating irrigation requirements.

1.2 State of art

Nowadays the observation of the crop conditions and area management are top priority. There are many advantages for using remote sensing data and technics. Contemporary tools for the analysis allow farmer to derive an up-to date information

about parcel crops, provide a real-time monitoring and track particular dynamic crop development.

There are a lot of applications of EO those supporting the irrigation management at farm level (Near real-time, advisory services etc.). Various tools have been developed in the past years aiming to support operational irrigation water management through the computation of actual crop ET and irrigation water requirements at plot scale over large areas. present an advanced and fully operational irrigation advisory service based on the utilisation of VIS–NIR satellite observations for crop water management at field and irrigation scheme levels; the service has been implemented in three different countries, by using a similar webGIS platform (Vuolo *et al.*, 2015)

Earth Observation (EO) technologies have emerged as valuable tools in supporting irrigation at farm scale. Near real-time, plot-level, irrigation advisory services have significantly improved water management practices in agriculture. However, it is important to note that the focus of this research is primarily on large-scale applications of EO for irrigation, rather than the specific services mentioned above.

EO can play a crucial role in water allocation by aiding in the identification of authorized and unauthorized irrigated areas. Satellite imagery and remote sensing data can be used to monitor land use patterns and identify areas where irrigation is permitted or restricted. This information can assist water authorities in effectively managing water resources and ensuring sustainable practices (Lockwood et al., 2014).

The need for accurate data on the distribution and diversity of crop areas is growing in significance when it comes to efficient irrigation management. Remote sensing technology offers solutions to the challenges associated with identifying and categorizing different crop types and their respective extents within irrigation systems or at the watershed scale. Moreover, the utilization of crop classification maps empowers managers and policymakers to allocate water resources optimally, thereby ensuring economically viable yields across vast geographical areas within the irrigation network (Perumal and Bhaskaran, 2010).

Accurate estimation of irrigation water requirements is essential for efficient irrigation management. EO technologies, such as satellite-based remote sensing, can

provide valuable data on various environmental factors that influence crop water demand. By analysing factors such as air temperature, relative humidity, solar radiation, wind speed, and vegetation indices derived from satellite imagery, farmers and irrigation planners can determine the optimal amount of water needed for different crops.

Water accounting is a critical aspect of irrigation management, as it helps in understanding the actual crop water usage. This latter can be evaluated by means of soil water balance models, which are nowadays able to accurately describe the soil and crop water dynamics (Coppola *et al.*, 2019; Feng *et al.*, 2023). However, soil water balance models require a detailed knowledge of soil hydraulic parameters (water retention and hydraulic conductivity), interaction with groundwater circulation, surface run-off and deep percolation. These data are not easily available, considering their significant spatial variability, especially when studying large areas like irrigation districts. Furthermore, actual irrigation volumes are needed as input in soil water balance models, in order to correctly describe the soil water flow dynamics. Irrigation volumes can be measured by meters, but these devices often face issues with malfunctioning and in general data are either missing or unreliable.

This reasoning gives a strong justification for developing alternative methods based on Earth Observation, with special concern to thermal data which are able to detect land evaporation (Kalma, McVicar and McCabe, 2008). EO can effectively contribute to water accounting by providing data on evapotranspiration (ET) rates for different crops (Garrido-Rubio et al., 2020), overcoming the limitations of soil water balance models and meter-based measurements.

One widely used approach to estimate irrigation requirement is through thermal data using surface energy balance models. Surface energy balance estimates sensible heat flux from land surface temperature and latent heat flux from latent heat as a residual term. One-source models, such as SEBAL (Surface Energy Balance Algorithm for Land), SEBS (Surface Energy Balance System), and METRIC (Mapping Evapotranspiration at High Resolution with Internalized Calibration), have gained popularity (Bastiaanssen et al., 1998; Su, 2002; Allen, Tasumi and Trezza, 2007)

On the other hand, two-source models like TSEB (Two-Source Energy Balance) and ALEXI (Atmosphere Land Exchange Inverse) have also been developed (Norman, Kustas and Humes, 1995; Anderson *et al.*, 1997).

The aforementioned thermal-based models have been abundantly employed, making use of observation data from Landsat (Anderson *et al.*, 2012), which is now the only operating platform providing medium-resolution acquisitions (100 m) in the thermal infrared. The acquired data is subsequently resampled to a spatial resolution of 30 metres, with a revisit period ranging from 8 to 16 days, depending on the exact location. Landsat LST data with accurate atmospheric correction are available on a global scale from NASA USGS website (Level 2 Collection 2 dataset: https://earthexplorer.usgs.gov/), but the temporal and spatial resolution are still representing a major limitation for applying surface energy balance models in highly fragmented area, such as agricultural systems in the Mediterranean regions. Furthermore, Level 2 are not available in near-real time, but with a 2-week latency due to the needed elaboration steps. This latter issue hampers their applicability for near real time operational services in support of irrigation management.

In order to tackle these obstacles presented by the fragmented agricultural farms in the study area, the study opted for the utilisation of Sentinel 2. The Sentinel 2 twin satellites offers a higher spatial resolution varying from (10 to 60) metres and a more frequent temporal resolution, allowing for observations to be made every 3 to 5 days. Thermal infrared in not available in Sentinel-2 but methods are being implemented for using shortwave infrared reflectance (SWIR) as a proxy for land surface water status (Sadeghi, Jones and Philpot, 2015).

In this study, the combination equation for ET calculation known as “one-step Penman-Monteith” (P-M) approach has been used in the first instance. This model is based on the assumption that crop covers uniform the soil surface as a "big leaf". This method postulates uniform behaviour of transpiration among all plants within a given area. The model incorporates energy balance and aerodynamic factors to calculate ETa and irrigation water requirement, taking into account the leaf stomatal resistance (Monteith and Unsworth, 2008). The calibration process ensures precise estimations

of ETa, considering the diverse characteristics of leaf resistance in various plant species and environmental settings.

In addition, another approach was employed, derived by Shuttleworth and Wallace, 1985 Shuttleworth and Wallace (1985), indicated as "S-W", where the combination equation approach is applied separately for the soil evaporation and the canopy transpiration, thus being applicable to non-uniform crop covers.

Both combination equation approaches, i.e., P-M and S-W, require as input the surface resistances (inverse of conductance) which depends on the biophysical characteristics of the vegetated surface (albedo, Leaf Area Index, crop height) and on the soil and crop water status.

To enhance the accuracy of evapotranspiration estimations, the Optical Trapezoidal Model (OPTRAM) was utilized to modulate both substrate and leaf canopy resistance with shortwave infrared reflectance throughout the entire irrigation period in the study area. This integration of OPTRAM provided valuable insights into the dynamic adjustments required for soil and leaf stomatal resistance, leading to improved estimations of evapotranspiration rates.

Subsequently, the evapotranspiration was estimated using both the P-M and S-W approaches. Additionally, the irrigation water requirements were calculated based on these estimations.

Moving from this baseline, the present study has investigated different approaches in using Sentinel-2 data for estimating irrigation water requirements at district scale in a typical Mediterranean agricultural system, highly fragmented. EO estimates will be compared with metered irrigation volumes for assessing.

1.3 Objectives

This research focuses on creating a functional remote sensing approach designed to accurately assess the irrigation water needs in the Mediterranean region. This region is known for its arid to semi-arid climate, water scarcity, and diverse landscape. To verify the effectiveness and accuracy of this methodology, the initial testing included assessing the feasibility of remote sensing-based techniques for

determining actual crop evapotranspiration and calculating irrigation water requirements, with a particular emphasis on water allocation in Southern Italy.

. The study applied a classification methodology to the district map, a crucial step in the assessment of water allocation and resource distribution.

In pursuit of this overarching goal, various scientific methodologies, including combination P-M approach and S-W techniques, were systematically investigated.

The P-M method was applied by modulating the value of leaf resistance, while the S-W approach facilitated simultaneous adjustments in leaf and soil resistance parameters with SWIR observations. This innovative approach was augmented by the integration of the Optical Trapezoid Model (OPTRAM), enabling the generation of multifaceted scenarios (actual irrigation requirement). The primary aim of this approach is to enhance the accuracy of ETa and irrigation water requirement estimation, considering the distinctive environmental attributes characteristic of the Mediterranean region.

1.4 Conceptual scheme

The schematic conceptual framework provides an overview of the thesis content, comprising three fundamental steps:

- The initial step involves determining the precise extent of irrigated areas (Chapter 2 & 3),
- The subsequent step focuses on estimating irrigation requirements at the district level, preceded by a comprehensive validation process of ET between combination equations (PM and S-W) and eddy covariance flux tower (Chapter 4 & 5),
- Finally, the third step involves the comparison of the estimated irrigation volume with the officially registered data (Chapter 5).

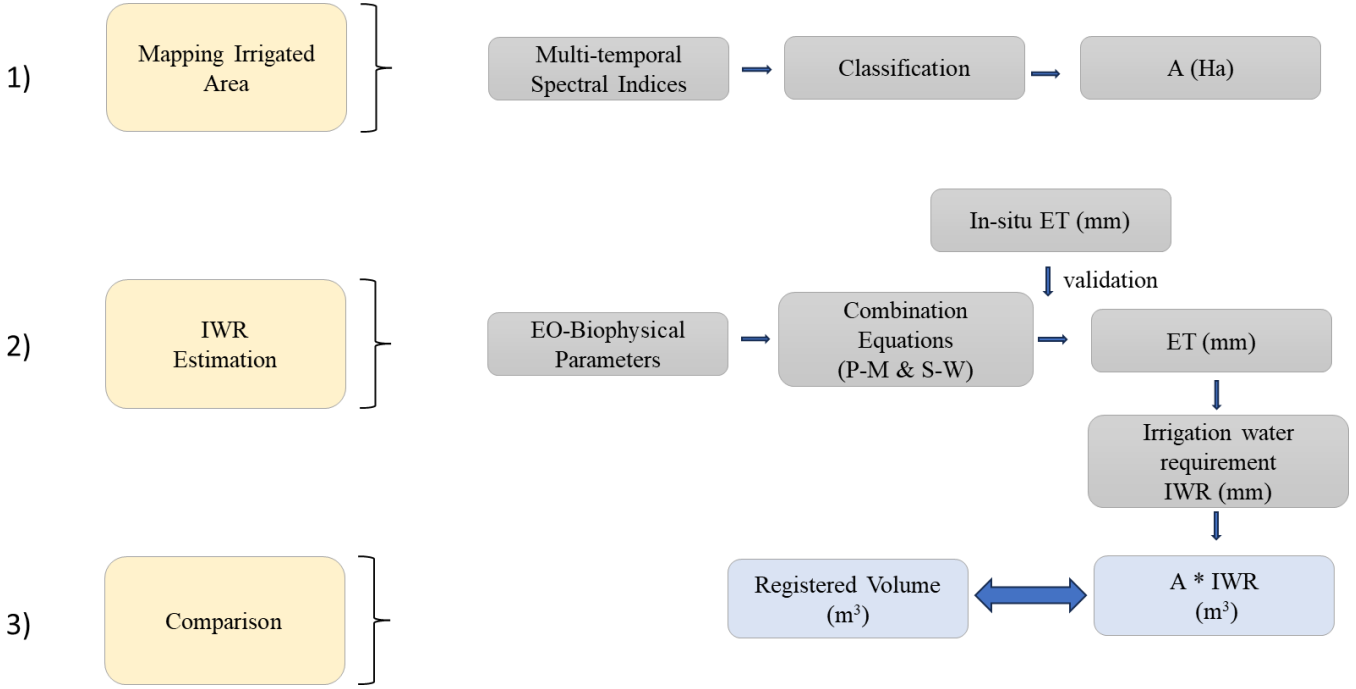
1)
Mapping Irrigated Area
Multi-temporal Spectral Indices
Classification
A (Ha)
2)
IWR Estimation
In-situ ET (mm)
validation
EO-Biophysical Parameters
Combination Equations (P-M & S-W)
ET (mm)
Irrigation water requirement IWR (mm)
3)
Comparison
Registered Volume (m3)
A * IWR (m3)

Chapter 2: Literature Review

2.1 Detecting irrigated area non-authorised water abstraction using EO

Since agriculture has the most detrimental impact on water resources, integrated methods must be used to manage water resources, particularly for irrigation (Bouwer, 2000; Giordano *et al.*, 2013). Water resources management is typically brought on by disparate interests involving shared water resources. The result is a rise in conflict between the many water users and objectives, particularly in the Mediterranean region. The Mediterranean region already experiences water shortage problems as a result of its meteorological characteristics, and it is anticipated that this situation will only worsen as time goes on (Jury and Vaux Jr, 2007; Portoghese *et al.*, 2013; Portoghese, Vurro and Lopez, 2015).

Lack of proper water allocation practices has also made water resources management challenging. water allocation procedures must meet the expectation of all stakeholders at the same time ensuring sustainability of the resources.

In particular, in Mediterranean countries, where irrigation water accounts for more than half of water abstracted and by up to 80% in some regions (Mills *et al.*, 2009).

However, a key requirement in each case is the ability to monitor farmers' water withdrawals in order to enforce rules governing individual abstraction rates (OECD, 2015), and determine future sustainable abstraction limits (Butler Jr *et al.*, 2018). Despite the importance of monitoring for water management, the overwhelming majority of agricultural water use worldwide both from groundwater and surface water remains unmetered (OECD, 2015).

Southern Mediterranean countries such as Cyprus, Greece, Italy, Malta, Portugal, and Spain are particularly concerned with non-authorised water abstraction. In Italy, Illegal abstraction volumes tend to range between 12% and 20% of total abstraction. More frequent droughts and increasing salinisation are making the problem

worse, but more intensive action by the forestry police in recent years has had an impact on these illegal activities (Dworak *et al.*, 2010).

EO-derived information can thus represent a substantial tool to direct and guide field inspections. The verification of abstracted volumes can be done by collecting records, through field inspections or using EO derived information.

Remote sensing has shown a great promise in identifying crops within an agricultural area or irrigation scheme.

The resultant information has been found to be useful for cropping patterns and allocation of water resources for improved crop production (Moran, Inoue and Barnes, 1997; Pinter Jr *et al.*, 2003; Nellis, Price and Rundquist, 2009).

EO represents another approach for the detection of non-authorised water abstractions. Satellite or airborne images data can be used to identify irrigated areas and estimate irrigation water requirement. Suspicious areas can be identified by comparing the map of irrigated areas that has been obtained through this technique with a map of irrigated land with water rights; or by comparing the estimated irrigation water requirement with the authorised amount of water to be abstracted (Pinter Jr *et al.*, 2003).

2.2 Multi temporal Time series of spectral indices

Observations made at regular intervals of time, such as daily, weekly, or monthly, constitute a time series (Australian Bureau of Statistics, 2023). The discrete timestamps are represented by x coordinates, whereas the variables value is shown by y coordinates in a two-dimensional display.

The primary elements of a time series are seasonal and trend changes, which can be found via time series analysis. The remaining variations in a series that cannot be traced to seasonality or trends are known as irregularities. These may be brought on by internal factors like random noise or external sources like natural disasters. It is possible to find underlying patterns in the series and more fully comprehend the underlying dynamics by analysing the irregularities (Shimabukuro *et al.*, 2014).

Due to the high temporal and poor spatial resolution of the data utilized in several research studies, the analysis of time series is a widely employed methodology. (Petitjean, Inglada and Gancarski, 2014; Khorasani *et al.*, 2016). Time series incorporate any transient changes and, as the analysis is based on observations from a certain time period, offer better analysis than any other datasets.

Spectral indices such as well-known NDVI – Normalized Difference vegetation index (Myneni *et al.*, 1995)– provide information about biomass development by using red and infrared reflectance values available historically on every sensor on orbiting platform, even since landsat-1 (https://landsat.gsfc.nasa.gov/satellites/landsat-1/). Hence the availability of time series NDVI from satellites, data improves knowledge of vegetation conditions and aids in evaluating and tracking changes to it (Ivits *et al.*, 2013).

Analysing time series data of vegetation and surface water bodies allows for the well-defined definition of significant seasonal changes and inter-annual trends (Haas, Bartholomé and Combal, 2009; Tulbure and Broich, 2013; Rembold *et al.*, 2015; Cristina *et al.*, 2016).

2.2.1 Classification

Several approaches for identifying land cover and, more specifically, crop types have been developed and tested during the last few decades. As previously said, approaches were constantly modified and enhanced, not only due to the diversity of agricultural landscapes, but also due to the rising number and quality of available data.

Various classification algorithms have been developed and widely used to construct land cover maps (Aplin and Atkinson, 2004). As can be seen from the brief explanations of these categories in Table 1, they range in logic from supervised to unsupervised; parametric to nonparametric to non-metric, or hard and soft (fuzzy) classification, or per-pixel, and sub-pixel (Keuchel *et al.*, 2003). However, there are two basic categories of classification procedures, both of which are used in the processing of remote sensing images: supervised classification and unsupervised classification.

These can be utilized as different ways, but they are frequently blended into hybrid methodologies that employ more than one method (Richards and Richards, 2022).

Unsupervised image classification is a method in which picture interpretation software separates a large number of unknown pixels in an image into classes or clusters based on their values of reflectance with no assistance from the analyst (Tou and Gonzalez, 1974). For unsupervised classification, the two most frequently employed clustering algorithms are K-means and Iterative Self-Organizing Data Analysis Technique (ISODATA). These two techniques rely solely on spectrally pixel-based statistics and assume no prior knowledge of the features of the themes under consideration. In contrast, supervised classification is a method in which the data analyst constructs tiny areas called training sites on the images that contain the predictor variable that is assessed in each sample unit and allocates prior classes to each of the sampling units. Since 1980, remote sensing (RS) has been used to map land cover and agricultural areas at different spatial and temporal scales (Pareeth *et al.*, 2019).

Many papers have reported that irrigated areas can be successfully mapped using different types of satellite instruments, such as optical sensors.

In terms of detecting changes in vegetation cover, classifying land use and land cover (LULC), estimating and foreseeing vegetation, mapping forest disturbance, etc., NDVI time series analysis provides more precise and effective findings(Kennedy, Yang and Cohen, 2010; Gómez, White and Wulder, 2016; Lyu, Lu and Mou, 2016).

One of the main methods implemented to derive this information is based on the use of satellite-based optical data. Single-date imagery acquired during the peak of the crop growing season can be used for classifying the irrigated areas, although the use of multi-temporal imagery approach is preferred as it covers the different phenology stages of the crops (Ghassemi *et al.*, 2022).

A common approach is based on the analysis of the NDVI time series, due to its ability to show a considerable difference between irrigated and non-irrigated pixels (Ozdogan *et al.*, 2006).

In the study on identifying irrigated and rainfed areas in Italy under semi-arid conditions, Falanga Bolognesi et al. (2020) concluded that NDVI and accumulated rainfall data can be combined to determine irrigated and rainfed areas.

As a stand-alone remote sensing method, Longo-Minnolo et al.(2022)was able to map irrigation areas using an unsupervised classification technique using Normalized Difference Vegetation Index (NDVI) data. In order to detect actual irrigated areas without using reference data, it used the OPtical TRApezoid Model (OPTRAM) in combination with the NDVI data. An application and validation method was used in Marchfield cropland (Austria).

2.3 In-Situ and Remote Sensing Methods for Evapotranspiration

2.3.1 In-situ direct measurement evapotranspiration

2.3.1.1 Eddy covariance

The measurement of energy balance via flux towers involves utilizing Eddy covariance systems to obtain data on both latent heat flux (λET) and sensible heat flux (H) across plant canopies. In addition to these measurements, supplementary instruments such as net radiometers and soil heat flux plates can be deployed to assess net radiation and ground heat flux (Wilson *et al.*, 2002).

A comprehensive flux tower setup facilitates the measurement of all surface energy balance components, often highlighting disparities between the turbulent fluxes recorded by the eddy correlation system (H + λET) and the independent measurements of net radiation and soil heat flux, collectively referred to as available energy (Rn−G0) (Foken and Wichura, 1996; Culf, Foken and Gash, 2004).

Energy balance closure failure can be attributed to various factors, including differences in instrument accuracy and footprint.

Among the various measurements of energy balance components, net radiation (Rn) and ground heat flux (Go) are commonly considered the most accurate. There are errors of approximately 10–20% for λET and H measurements, while net radiation measurements have an error rate of about 6% (Foken, 2008).

Despite the usually lower accuracy of G0 measurements, they exhibit lower magnitudes (approximately 15 W/m^2 for complete canopy cover). Consequently, it is highly advisable to assess energy balance closure by comparing available energy to the turbulent flux components (Wilson *et al.*, 2002).

A common approach to address energy balance closure issues involves adjusting the turbulent energy components (H and λET) to maintain the Bowen ratio (β) as an indicator of energy partition(Prueger *et al.*, 2005).

Bowen ratio developed by Bowen (1926), is calculated as the ratio of sensible heat flux (H) to latent heat flux (λET). Knowledge of β enables the partitioning of available energy between H and λET, with the computation of correction closure errors ΔH and ΔλET as following equations:

$$\Delta\lambda ET = \frac{(Rn - Go) - (1 - \beta)\lambda ET}{1 - \beta} \quad 2.1$$

$$\Delta H = \beta(\lambda ET + \Delta\lambda ET) - H \quad 2.2$$

This method enables the allocation of closure errors to the uncertain measurements (H and λET) in proportion to the energy magnitude of these fluxes. β values can become negative during dawn and sunset, corresponding to periods of minimal fluxes. Consequently, during these times, β becomes an inadequate indicator for characterizing energy distribution (Brutsaert, 2013).

2.3.1.2 Lysimeter

Lysimeters that use the principle of mass conservation to offer a direct measurement of evapotranspiration (ET) have been created. These lysimeters, which come in a variety of forms, sizes, and shapes, act as containers for measuring lateral and deep-water movement within a predetermined limit (Allen *et al.*, 1991). The fundamental advantage of lysimeters is their ability to estimate vegetation's water

consumption through direct mass measurements. However, it is important to note that using lysimeters requires extensive setup, and their application is frequently limited to monitoring individual trees or small agricultural fields (Verstraeten, Veroustraete and Feyen, 2008). One of the most significant disadvantages of lysimeters is their occasional restriction in root extension, and they often do not account for capillary rise since they presume the water table is located at a significant depth.

2.3.2 Remote sensing estimation of ET: the combination equations of Penman Monteith and Shuttleworth Wallace

Evapotranspiration plays a crucial role in determining the water needs of crops and is essential for efficiently managing water resources in irrigation. Remote Sensing (RS) stands as the primary method for spatially estimating actual evapotranspiration across extensive regions, even entire continents (Yebra *et al.*, 2013). The quest to estimate evapotranspiration through remote sensing started in the late 1980s (Jackson *et al.*, 1987). Over the last three decades, this field of research has gained significant momentum, thanks to the availability of new data sources with enhanced temporal and spatial resolution at a lower cost. Numerous remote sensing methods for estimating evapotranspiration have been developed and rigorously tested (Glenn *et al.*, 2007).

This study employs two primary combination approaches for estimating evapotranspiration: the one-step approach using P-M (Penman-Monteith) and the Shuttleworth and Wallace method. The equation combining Penman-Monteith to calculate evapotranspiration hinges on the concurrent solution of the surface energy balance equation and the turbulent transfer of heat and water vapor. This is achieved by considering resistance terms defined in various ways.

The EO-based FAO-PM method, initially proposed by (D'Urso and Menenti, 1995), is an operational approach that directly applies the FAO Penman-Monteith. It utilizes a combination of in-situ meteorological data and crop characteristics derived from optical satellite images (such as Leaf Area Index (LAI), crop height (hc), and surface albedo) to estimate the resistance factors of the P-M equation.

The S-W model is an approach for the direct estimation of ET components using two Penman-Monteith equations: one for plants and another for the soil surface, an idea introduced (Monteith, 1965). These two components are weighted using a set of coefficients representing the combination of soil and canopy resistances, as outlined by Shuttleworth and Wallace (1985). This model allows for the partitioning of ET into plant and soil components, with surface resistances regulating energy transfer between plants and soil and aerodynamic resistance controlling the transfer between the surface and the atmosphere.

Both of these approaches rely on crop biophysical parameters, including LAI, FVC, albedo, and crop height, to estimate evapotranspiration and irrigation water requirements. In the following chapter (2), we will delve into a comprehensive explanation of these approaches.

2.3.2.1 Crop biophysical parameters

As agricultural areas grow, it becomes increasingly important to develop methods for monitoring them at sufficiently high spatial resolution, in a simple and non-invasive way, so that crop management can be improved on a field scale, across the entire crop cycle, and even on a daily basis to manage irrigation (FAO, 2017).

As a means to build management techniques that are data-driven in order to increase production efficiency, in agricultural areas, it makes sense to think about the problem from two distinct points of view: one that takes into account, to the greatest extent possible, the variation in space of the primary biophysical characteristics of the crop and the soil, and another that takes into account the temporal patterns at frequent intervals, thus, to fulfil the need to frequently monitor over time these characteristics (Silvestro *et al.*, 2021).

There is a wide literature showing that EO data can be used to achieve the objectives. Increasingly advanced and accessible satellites are making it possible to monitor large areas with ever greater spatial resolutions and ever shorter time intervals thanks to advanced and accessible satellites. This type of satellite is exemplified by the

constellations of satellites available through the Copernicus programme (Jutz and Milagro Perez, 2017; Huang *et al.*, 2018, 2019).

Empirical retrieval methods are based on the assumption that a linear relationship exists between the biophysical parameter and the spectral data. Statistical category methods use mathematical functions to relate the biophysical parameter and the remote sensing data, while physically based retrieval methods are based on a radiative transfer model (RTM) which is used to infer the biophysical parameters from the remote sensing data (Pasqualotto *et al.*, 2019).

- Leaf area index:

As a crop management technique based on the application of differential resources at highly resolved spatial and temporal scales, precision agriculture requires readily accessible data on the crop state at a resolution that is consistent with its objectives (Rosso *et al.*, 2022).

One of the crop biophysical factors that provides the most helpful information on plant state is the leaf area index (LAI), which is measured as the ratio of (the top side) foliar area to projected ground area. Due to the fact that the quantity of LAI is directly related to quantitative aspects of photosynthesis, respiration, and canopy water exchange, any change in LAI can be correlated with changes in vegetation productivity brought on by problems with the health of plants or nutritional status (Bréda, 2003), making LAI an efficient testing parameter of plant status(Huang *et al.*, 2019).

Remote sensing data can accurately capture LAI information over a large area in a short period of time, as opposed to field measurements which are time-consuming and labour intensive. This means that more areas can be surveyed in a shorter amount of time, resulting in more accurate and comprehensive data (Gray and Song, 2012; Günlü *et al.*, 2017; Zhou *et al.*, 2017).

Numerous research have been carried out over the last two decades to estimate LAI utilizing different satellite images with varies spatial and temporal resolutions (Tian *et al.*, 2017; Brede *et al.*, 2020). Prediction of forest LAI has been proved using Landsat satellite images, particularly Landsat 7 and 8 (Soudani *et al.*, 2006; Kang *et al.*, 2021).

Additionally, Sentinel-2 imagery from the European Space Agency (ESA) has recently been used to detect numerous vegetation features involving LAI at local and regional scales because to its higher spatial and temporal resolution than Landsat satellite (Addabbo *et al.*, 2016; Wang *et al.*, 2022). Moreover, there are studies where the estimation of LAI is done using both Landsat and Sentinel-2 images (Ganguly *et al.*, 2012; Meyer *et al.*, 2019).

For the purpose of retrieving biophysical parameters, Verrelst et al. (2015) came to the conclusion that machine learning regression techniques and radiative transfer models integrated in training workflows may be implemented. The term "hybrid training workflows" refers to these processes.

As part of the estimation of Leaf Area Index (LAI) and canopy chlorophyll content (CCC), Pasqualotto et al. (2019) used a comparison of empirical approaches (vegetation indices), semi-empirical approaches (CLAIR model with fixed and calibrated extinction coefficients), as well as artificial neural network S2 products derived from Sentinel Application Platform Software (SNAP) biophysical processors (ANN S2 products).

Various LAI satellite products from operational services and customized solutions based on cutting-edge Earth Observation (EO) data like Landsat-7/8 and Sentinel-2A were analysed and validated by (Campos-Taberner *et al.*, 2018). The comparison was done to assess the general accuracy of rice LAI estimations, which constitute a key input at different scales (from regional to local).

- Fractional vegetation cover:

The fractional vegetation cover (FVC), which is often expressed in relation to a unit area, is the ratio of the vertically projected area of vegetation to the total surface extent. In the climatic, hydrologic, and geochemical cycles, fc is crucial (Jiang *et al.*, 2008). Via plant transpiration, photosynthesis, and surface albedo, FVC plays a significant role in the meteorological and hydrologic cycles (Jiang *et al.*, 2006; Jia *et al.*, 2016).

The FVC is a crucial biophysical parameter that participates in surface processes, and it is also one of the main requirements for the prediction of numerical weather, climate modelling at the regional and global scale (Avissar and Pielke, 1989; Trimble, 1990), and monitoring of global change. As well as being an important parameter for describing the surface vegetation, it is also a quantitative variable for the plant community on the ground surface, as well as a basic data point for characterizing ecosystems (Jing *et al.*, 2011).

Multiple worldwide FVC products have been created using data collected by the Advanced Very High Resolution Radiometer (AVHRR), and numerous algorithms have been invented for regaining fractional cover from satellites (Gutman and Ignatov, 1998; Baret *et al.*, 2007; Jia *et al.*, 2015).

Using remote sensing and calculating the leaf area index, partial vegetation cover might be indirectly calculated. FVC is obtained from LAI using a polynomial empirical expression whose coefficients are found from field measurements and are applicable to a variety of crops (Vuolo *et al.*, 2015).

Zhang et al. (2019) mentioned the advancement of remote sensing technology has produced an effective instrument for FVC estimate. The empirical model (EM), pixel decomposition model, artificial neural networks (ANN), decision tree classification.

Jia et al. (2015) presented general regression neural networks used in the study could accurately reproduce the high-spatial-resolution FVC data from the MODIS surface reflectance data, which enabled the production of a reliable global FVC product. This product was then evaluated using global statistics and a comparison with the high-spatial-resolution FVC data, demonstrating its reliability and usefulness.

Chapter 3: Materials

3.1 Study area

The case studies are irrigation district (District 10) in "Sinistra Ofanto" irrigation scheme in Fig. 1, located in southern Italy in the north-eastern part of Apulia region (province of Foggia).

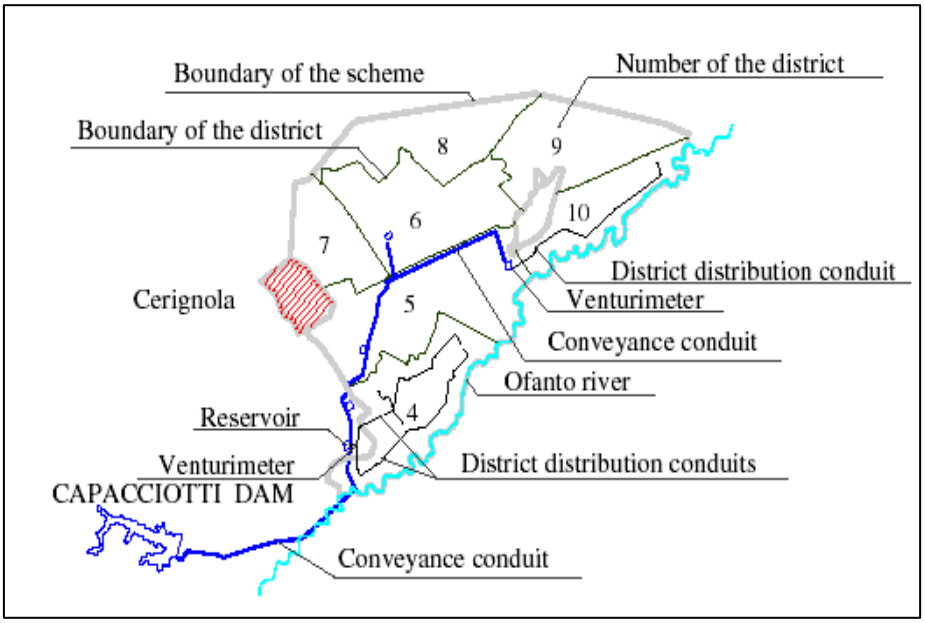

Fig. 1 - Sinistra Ofanto irrigation scheme (southern Italy).

3.1.1 Description of Sinistra Ofanto irrigation scheme

The "Sinistra Ofanto" irrigation system is located in southern Italy and covers an area of 22,500 ha. It was designed and constructed during 1980's for pressurized on-demand delivery schedule and is currently managed and operated by a local water users' organization (WUO), namely the "Consorzio per la bonifica della Capitanata"(CBC, 1984; Altieri, 1995). The area serviced by the system is subdivided into a "Low zone", where water is supplied to farms by gravity, and a "High zone"

where cropped fields are at higher elevations relative to the water source and irrigation water is conveyed and supplied by means of a lifting plant. The Low zone is composed by seven command areas called “districts”, each of them being sub-divided into smaller operational units called irrigation “sectors” that are composed by several grouped farms.

3.1.2 Description of the district N. 10

The study area corresponds to District 10, which belongs to the Low zone, and thus receives water by gravity from the source. It covers a widespread topographic area of about 2,000 ha, out of which the total irrigable area is 1,679 ha, and the site currently irrigated is 1,423 ha as depicted in Fig. 3. The current cropping pattern of the district under study was obtained from WUO records and reported in Fig. 2.

District 10 is supplied with irrigation water from a storage and compensation reservoir named “Reservoir 9-10”, having a total capacity of 47,000 m3. This reservoir receives water from the primary source, the Capacciotti dam, employing a conveyance pipeline and supplying water to Districts 9 and 10.

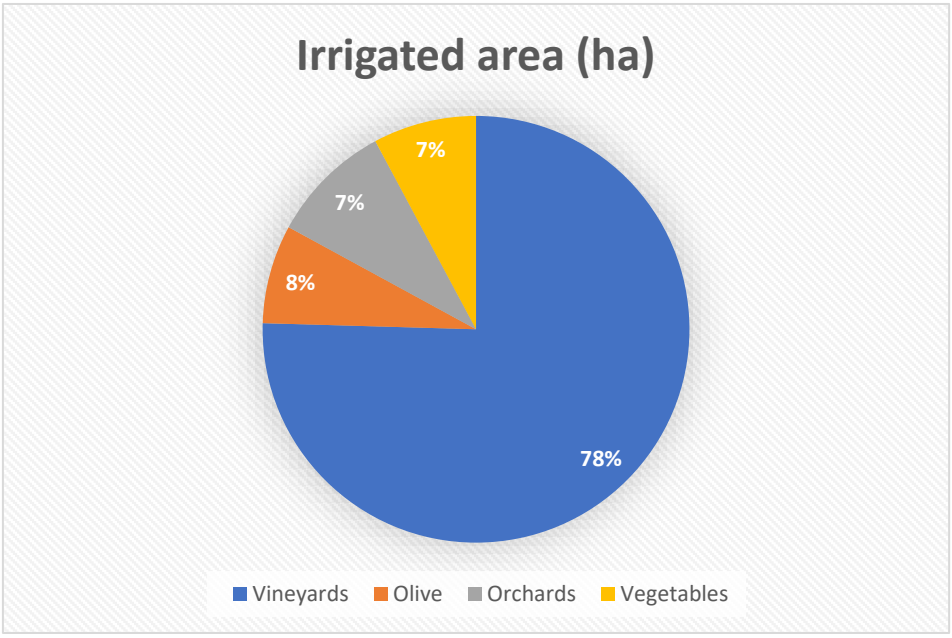

Fig. 2 - Cropping pattern in the irrigation District N. 10.

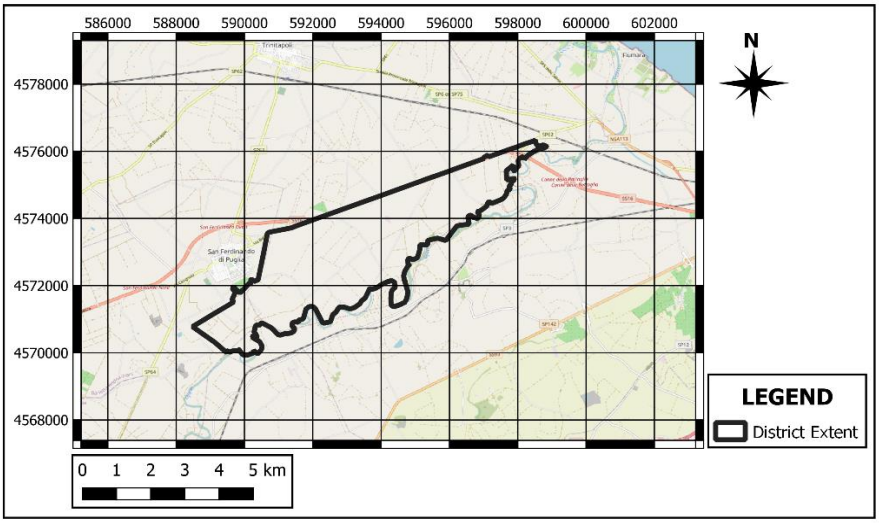

Fig. 3 - District N. 10 irrigation scheme.

The distribution network of District 10 is open branched. It is composed of buried pipelines equipped with delivery hydrants with a nominal discharge of 10 l s^{-1}, each supplying water to several cropped fields.

A restricted-demand delivery schedule operates the system. All farmers take water at their convenience with a maximum allowed flow rate of 10 l.s^{-1} and within the maximum seasonal allocated shares out of the total water supply available from the Capacciotti Dam. The service-oriented operation of the distribution network being conducted by the WUO ensures a minimum pressure head of at least 2 bars at each hydrant, which is suitable for trickle and micro-irrigation methods commonly used by farmers in the area.

The average farm size ranges from 1.5 to 2.5 ha, and each hydrant serves irrigated area ranging from 2.5 to a maximum of 4 or 5 ha; thus, the study area is characterized by many small land holdings. On the other hand, due to the favourable agro-climatic conditions, agriculture in the area is intensive and highly market-oriented. The climate is semi-arid to sub-humid and reported as “Maritime-Mediterranean”, which is typical of the coastal areas of the Mediterranean region, and the area falls

within Cfa category of the Koppen-Geiger climate classification, indicating a primary climate description of warm temperate (C), fully humid precipitation conditions (f), and hot summer temperatures (a) (Kottek *et al.*, 2006).

3.2 Meteorological data

A Mediterranean climate dominate the interested study area, Historical climatic data were obtained from TRINITAPOLI agrometeorological station (41°19'16.6"N 16°07'45.4"E), closest and most representative in the study area. Then climatic data parameters have been utilized for the next process in terms of estimation evapotranspiration and irrigation demand are average air temperature, relative humidity, wind speed and solar radiation, where the precipitation measurement was used to estimate the irrigation water requirement. As illustrated in Fig. 4 and Fig. 5, the meteorological data collected were primarily for both years 2020 and 2021 on a daily scale.

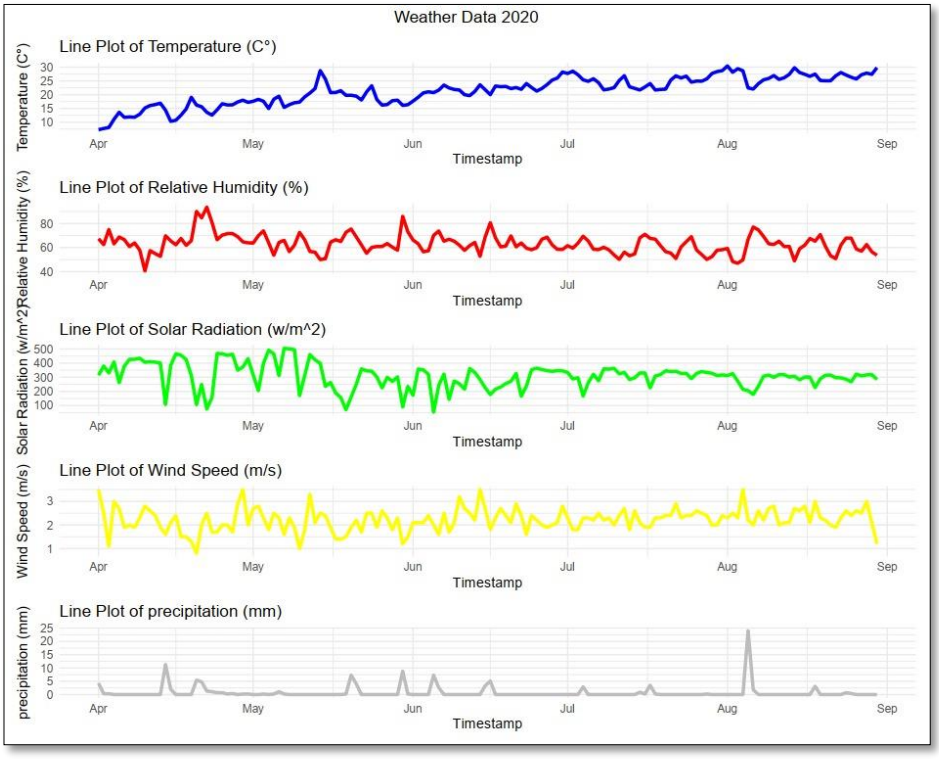

Fig. 4 - Meteorological data for District N. 10 during the 2020 irrigation season

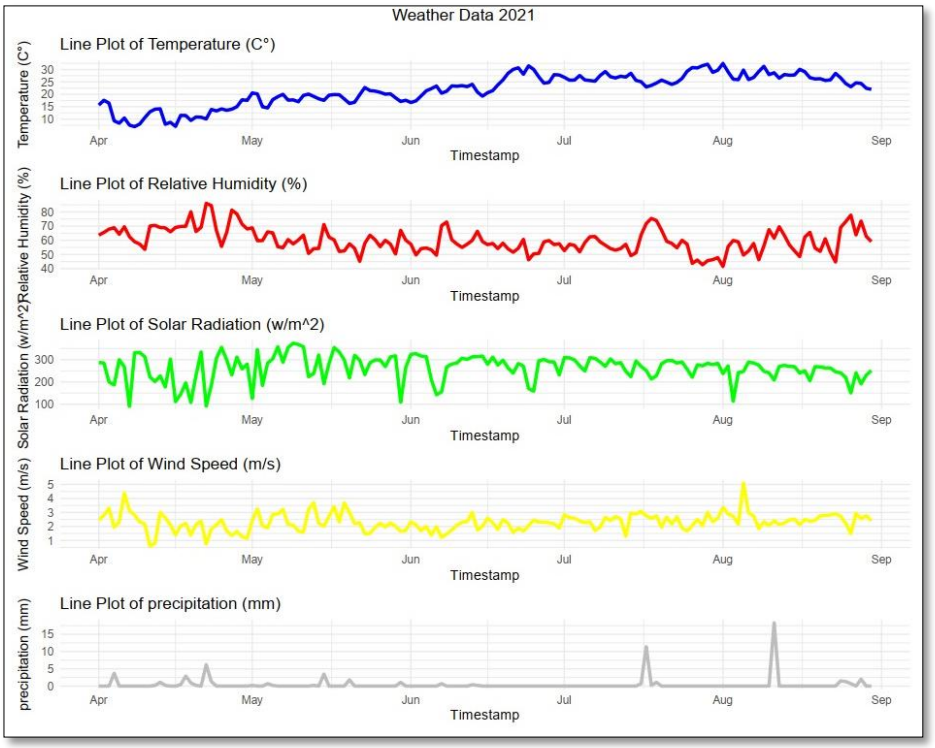

Fig. 5 - Meteorological data for District N. 10 during the 2021 irrigation season

3.3 Registered Irrigation volumes

Registered irrigation volumes were provided by the irrigation Consortium of Capitanata, which is the irrigation authority for the study area District N. 10. The consortium measures the irrigation volumes by flow meter installed at the upstream end of the interested area for the year 2020 and 2021. Table 1 shows the periods where the irrigation data were collected.

These data were limited for specific periods due to the frequent malfunction of the flowmeter, and hence, only the periods had available, reliable, irrigation data. Notably, the year 2021 posed a distinctive challenge, as continual flowmeter malfunctions prevented the complete recording of the specified irrigation volume.

Registered irrigation volumes in the study area of district 10 are provided by the irrigation Consortium of Capitanata.

Table 1 - Registered Irrigation volumes within District N. 10 for the years 2020 and 2021.

Year	Periods of collected irrigation data
2020	From 10 July to 30 August
2021	From 30 June to 30 August (not complete)

Fig. 6 - The flow meter and irrigation pipeline in pressurized irrigation system at District N. 10.

3.4 Sentinel 2

Sentinel-2 is a medium resolution optical remote sensing mission for earth observation that is a part of the Copernicus program. Its resolution is between 10 and 60 meters. It comprises the identical Sentinel-2A and Sentinel-2B satellite systems, which were launched on June 23, 2015, and March 6, 2017, respectively. Both are in the same orbit, 180 degrees apart. Multi-Spectral Instruments (MSI) on both satellites

are capable of capturing 13 spectral bands in the Visible and Near Infrared (VNIR) and SWIR.

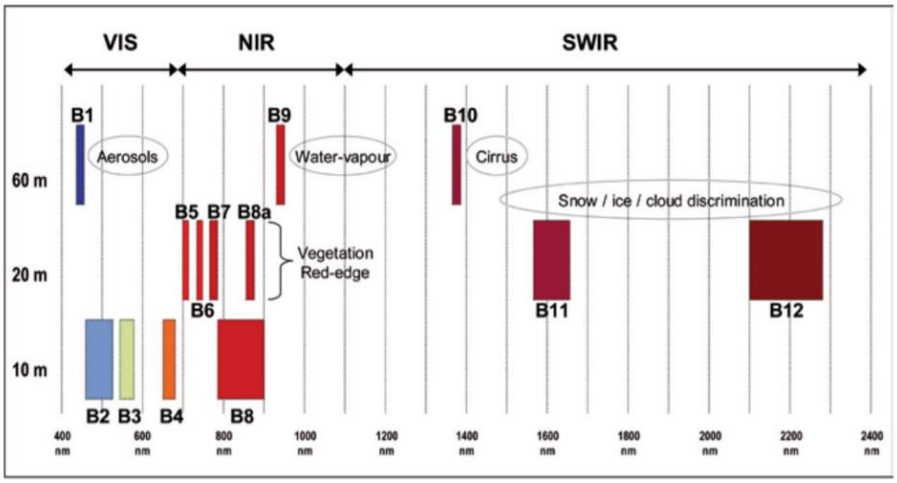

Fig. 7 - Spatial and spectral reflectance of the sentinel 2 bands at different spatial resolution ranging from 10 m to 60 m (Gatti and Bertolini, 2013).

The constellation of Sentinel-2A and 2B provide a high temporal resolution with a combined revisit time of 5 days in the equator. Given its reasonably good spatio-temporal resolution and spectral resolution, the satellite images obtained from this pair operated by the European Space Agency (ESA) can be used in monitoring changes in the earth's surface, including inland water bodies, vegetation cover, LULC, and in diverse other scientific and humanitarian applications (Jutz and Milagro Perez, 2017) .However, this technology is incapable of capturing the thermal spectrum. Fig. 7 exhibits spatial resolution and the bands of MSI.

Table 2 - Spectral bands of sentinel 2

Sentinel-2 Bands		Central Wavelength [μm]	Resolution [m]
Band 1	Coastal aerosol	0.443	60
Band 2	Blue	0.490	10
Band 3	Green	0.560	10
Band 4	Red	0.665	10
Band 5	Vegetation Red Edge	0.705	20
Band 6	Vegetation Red Edge	0.740	20
Band 7	Vegetation Red Edge	0.783	20
Band 8	NIR	0.842	10
Band 8a	Vegetation Red Edge	0.865	20
Band 9	Water vapor	0.945	60
Band 10	SWIR- Cirrus	1.375	60
Band 11	SWIR	1.610	20
Band 12	SWIR	2.190	20

3.5 Satellite images acquisition

The selected Sentinel 2A and 2B satellite images (L 2A) were obtained to cover the entire irrigation season for District N. 10 “Sinistra Ofanto” during 2020 and 2021, the time interval for the irrigation period started from April till September and The images were acquired on multiple days, It was particularly obtained from Sentinel 2A and 2B over the study area with 31 cloud-free satellite images for 2020 and 27 cloud-free satellite images for 2021, as it is shown in Table 3.

Table 3 - List of Sentinel-2 satellite images level 2A selected for District N. 10 in the years 2020 and 2021.

Acquisition date	Platform	Acquisition date	Platform
2021-03-30	Sentinel-2B	2020-04-09	Sentinel-2A
2021-04-09	Sentinel-2B	2020-04-12	Sentinel-2A
2021-05-09	Sentinel-2B	2020-04-24	Sentinel-2B
2021-05-14	Sentinel-2A	2020-04-27	Sentinel-2B
2021-05-24	Sentinel-2A	2020-05-04	Sentinel-2B
2021-05-29	Sentinel-2B	2020-05-09	Sentinel-2A
2021-06-03	Sentinel-2A	2020-05-12	Sentinel-2A
2021-06-13	Sentinel-2A	2020-05-22	Sentinel-2A
2021-06-23	Sentinel-2A	2020-05-24	Sentinel-2B
2021-06-28	Sentinel-2B	2020-06-03	Sentinel-2B
2021-07-01	Sentinel-2B	2020-06-13	Sentinel-2B
2021-07-06	Sentinel-2A	2020-06-26	Sentinel-2B
2021-07-11	Sentinel-2B	2020-06-28	Sentinel-2A
2021-07-16	Sentinel-2A	2020-07-03	Sentinel-2B
2021-07-21	Sentinel-2B	2020-07-08	Sentinel-2A
2021-07-23	Sentinel-2A	2020-07-11	Sentinel-2A
2021-07-28	Sentinel-2B	2020-07-21	Sentinel-2A
2021-07-31	Sentinel-2B	2020-07-23	Sentinel-2B
2021-08-02	Sentinel-2A	2020-07-26	Sentinel-2B
2021-08-07	Sentinel-2B	2020-07-28	Sentinel-2A
2021-08-10	Sentinel-2B	2020-07-31	Sentinel-2A
2021-08-12	Sentinel-2A	2020-08-02	Sentinel-2B
2021-08-15	Sentinel-2A	2020-08-10	Sentinel-2A
2021-08-20	Sentinel-2B	2020-08-12	Sentinel-2B
2021-08-22	Sentinel-2A	2020-08-15	Sentinel-2B
2021-08-27	Sentinel-2B	2020-08-17	Sentinel-2A
2021-08-30	Sentinel-2B	2020-08-20	Sentinel-2A
		2020-08-27	Sentinel-2A
		2020-08-30	Sentinel-2A
		2020-09-06	Sentinel-2A
		2020-09-09	Sentinel-2A
		2020-09-11	Sentinel-2B

	2020-09-14	Sentinel-2B
	2020-09-16	Sentinel-2A
	2020-09-19	Sentinel-2A

Chapter 4: Methods

4.1 Satellite Images pre-processing

Once the cloud-free images have been identified, the next step is to subset the bands. A band refers to a defined wavelength range detected by the satellite sensors. When working with satellite images for irrigation monitoring, it is essential to subset the images to display only the required bands, including B2, B3, B4, B5, B6, B7, B8, B8A, B11, and B12. This step is imperative for deriving essential indices, such as normalized difference vegetation index (NDVI), short transformed infrared reflectance index (STR) and albedo, which play a pivotal role in this research.

To achieve uniformity in raster data size, a resampling process was applied, using the nearest-neighbour method, to adjust all Sentinel-2 bands with a spatial resolution of 20m (B5, B6, B7, B8a) and 60 m (B11, and B12) to 10m, aligning them with the existing 10m bands (B2, B3, B4, and B8).

4.2 Biophysical parameters retrieval

In this study, the biophysical parameters used for estimating the evapotranspiration are LAI and FVC, as described in 2.3.2.1. LAI represents the total one-sided area of photosynthetic tissue per unit of ground area and FVC is the ratio of vertically projected area of vegetation to the total surface extent, generally expressed in relation to a unit area. The SNAP (Weiss, Baret and Jay, 2020) toolbox was used to retrieve the biophysical parameters during 2020 and 2021 in the study area. This software requires as input multispectral raster of equal size, either 10 or 20 m in the case of Sentinel-2.

Artificial neural network ANN-based retrieval algorithm is used for these parameters, in this case, as a result of training the network with PROSPECT and SAIL radiative transfer models, canopy characteristics were estimated from the associated SENTINEL2 top of canopy (TOC) reflectance data. The LAI is derived via the ANN

algorithm by inputting eight spectral bands (B3–B7, B8a, B11, and B12) resampled to 10 m pixels. Validation of this approach has been done on a variety of crops (Pasqualotto et al., 2019), FVC can also be derived using the coupled model, as shown in the Fig. 8.

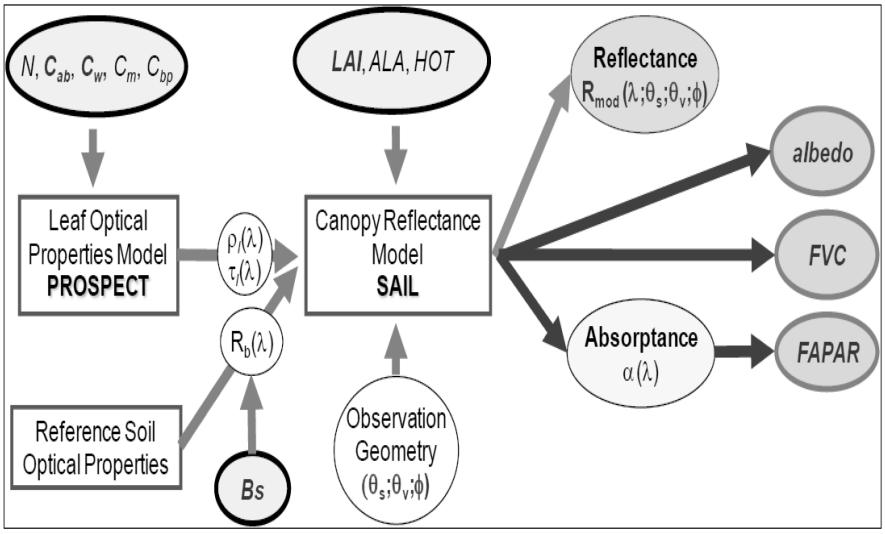

Fig. 8 - The coupled PROSPECT+SAIL model that generates the training database made of TOC reflectance's and corresponding biophysical variables (Verhoef, 1984; Jacquemoud and Baret, 1990; Weiss, Baret and Jay, 2020).

When computing the net radiant flux in the ET models, it is needed to calculate the hemispherical and spectrally integrated surface albedo. By accounting for atmospheric corrections in L2A images, as used herein, the albedo can be derived as a weighted sum of surface spectral reflectance (ρλ) with broadband coefficients (ωλ) in determining the fraction of solar irradiance for each sensor band (Menenti, Bastiaanssen and Van Eick, 1989; D'Urso and Calera Belmonte, 2006).

The albedo is calculated using Eq. (3.1):

$$r = \sum_{\lambda=1}^{n} \rho_\lambda \omega_\lambda \qquad 4.1$$

The coefficient used to calculate the albedo ($\omega_{\lambda i}$) are presented in Table 4 (D'Urso et al., 2021).

The biophysical parameters, specifically Leaf Area Index (LAI), Fraction of Vegetation Cover (FVC), and Albedo, were subject to linear interpolation to facilitate daily-scale utilization in subsequent processing. This adjustment was necessitated by the intermittent acquisition of parameters throughout the day, particularly when utilizing Sentinel-2 satellite images with a relatively wide temporal acquisition window ranging from 3 to 5 days across two orbits. The interpolated parameters enabled the estimation of daily Evapotranspiration (ET) and the generation of Irrigation maps, aligning with meteorological data. This emphasis on incorporating meteorological information represents a crucial aspect of this study, facilitating comparisons with registered irrigation volumes on a daily scale (Li et al., 2017).

Table 4 - Multispectral imager (MSI) characteristics and coefficients for calculating hemispherical albedo on Sentinel-2 satellites.

Band Number	Center (λ) [μm]	Spectral width (Δλ) [μm]	E_{λ}^{0} [W m^{-2}]	$\omega_{\lambda i}$ [-]
B1	0.443	0.02	1893	-
B2	0.49	0.065	1927	0.1836
B3	0.56	0.035	1846	0.1759
B4	0.665	0.03	1528	0.1456
B5	0.705	0.015	1413	0.1347
B6	0.74	0.015	1294	0.1233
B7	0.783	0.02	1190	0.1134
B8	0.842	0.115	1050	0.1001
B8a	0.865	0.02	970	-
B9	0.945	0.02	831	-
B10	1.375	0.03	360	-
B11	1.61	0.09	242	0.0231
B12	2.19	0.18	3	0.0003
			Sum	1.0000

4.3 Mapping irrigated area

The detection of the irrigated areas was performed a preliminary unsupervised classification of the normalized difference vegetation index (NDVI) using the full

temporal trajectory time series imagery. The NDVI is a normalized ratio, computed by combining the reflectance values from Sentinel 2 satellite in the Near Infrared (NIR) and Red spectral bands (RED) taking into consideration the spatial resolution of 10 meters both bands.

$$NDVI = \frac{(NIR - RED)}{(NIR + RED)} \qquad 4.2$$

Temporal time series was extracted along irrigation season for both years 2020 and 2021, which express on the phenological statement during the seasons, thus, it can be focal index to start detecting the irrigated areas according to NDVI layer-stack maps.

This method requires no prior knowledge of the area in terms of ground truth. This classification approach is performed to detect irrigation area, and the method applied for clustering is K-mean, which is simple and fast clustering technic, and before that, the elbow method is a technique used to estimate the optimal number of clusters in a K-means clustering analysis (Yang *et al.*, 2021). The process involves plotting the sum of squared distances (or within-cluster sum of squares, WSS) for each number of clusters against the number of clusters and looking for the "elbow point" in the plot, where the decrease in WSS starts to level off. From the Fig. 9 the elbow point represents the number of clusters of the NDVI where adding additional clusters does not significantly decrease the WSS. The appropriate number of clusters was selected at 50 classes, which follows the turning point.

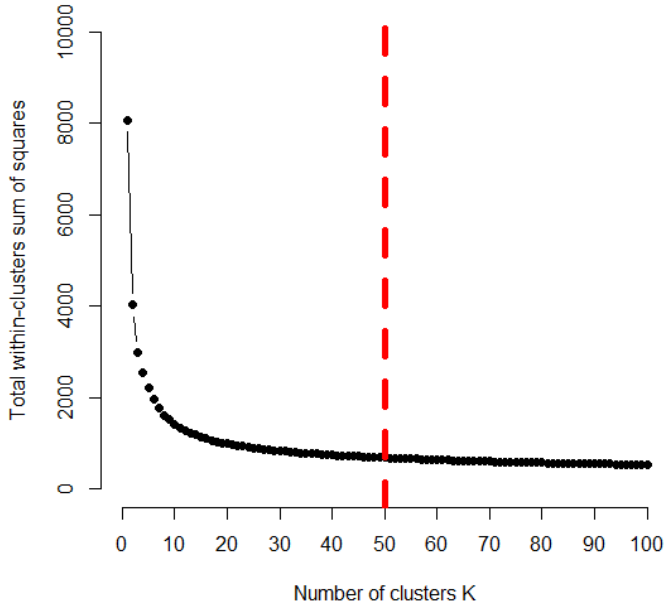

Fig. 9 – Elbow method plot.

K-mean clustering method is conducted using (Orfeo – ToolBox) by taking into account the merge NDVI stack-layers for the entire irrigation season, following the main principle of k-means is to compile a prototype or center of mass (centroid) from a dimensionless dataset n. k-means requires input of the number of classes as much as k and divides the amount of data n into class k based on the similarity with the class centroid (Giyanto, 2008). Determinate of the centroid value in k-means using these equation (Wakhidah, 2010):

$$Ci = \frac{1}{M}\sum_{j=1}^{M} xj \qquad 4.3$$

Data that has the shortest distance with the centroid will be entered into the class in the centroid. Calculation to determine the distance between centroid points with each point of the object using following equation:

$$d = \sqrt{(x1 - x2)^2 + (y1 - y2)^2} \qquad 4.4$$

Overall, the analysis involves the information from the K-means clustering, NDVI mean and variance trends, to determine whether each cluster represents a potentially irrigated or not irrigated area. After that we grouped the classes according to their phenological pattern, where the trend indicates consistent growth over time, it may suggest the presence of irrigated area. This link is established through an analysis of both rainfall data and the crop phenology curves, where the temporal trends of NDVI mean and variance are plotted for each class (Ozdogan *et al.*, 2010). Thus, the study area was divided into three thematic groups based on the time series of NDVI mean values and standard deviations. Those three groups are: a) group 0 which represents not irrigated areas, b) group (1) which represents irrigated trees, and c) group 2 which represents irrigated herbaceous.

4.4 One-step Penman Monteith approach

The well-known Penman-Monteith approach (hereafter, PM) combines the principles of surface energy balance the vertical heat and vapour fluxes by applying different surface resistances:

$$\mathrm{ET_p} = \lambda \left[\frac{\Delta A + \rho c_p \mathrm{D} / r_a^h}{\Delta + \gamma \left(1 + r_s^c / r_a^h\right)} \right] \qquad 4.5$$

Where:

ETp is crop evapotranspiration,

λ is latent heat of vaporization (J/Kg),

Δ is the latent heat for vaporization (J/Kg),

A is the available energy flux density (W/m2),

ρ is the air density (Kg/m3),

cp is air specific heat (J/Kg/ C^{o}),

D is the vapor pressure deficit at the screen level where the air temperature is measured (KPa),

γ is the thermodynamic psychometric constant (KPa/C^{o}),

rah is the aerodynamic resistance for sensible and latent heats (s/m), and

r_s^c is the canopy resistance (s/m).

The available energy flux is the difference between the net radiation, Rn, and the soil heat flux, G. The Rn can be calculated as:

$$\mathrm{R_n} = (1-\alpha)K + L^* \quad 4.6$$

Where α is the spectrally integrated surface albedo, K is the incoming shortwave radiation and L* is the net incoming longwave radiation. The aerodynamic resistance to sensible heat can be obtained as:

$$\mathrm{r_a^h} = \frac{\ln\left(\frac{z_u - 0.66h_c}{0.123h_c}\right)\ln\left(\frac{z_T - 0.66h_c}{0.0123h_c}\right)}{k^2 u} \quad 4.7$$

Where hc is the canopy height, k is the von Karman's constant which can be taken as 0.41, zu and zT are the measurement heights for wind speed u and temperature T, d0 is the zero-plane displacement height and z0m and z0h represent the roughness lengths for momentum and heat. The values of d0, z0m and z0h are taken as proportional to the canopy height hc (Brutsaert, 1982), with factors 0.67, 0.123 and 0.0123, respectively.

The bulk stomatal resistance was given by (Szeicz and Long, 1969) as:

$$r_s^c = \begin{cases} \dfrac{r_{leaf}}{0.5LAI} & |LAI \leq 4 \\ \dfrac{r_{leaf}}{2} & |LAI < 4 \end{cases} \quad 4.8$$

Where r_{leaf} is the leaf resistance which is the reciprocal of the stomatal conductance; its value reaches a minimum for non-stressed crop, i.e. 100 s/m for herbaceous and 200 s/m for tree crops (Körner, 1994; Kelliher et al., 1995). Under stress conditions due to limited soil water availability, the resistance value increases, thus determining a reduction in the evapotranspiration flux.

PM approach requires meteorological data and leaf and canopy resistances. In order to separate the transpiration from evapotranspiration, (Ritchie, 1972) equation was applied using LAI:

$$\mathrm{E_{s,p}} = ET_p e^{-c.LAI} \quad 4.9$$

$$\mathrm{T}_p = ET_p - \mathrm{E}_{s,p} \quad 4.10$$

c is an extinction coefficient, the partitioning between soil evaporation $E_{s,p}$ and transpiration T_p is based on the assumption that LAI is uniform for all the canopy cover.

However, the PM approach assumes that the leaves completely cover the soil, i.e., the big-leaf assumption (Monteith and Unsworth, 2008). This assumption could lead to underestimation of bare soil evaporation when applied to sparse vegetation such as tree crops (D'Urso, 2001).

4.5 Shuttleworth and Wallace approach

Shuttleworth and Wallace (1985) extended the application of PM approach by partitioning the evapotranspiration between the bare soils and the canopy covers. The evapotranspiration in Shuttleworth and Wallace (1985) (hereafter, SW) is given by:

$$\mathrm{ET_p} = \lambda E_c + \lambda E_s = \frac{\Delta(A - A_s) + \frac{\rho c_p D_0}{r_a^c}}{\Delta + \gamma\left(1 + \frac{r_s^c}{r_a^c}\right)} + \frac{\Delta A_s + \frac{\rho c_p D_0}{r_a^s}}{\Delta + \gamma\left(1 + \frac{r_s^s}{r_a^s}\right)} \quad 4.11$$

Where D0 is the vapor pressure deficit at the canopy height, given by:

$$\mathrm{D_0} = D + \frac{\Delta A - (\Delta + \gamma)\lambda \mathrm{E}\ \mathrm{r_a^a}}{\rho c_p} \quad 4.12$$

The available energy at soil surface, As, is calculated from the net radiation at the soil surface, Rns. The latter can be calculated from Rn using Beer's law:

$$\mathrm{R_{ns}} = R_n \exp\left(-0.5LAI\right) \quad 4.13$$

In SW approach, the vapor flux is driven by two aerodynamic resistances: from canopy level to the reference screen height, r^a_a, and from the soil surface to the canopy level, r^a_s. The two resistances values change linearly between two limits, w corresponding to closed canopy at LAI >4, and 0 corresponding to bare soils. The resistances can then be described as:

$$\mathrm{r_a^s} = \begin{cases} \frac{LAI}{4} r_a^s(\omega) + \frac{(4 - LAI)}{4} r_a^s(0) & at\ LAI \le 4 \\ r_a^s(\omega) & at\ LAI > 4 \end{cases} \quad 4.14$$

$$\mathrm{r}_{\mathrm{a}}^{a} = \begin{cases} \frac{LAI}{4} r_a^a(\omega) + \frac{(4 - LAI)}{4} r_a^a(0) & at\ LAI \leq 4 \\ r_a^a(\omega) & at\ LAI > 4 \end{cases} \quad 4.15$$

Where:

$$\mathrm{r}_{\mathrm{a}}^{s}(\omega) = \frac{\ln\left(\frac{z - d_0}{z_0}\right)}{k^2 u} \frac{h_c}{n(h_c - d_0)} \left[\exp n - \exp\left(n\left(1 - \frac{d_0 + z_0}{h_c}\right)\right)\right] \quad 4.16$$

$$r_a^s(0) = \frac{\ln\left(\frac{z}{z_0'}\right) \ln\left(\frac{d_0 + z_0}{z_0'}\right)}{k^2 u} \quad 4.17$$

$$r_a^a(\omega) = \frac{ln\left(\frac{z - d_0}{z_0}\right)}{k^2 u} \left[\ln\left(\frac{z - d_0}{h_c - d_0}\right) + \frac{h_c}{n(h_c - d_0)} \left[\exp\left(n\left(1 - \frac{d_0 + z_0}{h_c}\right) - 1\right)\right]\right] \quad 4.18$$

$$r_a^a(0) = \frac{\left[\ln\left(\frac{z}{z_0'}\right)\right]^2}{k^2 u} - r_a^s(0) \quad 4.19$$

Where z0 and z'0 are the roughness lengths at closed canopies and bare soils, respectively. The z0 is equal to 0.05 hc (Raupach, 1994; Verhoef, McNaughton and Jacobs, 1997). The z'0 can be considered a constant value of 0.01 m. The eddy diffusivity decay coefficient, n, can be considered a constant at the value of 2.5 (Shuttleworth and Wallace, 1985; Ortega-Farias et al., 2007).

Consequently, by rewriting Equation (4.11) in the manner shown below, it is possible to eliminate the vapour pressure deficit at canopy height D0:

$$\lambda \mathrm{E} = C_c PM_c + C_s PM_s \tag{4.20}$$

$$PM_c = \frac{\Delta \mathrm{A} + (\rho c_p \mathrm{D} - \Delta r_a^c A_c)/(r_a^a + r_a^c)}{\Delta + \gamma(1 + \frac{r_s^c}{r_a^a + r_a^c})} \tag{4.21}$$

$$PM_s = \frac{\Delta \mathrm{A} + (\rho c_p \mathrm{D} - \Delta r_a^s A_s)/(r_a^a + r_a^s)}{\Delta + \gamma(1 + \frac{r_s^s}{r_a^a + r_a^s})} \tag{4.22}$$

The two coefficients Cc and Cs are given by the equations:

$$C_c = \frac{1}{\left[1 + \frac{R_c R_a}{R_s(R_c + R_a)}\right]} \tag{4.23}$$

$$C_s = \frac{1}{\left[1 + \frac{R_s R_a}{R_c(R_s + R_a)}\right]} \tag{4.24}$$

With:

$$\mathrm{R}_a = (\Delta - \gamma) r_a^a \tag{4.25}$$

$$\mathrm{R}_s = (\Delta - \gamma) r_a^s + \gamma r_s^s \tag{4.26}$$

$$\mathrm{R}_c = (\Delta - \gamma) r_a^c + \gamma r_s^c \tag{4.27}$$

This mathematical equation enables the computation of λE as described in Equation (4.20). The resultant value can subsequently be applied in Equation (4.12) to

derive Do, and consequently, ascertain the values of λE_c and λE_s, as determined by Equation (4.21).

4.6 Optical trapezoid model (OPTRAM)

OPTRAM is based on the normalized difference vegetation index (NDVI) and shortwave infrared transformed reflectance (STR) spaces pixel distribution.

Short wave transformed reflectance STR is provided by:

$$STR = \frac{(1 - \rho_{SWIR})^2}{2\,\rho_{SWIR}} \qquad 4.28$$

Where SWIR band is surface reflectance from the Sentinel satellite band 12 (2190 nm).

The Fig. 10 exhibits STR-NDVI feature space takes the shape of a trapezoid when the relationship between soil and vegetation water content is assumed to be linear (Sadeghi et al., 2017).

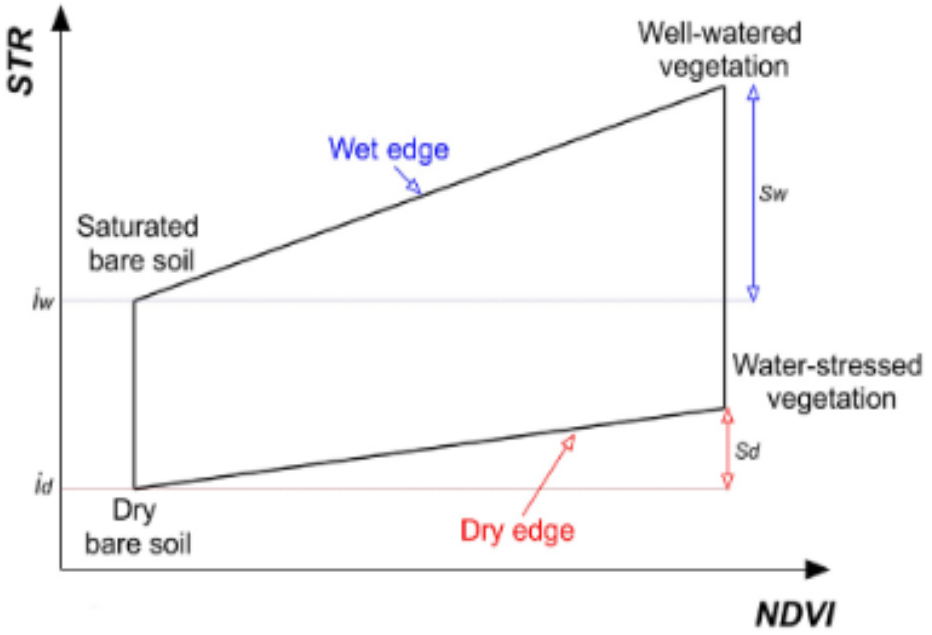

Fig. 10 - Optical trapezoid model between STR and NDVI (Sadeghi *et al.*, 2017)

D'Urso et al. (2021), proposed a method to modulate the leaf stomatal resistance and the substrate between upper and down edges as depicted by using the water index in Fig. 11.In this study, we adopt the aforementioned technique that integrates the S-W and P-M approaches. In the following equations, we may establish the Optram model.

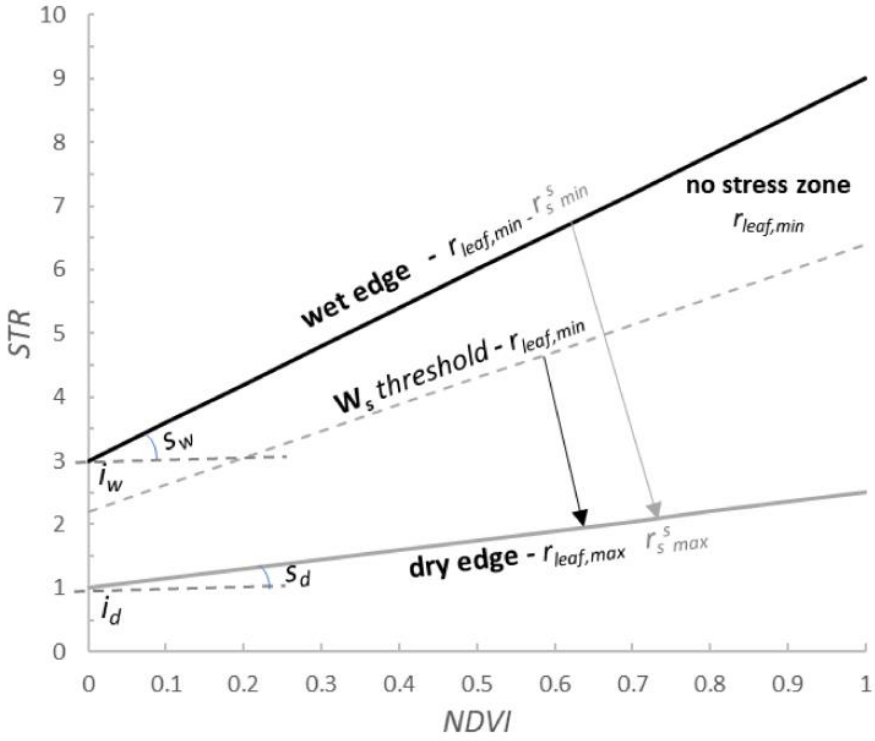

Fig. 11 - NDVI-STR space for OPTRAM method and proposed modulation of substrate and leaf stomatal resistance (D'Urso *et al.*, 2021).

The STR and NDVI were calculated for each satellite image from sentinel 2 during the irrigation season for 2020 and 2021, then the two-dimensional scatter STR_NDVI is confined by two edges corresponding two dry and wet edges. These

boundaries correspond to the time series pixels of STR-NDVI over atwo year period. Specifically, the data spans from April to September for the years 2020 and 2021.

By determining the slope and intercept of the wet (Sw, iw) and dry (sd, id) edges, we define the two limits in the STR-NDVI boundaries following the equations:

$$STR_d = i_d + s_d NDVI \quad 4.29$$

$$STR_w = i_w + s_w NDVI \quad 4.30$$

Then the water index "W" calculated for each pixel:

$$W = \frac{STR - STR_d}{STR_w - STR_d} \quad 4.31$$

When using Sentinel-2 short wave infrared band 12, the water index that is displayed is a good indicator for soil water saturation, then it should be utilized to modulate the resistances of the substrate and leaf canopy between wet (W=1) and dry (W=0) conditions (D'Urso *et al.*, 2021).

The Fig. 12 clearly shows that the water index preserves the minimal leaf resistance as a constant value unless it decreases by less than the stipulated value (W=0.6) of the water index; in this case, the plant is regarded as toward stress condition (Keulen and Seligman, 1987; Feddes *et al.*, 1988).

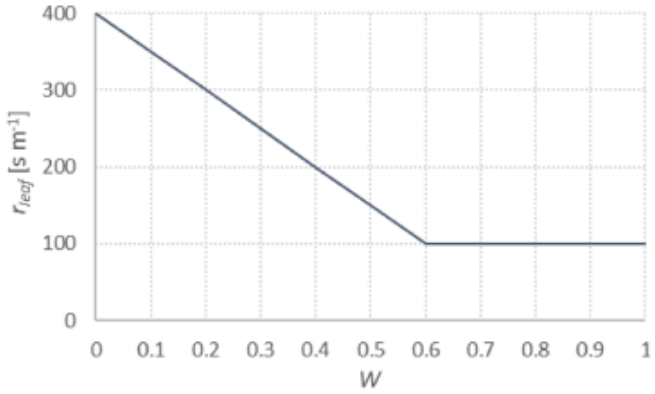

Fig. 12 - Variation of leaf resistance with water index (D'Urso *et al.*, 2021).

Nevertheless, the substrate resistance is inversely related to the water index, substrate resistance rs decreasing by increasing the water index (Shuttleworth and Wallace, 1985) as shown in the Fig. 13.

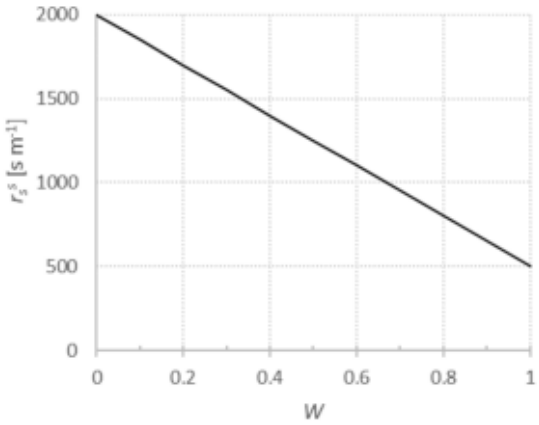

Fig. 13 - Variation of substrate resistance with water index (D'Urso *et al.*, 2021).

The wet and dry boundaries of the STR-NDVI feature space, delineating its upper and lower sides, were employed to compute the water index (W) for individual pixels. This computation was based on the variables NDVI and STR, as depicted in the Fig. 11.

4.7 Different scenarios to estimate evapotranspiration

In the study area (District 10), a comprehensive scientific inquiry was undertaken, employing combination equations for the evaluation of local irrigation practices. Within this research, combination approaches like Penman-Monteith (P-M) and Shuttleworth and Wallace (S-W) were carefully applied in a singular technical step to rigorously examine and quantify evapotranspiration (ET). This comprehensive procedure involved canopy parameters, notably the Leaf Area Index (LAI) and surface albedo. These critical parameters were meticulously derived from data acquired by the

Sentinel-2 (S2) satellite system, playing an important part in making accurate estimate of irrigation volumes.

An important aspect of this study was calibrating the model, which played a key role in the research. Specific adjustments were executed, with particular emphasis placed on key factors such as crop height (hc) and leaf stomatal resistance (r_{leaf}). Notably, the standardization of crop height (hc) was rigorously set at 0.4 meters for herbaceous crops and 1.2 meters for tree crops, despite the dominance of the radiative component in evapotranspiration estimation through the Penman-Monteith method in irrigated environments, the adoption of fixed crop height values for both herbaceous and tree crops demonstrates minimal impact on final accuracy (Calera *et al.*, 2017). Within our district-specific study, the precise determination of singular values for various tree or herbaceous groups remains a challenge. Consequently, the implemented fixed values serve as a pragmatic approximation, effectively characterizing an average crop height. This standardization was underpinned by the premise that, during the irrigated season, the influence of crop height (hc) on the estimation of evapotranspiration is deemed negligible in contrast to the impact of incoming solar radiation (Vuolo et al., 2015; Belfiore et al., 2023). The subsequent scenarios were exclusively employed for perennial crops (trees) as classified on the irrigation map. For herbaceous crops, we assumed standard conditions with minimal leaf resistance ($r_{leaf} = 100$ s/m) in order to estimate evapotranspiration (ET).

Within the ambit of the Penman-Monteith methodology, the study presented four distinct scenarios, denoted as S1, S2, S3, and S4, encompassing variations in leaf resistance (r_{leaf}). Herbaceous crops were maintained at constant values under standard conditions, with crop height (hc) set at 0.4 meter and leaf stomatal resistance (r_{leaf}) fixed at 100 s/m. In contrast, tree crops were maintained with a constant crop height of 1.2 meters, while variations in leaf resistance (r_{leaf}) were contingent upon the stress conditions experienced. Specifically, when tree crops encountered stress conditions, such as those induced by deficit irrigation practices, notably prevalent in District 10, especially in the context of the dominant grapevine crop, leaf resistance increased to a level of 400 s/m (Möller *et al.*, 2007; D'Urso *et al.*, 2021).

Furthermore, the Ritchie equation (4.10) was applied to isolate the transpiration (Tp) component from the plant, effectively eliminating soil evaporation (Es) due to the sparse canopy coverage present in the irrigated area, primarily cultivated with perennial crops equipped with drip irrigation systems. Based on the previous explanation of the fourth scenarios, we can conclude that the range of assumptions, spanning from no-stress (r_{leaf} = 200 s/m) to limited-stress (r_{leaf} = 400 s/m), was utilized to assess the farmer's response to either meeting the crop's water requirements or practicing deficit irrigation (verification needed when compared to registered irrigation volume).

The study extended its scope to include additional scenarios, specifically denoted as S5, S6, and S7. These scenarios involved the adaptation of the OPTRAM model to estimate ETa when utilizing both the Penman-Monteith (P-M) approach and the Shuttleworth and Wallace (S-W) methodology. The S-W approach is characterized as a combination equation tailored for sparse canopy conditions, encompassing the calculation of both soil evaporation (Es) and plant transpiration (Tp). The OPTRAM model was then employed to modulate leaf and substrate resistances. It is noteworthy that a range of values for leaf resistance (r_{leaf}) spanning from 100 s/m to 400 s/m was assumed, in conjunction with the application of maximum irrigation deficit applied by farmers to perennial crops (D'Urso *et al.*, 2021). Additionally, soil resistance (r_{soil}) was considered to range from no-stress (r_{soil} =500 s/m) to limited-stress (r_{soil} =2000 s/m). Notably, when implementing the OPTRAM model, two distinct estimation scenarios, denoted as S5 and S6, were generated when incorporating S-W in the calculation of both evapotranspiration and transpiration for perennial crops. In contrast, the P-M approach (with OPTRAM) exclusively addressed evapotranspiration in scenario S7. The tables listed below provide clear clarification of the scenarios.

Table 5 - Scenarios when using Penman-Monteith with different leaf resistances.

Scenarios	Method	r_{leaf}	ET
S1	P-M	200 s/m	No stress
S2	P-M	400 s/m	limited stress

Table 6 - Scenario when using Penman-Monteith, calculate transpiration by applying Ritchie equation (4.10)

Scenarios	Method	r_{leaf}	Tp
S3	P-M*	200 s/m	No stress
S4	P-M*	400 s/m	limited stress

Table 7 - Scenarios when use Shuttleworth and Wallace integrated with OPTRAM, modulating r_{soil} (500 s/m to 2000 s/m) and r_{leaf} (100 m/s to 400 m/s)

Scenarios	Method	OPTRAM	ET	Tp
S5	S-W	×	Actual	----------
S6	S-W	×	----------	Actual

Table 8 - Scenario when use Penman Monteith integrated with OPTRAM, modulating r_{leaf} (100 m/s to 400 m/s

Scenarios	Method	OPTRAM	ET
S7	$P\text{-}M_{Optram}$	×	Actual

4.8 Irrigation water requirement:

The calculation of irrigation water requirement was carried out for seven distinct scenarios, the scenarios were mentioned in this chapter.

The irrigation water requirement concept is defined as the net depth of water that needs to be applied to the crop. It quantifies the amount of water necessary to meet the crop's evapotranspiration demands, which refers to the combined loss of water through both evaporation from the soil surface and transpiration from the plant (Allen et al., 1998).

Mathematically, the net irrigation requirement (IWR) is determined by subtracting the effective rainfall from the total evapotranspiration of the crop (ET_{crop}). This can be represented by the following:

$$IWR = ET_{crop} - P_n \quad 4.32$$

Where ET_{crop} is crop evapotranspiration (mm) and P_n is the effective rainfall.

The amount of the intercepted precipitation water from crop surface is subtracted from the total precipitation to obtain the net precipitation (Braden, 1985):

$$P_n = P - \alpha LAI \left(1 - \frac{1}{1 + \frac{\mathrm{FVC}.P}{\alpha.LAI}} \right) \quad 4.33$$

Where P is the precipitation above the canopy in (mm), α is an empirical parameter represents the crop saturation per unit of foliage area (2.88 mm/day for most crops).

to calculate the gross irrigation water requirement (GIWR), which accounts for the efficiency of the irrigation system, the net irrigation requirement (IWR) is divided by the irrigation efficiency (eff), which is a dimensionless parameter representing the system's effectiveness in delivering water to the crop. In the study area, the irrigation efficiency (eff) was determined to be 0.85, assuming drip irrigation as the method of irrigation for perineal crops, and 0.75 for the herbaceous, assuming sprinkler irrigation.

It is essential to emphasize that GIWR was rigorously assessed in relation to the registered irrigation volumes on a district scale.

4.9 Flow chart:

The flowchart illustrates the process for determining the irrigation water requirement by employing various models to initially estimate evapotranspiration (ET) and transpiration (Tp), as detailed in chapter (4.7).

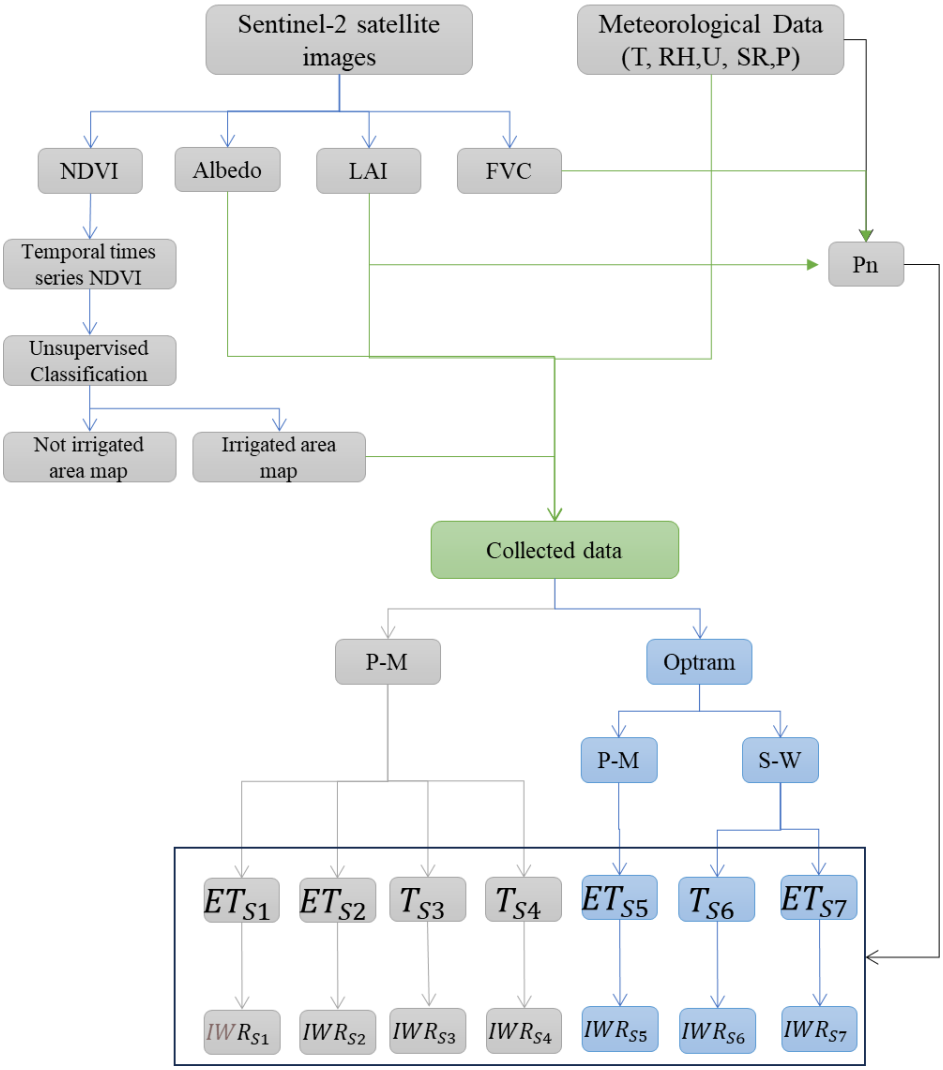

Fig. 14 - Overview of step processing to estimate irrigation water requirements.

4.10 Implementation of validation models in eddy covariance flux tower ET measurements:

In this subsection, the validation of the prior methods, denoted as P-M and S-W, is conducted by means of eddy covariance flux measurements, both with and without the incorporation of OPTRAM. For this purpose, considering the impracticality of installing this type of instrumentation in the study area, i.e., lack of homogenous field of suitable dimensions, a dataset collected in the Murray Darling Basin (Australia) on irrigated herbaceous crop has been considered and shares climate characteristics with District 10, featuring warm temperate conditions, fully humid precipitation, and high temperatures during the summer months (Kottek *et al.*, 2006). Despite the location and the crop type, this validation serves as a robust means of assessing the accuracy of estimated evapotranspiration (ET) when compared to the ETa values derived from an eddy covariance flux tower.

The validation models discussed in preceding sections were similarly applied in an Australian study area as part of the COALA project (https://www.coalaproject.eu/). This particular study took place in GVC's alfalfa field, where an eddy covariance flux tower was erected to encompass observations from March 19 to May 17, 2022.

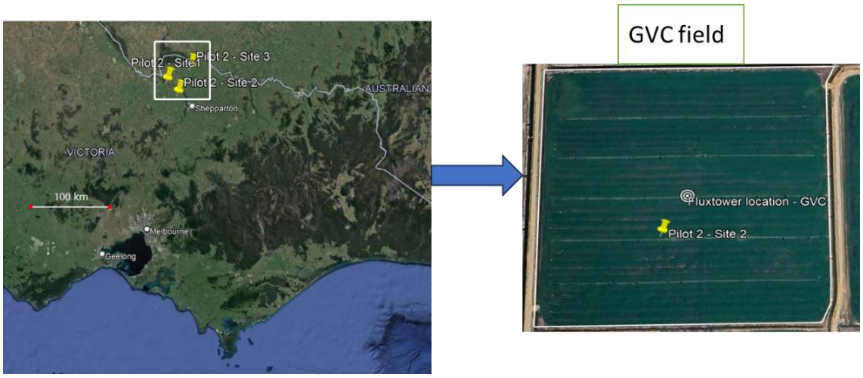

Fig. 15 - GVC alfalfa (right) field located in Goulburn-Murray (Australia)

The raw 20Hz eddy covariance data downloaded from the flux tower were processed to half-hourly data via EddyPro software. Post-processing procedures, including quality control, gap filling, and energy balance closure correction, were also conducted to improve the data quality.

Sentinel 2 satellite image cloud-free were collected to cover the irrigation season, as depicted in Table 9.

Table 9 – List of Sentinel-2 satellite images selected for GVC field.

Level	Doy	Date
L2A	325	21/11/2021
	345	11/12/2021
	350	16/12/2021
	355	21/12/2021
	365	31/12/2021
	20	20/01/2022
	25	25/01/2022
	35	04/02/2022
	45	14/02/2022
	50	19/02/2022
	65	06/03/2022
	70	11/03/2022
	80	21/03/2022
	85	26/03/2022
	90	31/03/2022
	95	05/04/2022
	125	05/05/2022
	140	20/05/2022

It was followed the same methodology:

In detail, the validation of the ET was based on the following steps:

- Retrieve Earth Observation (EO) input data as LAI, surface albedo, NDVI and STR data from Sentinel-2,
- Interpolation of EO data on a day scale, using the linear approach for LAI, surface albedo and NDVI and the stepwise approach for STR,

- Filtering and selection of interpolated EO data coinciding with valid ET values acquired from the flux tower, (procedures undertaken by COALA project https://www.coalaproject.eu/),
- Validation of the ET estimates obtained with the PM and SW models without OPTRAM parametrization, assuming no water stress conditions and constant values for leaf resistance (r_{leaf}=100 sm^{-1}) and soil resistance only for SW model (r_{soil}= 500 sm^{-1}),
- Validation of the ET estimates obtained with the PM and SW models without OPTRAM parametrization, assuming no water stress conditions and variable ranging values for leaf resitance (from r_{leaf}=100 sm^{-1} to r_{leaf}=200 sm^{-1}) and soil resistance only for SW model (from r_{soil}=500 sm^{-1} to r_{soil}=2000 sm^{-1}).

The OPTRAM model was parameterised using time series of NDVI and STR indices, covering a large area of more than 7000 hectares during the irrigation season as depicted in Table 9. This approach was adopted to take into account the local conditions and their spatial and temporal variability within the study area.

It's important to note that only 'agricultural pixels' were considered in the analysis, identified through the utilization of the ESA World-Cover 2021 map, a global land cover product at 10 m resolution based on Sentinel-1 and Sentinel-2 data. The values representing the intercept and slope for the wet and dry edges in the lines were determined for whole extent area included GVC fields, as shown in Table 10. These values had a crucial role in the calculation of the water index, referred to as W, for each date.

Table 10 - Optram parametrization within GVC for irrigation season.

	Dry Edge		Wet Edge	
	Id	Sd	Iw	Sw
Year2020	0	1	5.1	9.4

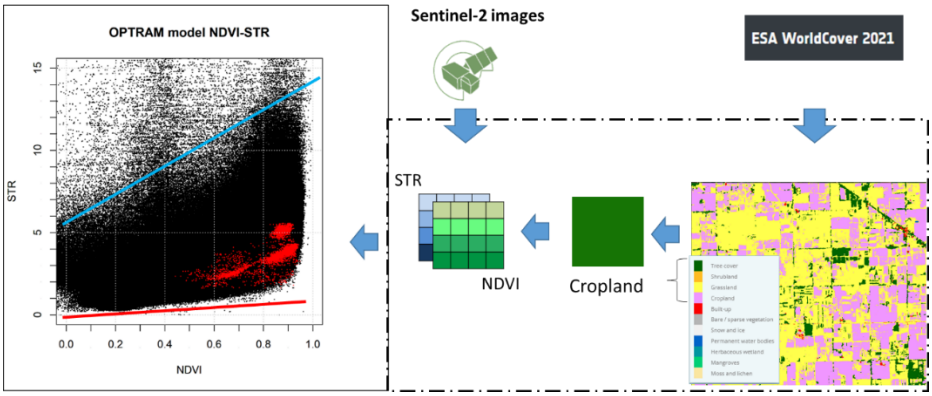

Fig. 16 - Spatial and temporal domains considered for OPTRAM model based on 17 Sentinel-2 acquisitions over GVC site collected from November 2021 to May 2022. The distribution of NDVI-STR for the pixels within GVC's alfalfa field is illustrated in red.

4.11 Statistical performance metrics

The subsequent metrics were computed to evaluate the performance of the estimated irrigation volumes across various scenarios. Let Oi and Esti represent the observed and estimated values, respectively, 'n' denote the total number of observations.

Root mean square error:

$$\mathrm{RMSE} = \sqrt{\frac{\sum_{i=1}^{n}(O_i - Est_i)^2}{n}}$$	4.34

Mean absolute error:

$$MAE = \frac{\sum_{i=1}^{n}\lvert Est_i - O_i\rvert}{n}$$	4.35

Mean bias error:

$$MBE = \frac{1}{n}\sum_{i=1}^{n}(Est_i - O_i)$$	4.36

Pearson correlation coefficient:

$$\text{Pearson} = \frac{\sum_{i=1}^{n}(O_i - O_i^*)(Est_i - Est_i^*)}{\sqrt{\sum_{i=1}^{n}(Est_i - Est_e^*)^2(O_i - O_i^*)^2}}$$	4.37

Kling-Gupta efficiency (KGE):

$$\text{KGE} = 1 - \sqrt{(r-1)^2 + (\frac{\alpha_{Obs}}{\alpha_{Est}} - 1)^2 + (\frac{\mu_{Obs}}{\mu_{Est}} - 1)^2}$$	4.38

The KGE combines the correlation coefficient (r), the variability error, and the bias error, KGE range were specified between -0.4 to 1 (Brombacher et al., 2022). It was conducted a t-test and compared the t-test results by assessing the p-value against a threshold of 0.01, specifically in the context of irrigation. Even a coefficient of determination R^2 were calculated to assess a goodness of fit between the estimated and observed irrigation volumes.

Chapter 5: Results and Discussions

In this chapter, we discuss the final results for District N. 10 (Sinistra Ofanto irrigation scheme), covering details from sections 5.1 to 5.7. In these sections, we elaborate the use of combination P-M and S-W methods, along with the Optical Trapezoid model. This combination helps us estimate evapotranspiration and determine the necessary irrigation volumes on a daily and time-specific basis.

Moving on to section 5.8, we extend our analysis to a farm-scale application of the same methods. Here, we compare the estimated evapotranspiration with measurements from an eddy covariance flux tower, focusing on an alfalfa crop in Australia. This comparison gives us insights into how well our methods perform in a practical agricultural setting.

5.1 Biophysical parameters retrievals for District N. 10

In this study, the accurate retrieval of Leaf Area Index (LAI) and albedo crucial for P-M and S-W method estimation, is facilitated by employing Artificial Neural Networks (ANN) by using SNAP to retrieve LAI. LAI, representing the amount of leaf area per unit ground area, significantly influences the interception of solar radiation by the vegetation canopy, impacting the energy balance. Simultaneously, Albedo is derived as a weighted sum of surface spectral reflectance (ρλ) with broadband coefficients (ωλ) using Equation (4.1), determining the fraction of solar irradiance for each sensor band. As illustrated in Fig. 17 and Fig. 18 for LAI and Albedo maps on the respective dates, these parameters provide insights into their spatial distribution across the district N. 10.

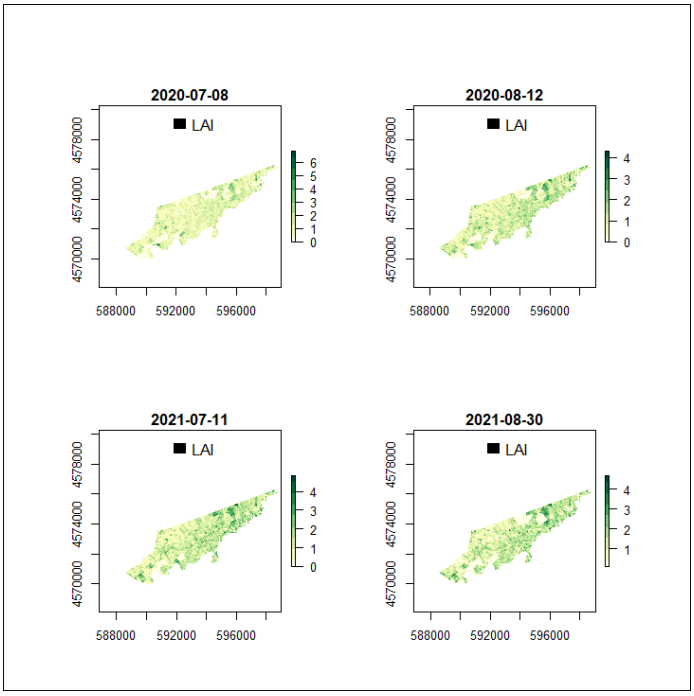

Fig. 17 – Spatial distribution of leaf area index (LAI) maps in the District N. 10 for 2020 and 2021.

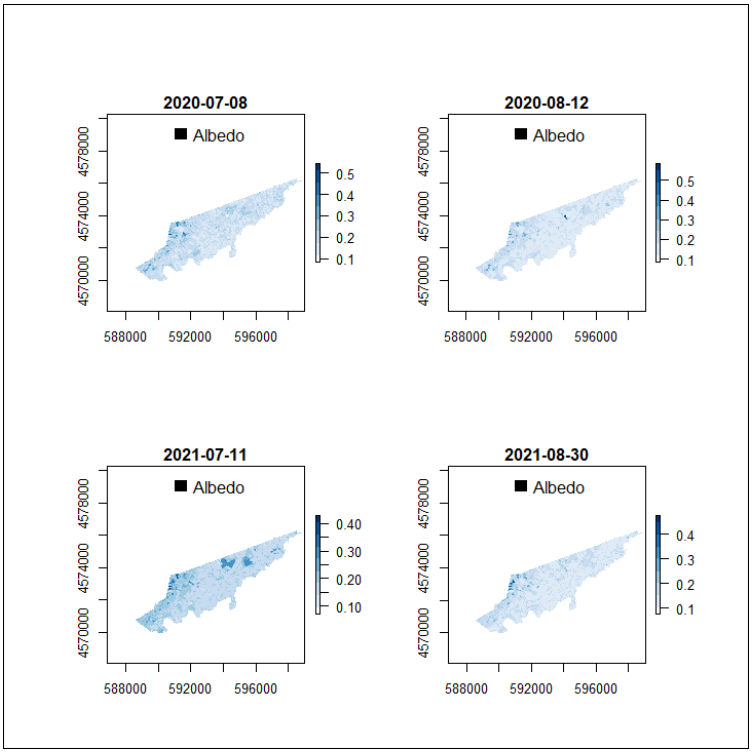

Fig. 18- Spatial distribution of albedo maps in the District N. 10 for 2020 and 2021.

Additionally, Fig. 19 depicts fractional vegetation cover (FVC) on the same date, is essential for irrigation requirement estimation. Notably, Albedo and FVC values range from 0 to 1. The integration of LAI and FVC maps allows for the calculation of effective precipitation using (Braden, 1985) equation (4.33) at a pixel scale, contributing to a comprehensive depiction of irrigation requirements presented in the final result. This study underscores the significance of LAI and Albedo in the Penman-Monteith method and emphasizes the role of FVC, with due consideration to the normalized range of Albedo and FVC values, offering valuable insights for localized water resource management.

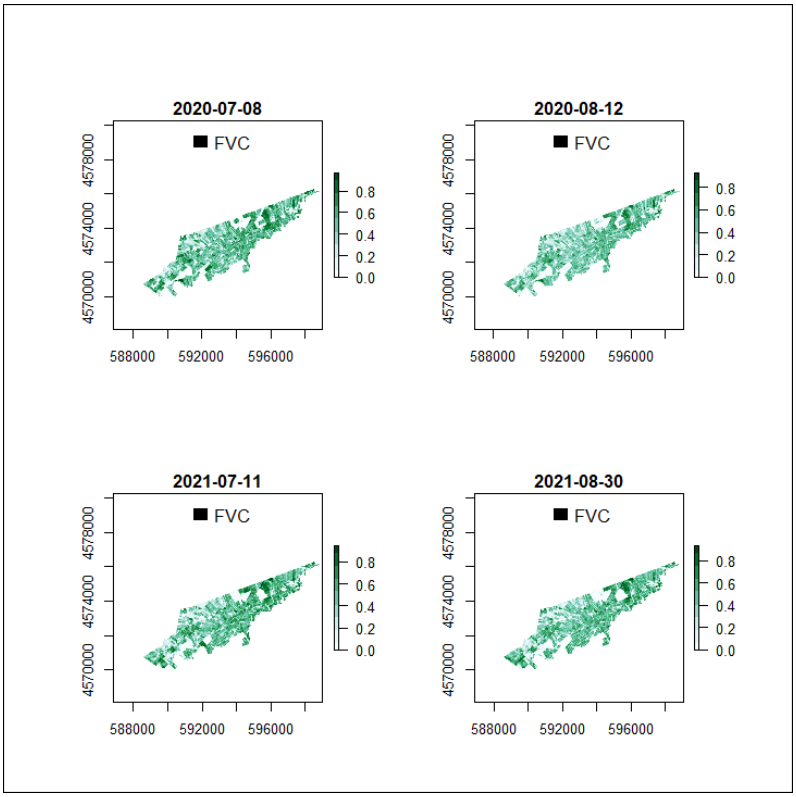

Fig. 19- Spatial distribution of fractional vegetation cover (FVC) maps in the District N. 10 for 2020 and 2021.

5.2 Mapping actual irrigated areas

In the "Sinistra Ofanto" irrigation scheme, with a focus on District 10, a comprehensive study was conducted over the years 2020 and 2021. The main objective was to understand how the land is utilized in this specific area. To achieve this, unsupervised classification methods, particularly the K-means clustering technique, were employed. This technique helped organize the landscape into 50 distinct categories, providing a clearer insight into the types of land cover present in District 10.

This classification process was carried out separately for each year, specifically during the months of active irrigation, which run from April to September for the two

years 2020 and 2021. This period was chosen to capture changes in land cover during the peak of agricultural activity.

The study primarily identified three main types of thematic classes areas: areas that were not irrigated, areas with irrigated tree crops, and portions with irrigated herbaceous. This classification was achieved by analysing changes in vegetation using a specialized index NDVI time series linked to precipitation (Ozdogan *et al.*, 2010), which helps gauge the health and density of plants across District 10.

Fig. 20 illustrates the spatial distribution of NDVI maps, showcasing the color-coded representation of NDVI value change across the district 10 on selected days in both 2020 and 2021.

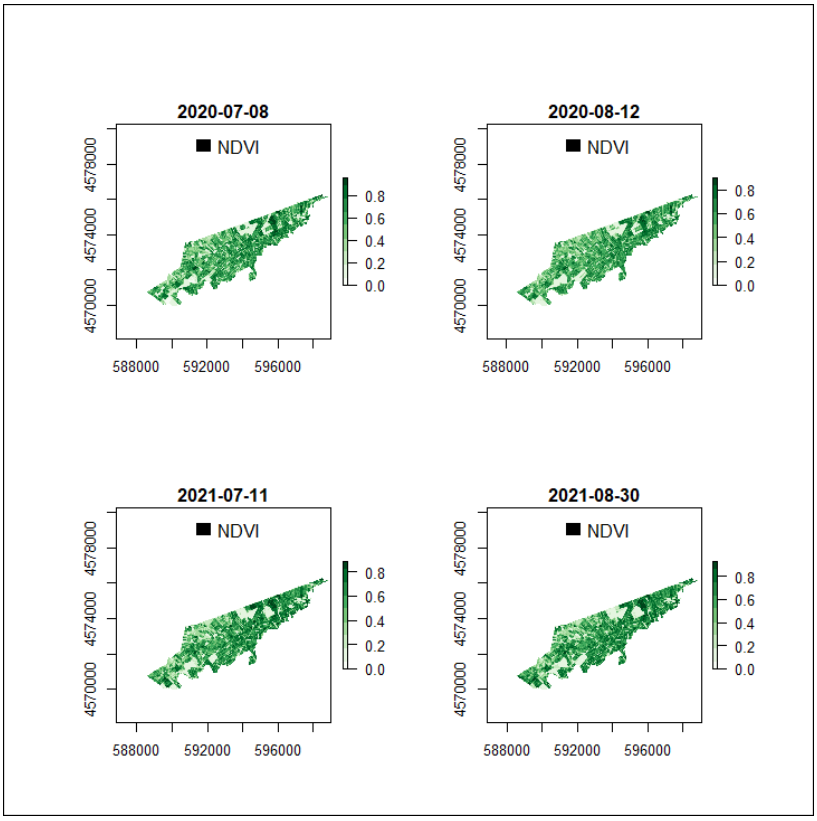

Fig. 20 – Spatial distribution of normalise difference vegetation index mapping in the District N. 10 for 2020 and 2021.

Fig. 21 depicts three discernible instances of multi-temporal NDVI time series, each characterized by the mean and standard deviation for every class within the classification scheme. These classes correspond to the three identified groups: (a) not irrigated, (b) irrigated trees, and (c) irrigated herbaceous, facilitating conclusive classification in 2020. The consistent application of the identical methodology endured throughout the entirety of 2021.

It's important to note that the choice of unsupervised classification was made due to the lack of available "ground truth" information for validation. In simpler terms, there wasn't exact reference data to compare with, so this approach allowed patterns in the data to be discovered without needing precise labels.

In practical terms, the maps generated from this classification (Fig. 22 and Fig. 23) played a crucial role in estimating the irrigation water requirements for District 10. By understanding the types of land cover in various areas.

In the context of the study, it's essential to highlight the specific land areas dedicated to irrigated trees and irrigated herbaceous crops for the years 2020 and 2021. The allocated area for irrigated trees in 2020 was **1458.6** hectares, while the area designated for irrigated herbaceous crops was **49.94** hectares.

Moving on to the year 2021, the Fig. 23 demonstrate a slight shift. The area dedicated to irrigated trees in 2021 was **1467.13** hectares, indicating a minor reduction. In contrast, the region designated for irrigated herbaceous crops reduced to **27.69** hectares.

This process offers a quantitative insight into the allocation of land for specific agricultural activities within the study area for both years. This information contributes to a more comprehensive understanding of the land cover and their variations over the analysed period.

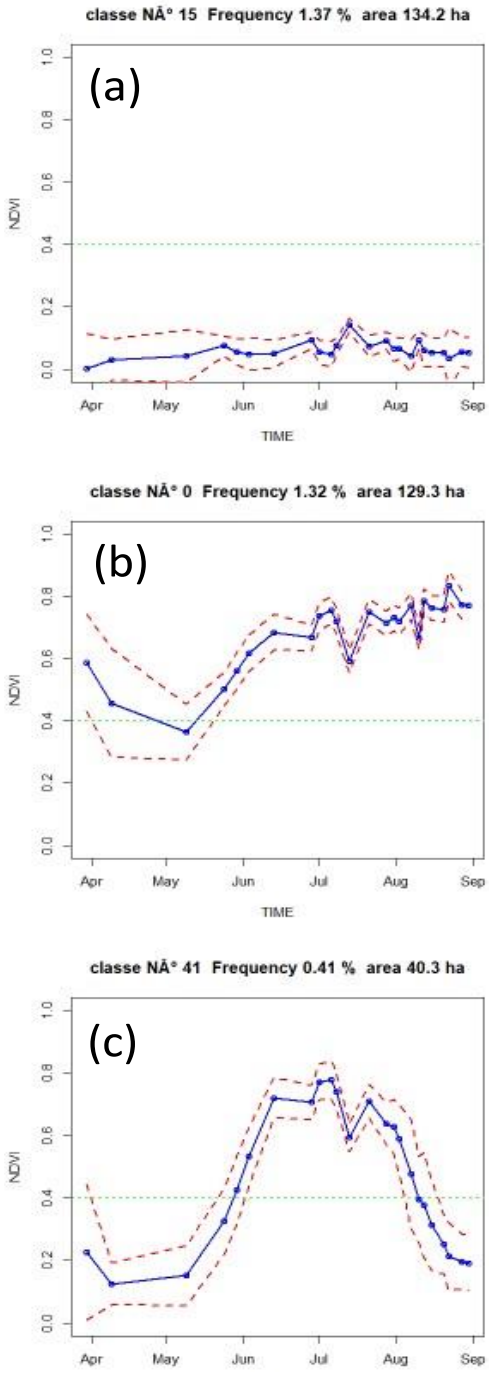

Fig. 21 – Example of NDVI temporal pattern labelled a) not irrigated areas, b) irrigated trees and c) irrigated herbaceous.

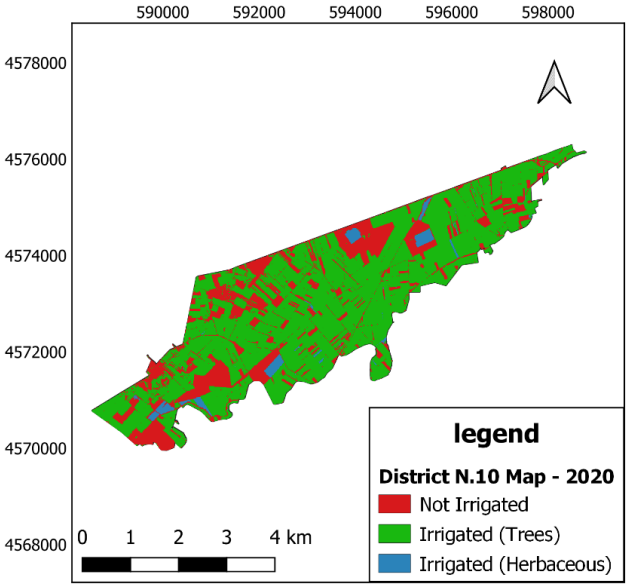

Fig. 22 - classified irrigation map at district N. 10 for 2020.

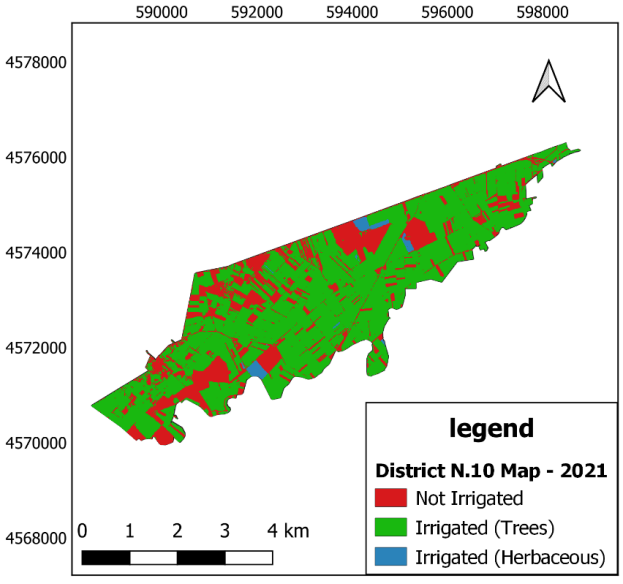

Fig. 23 – classified irrigation map at district N. 10 for 2021.

5.3 OPTRAM parametrization:

The OPTRAM model's parameters were determined through an analysis of pixel distribution scatterplots within the STR-NDVI space, a key aspect of our study.

It is advisable to display not only the spatial distribution of NDVI, as depicted in Fig. 20, but also to present Figure 2, elucidating the spatial distribution of shortwave infrared transformed reflectance (STR) for two specifically chosen days within District 10 for the years 2020 and 2021.

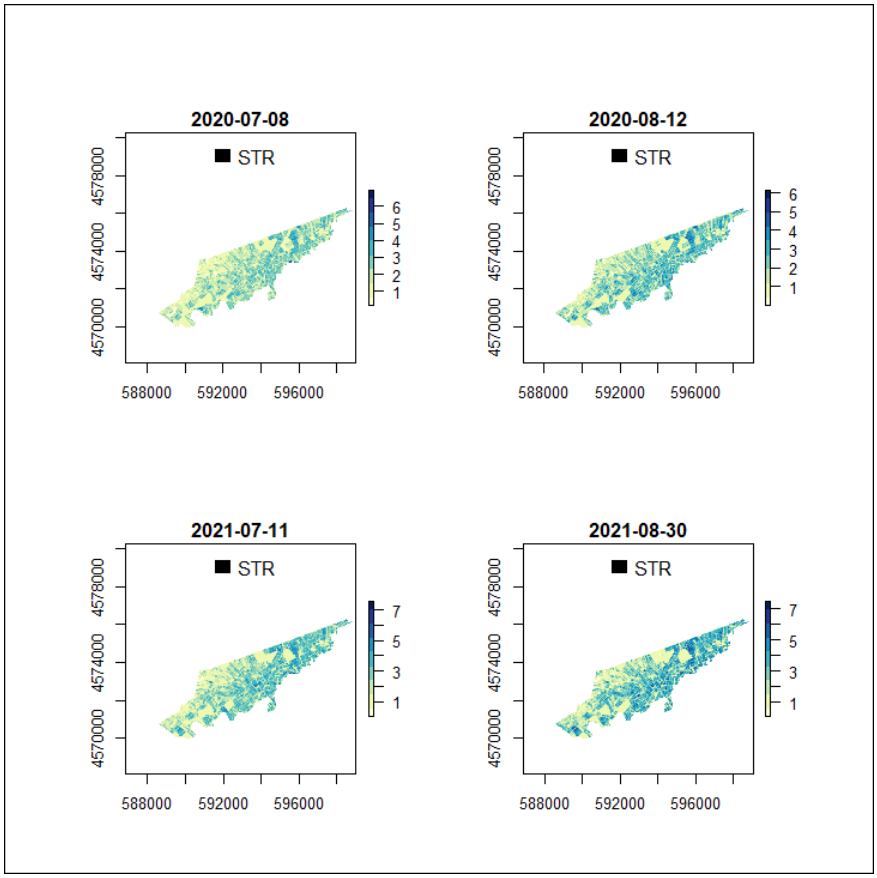

Fig. 24 – Spatial distribution of shortwave infrared transformed reflectance STR mapping in the District N. 10 for 2020 and 2021.

The OPTRAM model Equations (4.29 and 4.30) were skilfully parametrized for district N. 10 by examining the pixel distribution within the STR-NDVI space. This

process was carried out separately for each available image for the years 2020 and 2021. In addition to this, we sought to create a universal parameterization by integrating pixel distributions from all selected images into a single trapezoid.

To ensure the accuracy of our model, we identified the dry (i_d and s_d) and wet (i_w and s_w) edges within the STR-NDVI spaces through visual inspection as suggested by Sadeghi et al., (2017). These edges were chosen to encompass the majority of the pixels, a crucial step in our methodology. While the identification of these edges was done visually, it is important to note that this does not pose a significant limitation to our approach. The shape of the pixel distribution in the NDVI-STR space remains consistent for a given location at any time, irrespective of surface and meteorological conditions. It is worth mentioning that pixels excluded above the wet edge were deemed oversaturated or shadowed pixels. This underscores the importance of the accurate definition of the dry and wet edges, especially in relation to oversaturated pixels, which must be excluded from the NDVI-STR domain to maintain the integrity of our analysis, as depicted in Fig. 25 and Fig. 26.

For district N.10 fields, the values of the intercept and slope of the lines representing the wet and dry edges were determined as depicted in the Table 11, and these values played a critical role in calculating the water index, denoted as W, for each date.

Table 11 – Optram parametrization within District N. 10 for 2020 and 2021.

	Dry Edge		Wet Edge	
	Id	Sd	Iw	Sw
Year2020	0	0.8	1.8	9.2
Year2021	0	0.9	2	9.8

Furthermore, our adoption of these limits allowed us to determine substrate, leaf and canopy resistances, which are fundamental components of our study to estimate ETa by using S-W, and the usage of modulated leaf resistance is to estimate ET from P-M. The rigorous parameterization process, guided by pixel distribution within

the STR-NDVI space and the careful identification of dry and wet edges, provides a solid foundation for our OPTRAM model's analysis for the years 2020 and 2021.

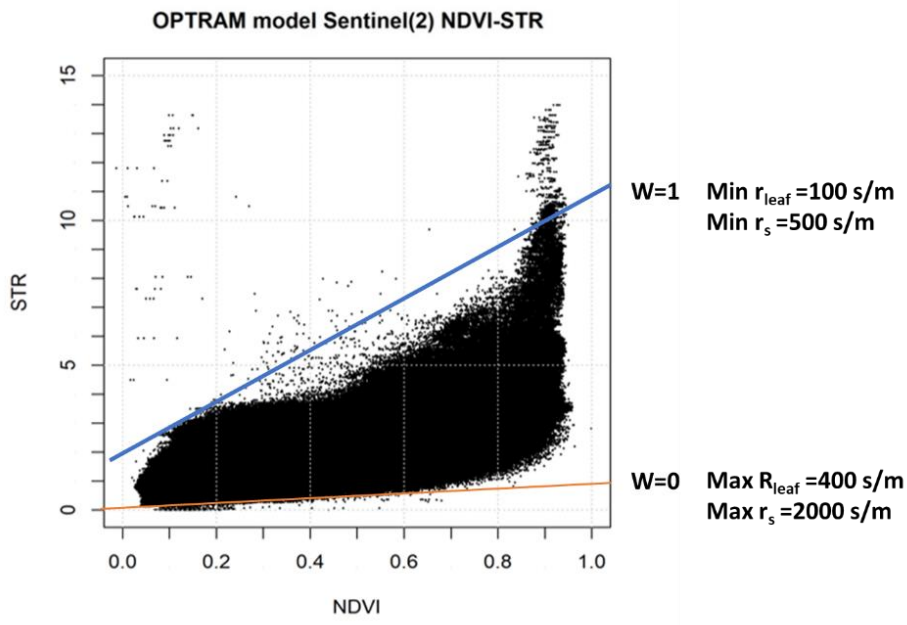

Fig. 25 - Spatial and temporal domains considered for OPTRAM model. The distribution of NDVI-STR for the pixels within District N. 10 for 2020.

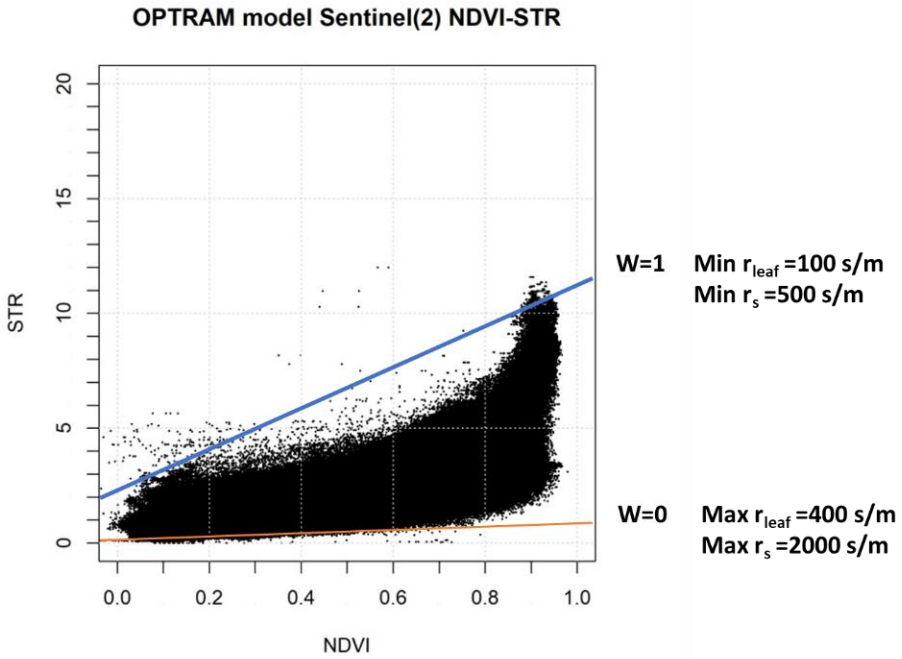

Fig. 26 - Spatial and temporal domains considered for OPTRAM model. The distribution of NDVI-STR for the pixels within District N. 10 for 2021.

5.4 Evaluation daily irrigation volumes

The study conducted an analysis of seven distinct scenarios, each tailored to evaluate the precision of irrigation volume estimations. In all four scenarios, it was conducted daily comparisons spanning a two-year period, including the year 2021, despite the limited availability of registered volumes due to the malfunctioning of the flow meter during that year. This methodology proved crucial in showcasing the practicality and relevance of these scenarios, as it incorporated the most up-to-date meteorological data and integrated a newly generated classified map for the same year 2021. Consequently, it allowed us to undertake a comprehensive assessment, comparing the estimated irrigation volumes against the recorded data and shedding light on the model's performance over both 2020 and 2021.

As depicted in Fig. 27 and Fig. 28, S1 revealed a consistent overestimation of irrigation volume in both 2020 and 2021, highlighting a tendency to predict higher water requirements than those actual used. S2, despite minor overestimations in major days of 2020, demonstrated an overall reasonable alignment with recorded data.

From Fig. 27 and Fig. 28, S3, which focused on transpiration and incorporated slight overestimations on some days, particularly in 2020, showed a substantial correlation with recorded irrigation volumes. In 2021, it achieved a closer approximation, occasionally overestimating. Finally, the last S4, concentrating exclusively on plant transpiration while ignoring soil evaporation, consistently resulted in notable underestimation for both 2020 and 2021.

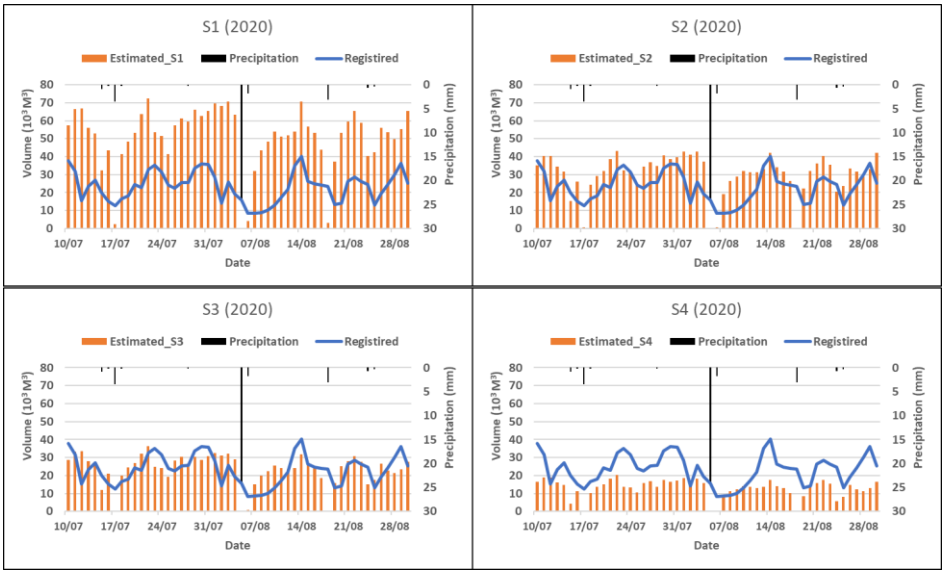

Fig. 27 - Daily pattern comparison for scenarios S1, S2, S3, and S4 between the estimated and registered irrigation volume for July and August 2020.

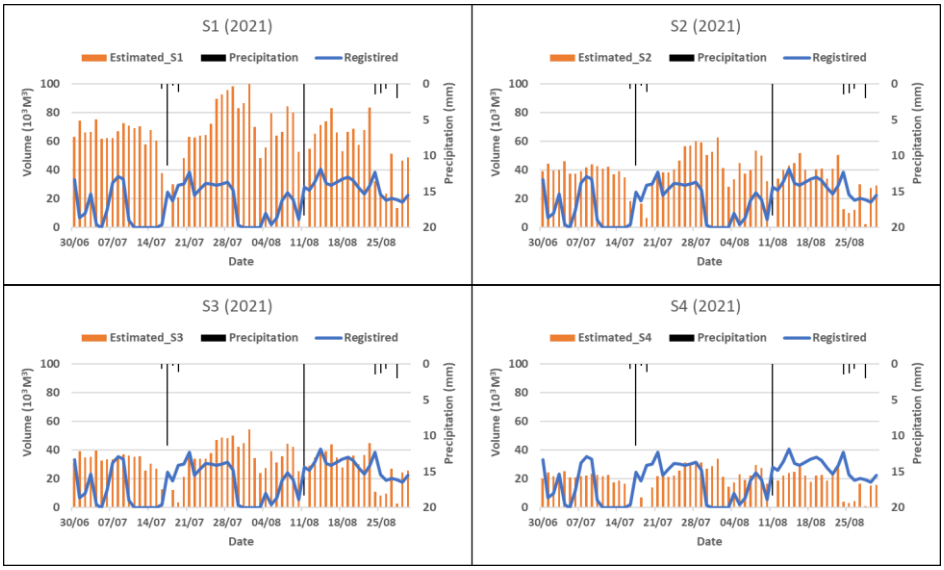

Fig. 28 - Daily pattern comparison for scenarios S1, S2, S3, and S4 between the estimated and registered irrigation volume for July and August 2021.

As shown in Fig. 29 and Fig. 30, S6, which emphasized transpiration and demonstrated fewer instances of overestimation, especially in 2020, exhibited a strong correlation with the recorded irrigation volumes. In 2021, it achieved a closer match, occasionally tending to overestimate based on the available recorded volumes. In contrast, both S5 and S7, which exclusively focused on evapotranspiration, consistently showed.

The Fig. 31 present three examples of irrigation maps were generated using Sentinel-2 satellite. These maps were created through pixel-based calculations, leveraging the high spatial precision and frequent temporal acquisitions afforded by Sentinel-2 data.

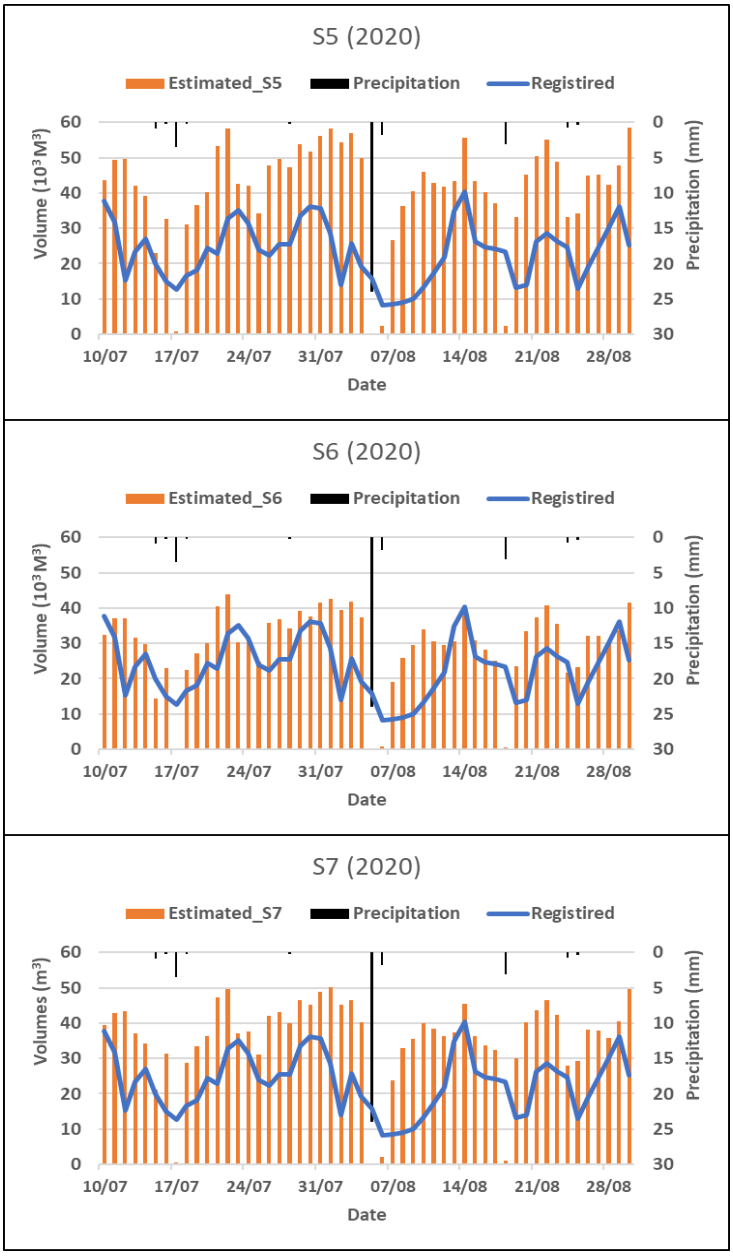

Fig. 29 - Daily pattern comparison for scenarios S5, S6 and S7 between the estimated and registered irrigation volume for July and August 2020.

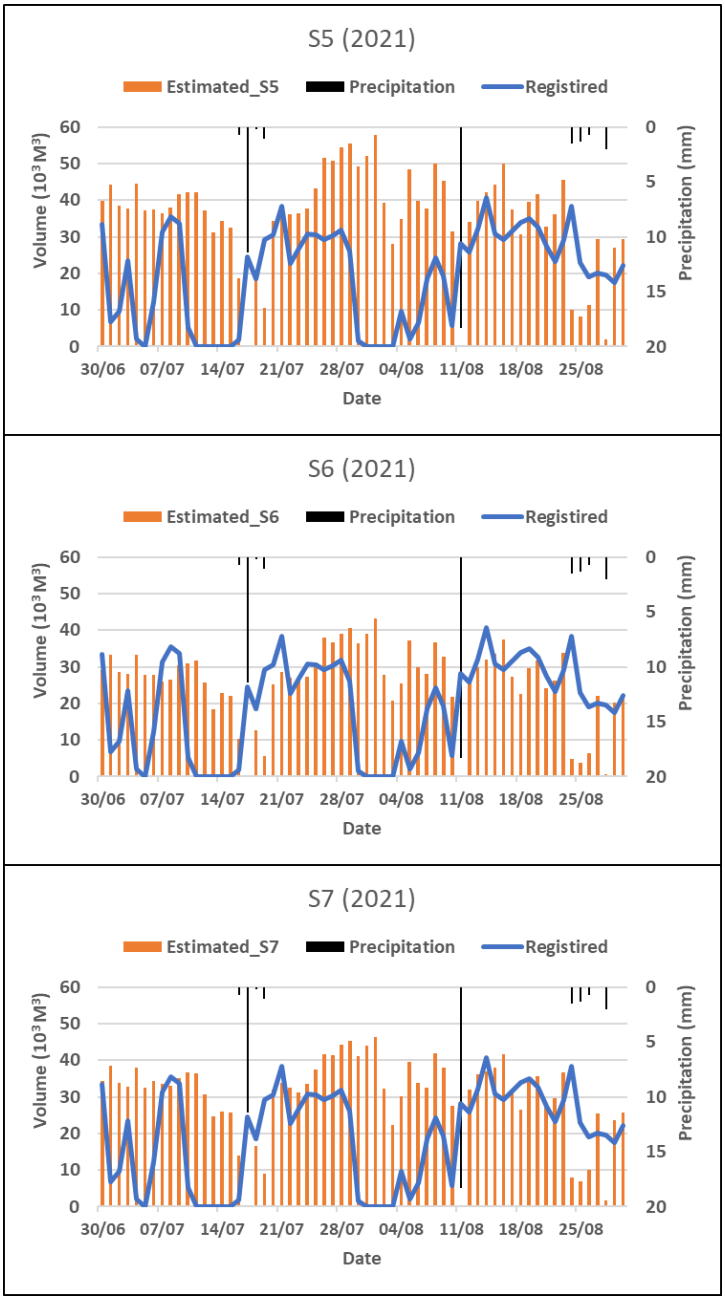

Fig. 30 - Daily pattern comparison for scenarios S5, S6 and S7 between the estimated and registered irrigation volume for July and August 2021.

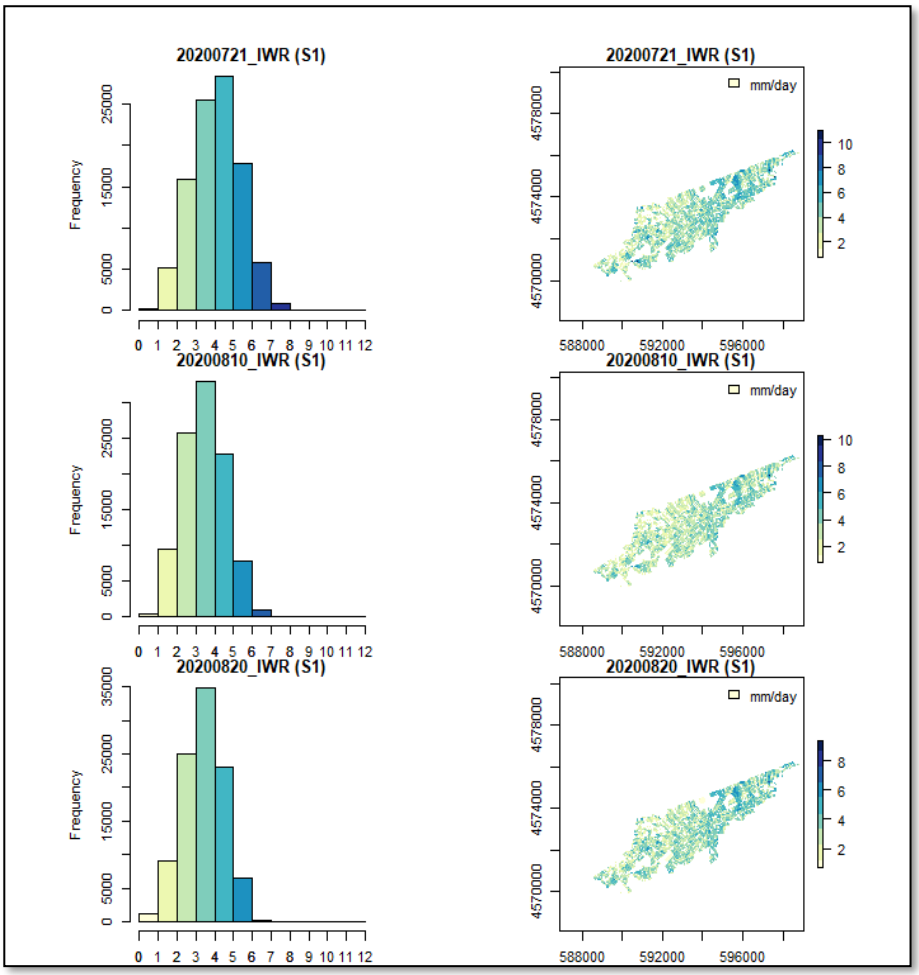

Fig. 31 - Maps depicting district 10's irrigation water estimated throughout the year 2020.

5.5 Evaluation cumulative irrigation volumes

Comparing cumulative daily irrigation volume estimated with cumulative irrigation registered for district N.10 in July and August 2020, rather than doing a daily comparison, offers a more detailed perspective. This approach enables us to capture patterns in irrigation management strategies and farmer behaviour over an extended period.

Analysing cumulative data over two months allows us to understand how irrigation practices evolve throughout the irrigation season. This can shed light on the long-term strategies employed by farmers in response to changing environmental conditions and resource availability.

By focusing on cumulative volumes, we can identify trends and fluctuations in irrigation usage that may not be apparent on a daily basis. This approach helps us gain insights into the overall water management practices in the district and how they vary across different scenarios.

Given the registered volume limitations in 2021, concentrating on the seven scenarios from 2020 becomes crucial for a comprehensive analysis. This ensures that we have a sufficient dataset to draw meaningful conclusions about irrigation management strategies in that specific year.

In this study, seven scenarios were carefully examined. These scenarios were evaluated by analysing the actual recorded irrigation volumes in district N.10 for the year of 2020. The key focus was on understanding how well these scenarios matched the irrigation recorded.

Now, looking specifically at scenarios S1 and S4, which are illustrated in Fig. 32, we observed distinctive trends in the daily cumulative irrigation. In the case of scenario S1, there was a consistent overestimation of irrigation. This means that the model or system used for scenario S1 consistently predicted higher irrigation volumes than what were actually recorded. This overestimation was particularly noticeable during the period from July 10th to August 30th, 2020. In contrast, for scenario S4, the model or system consistently underestimated irrigation, showing significantly lower values compared to the real-world recorded data during the same period.

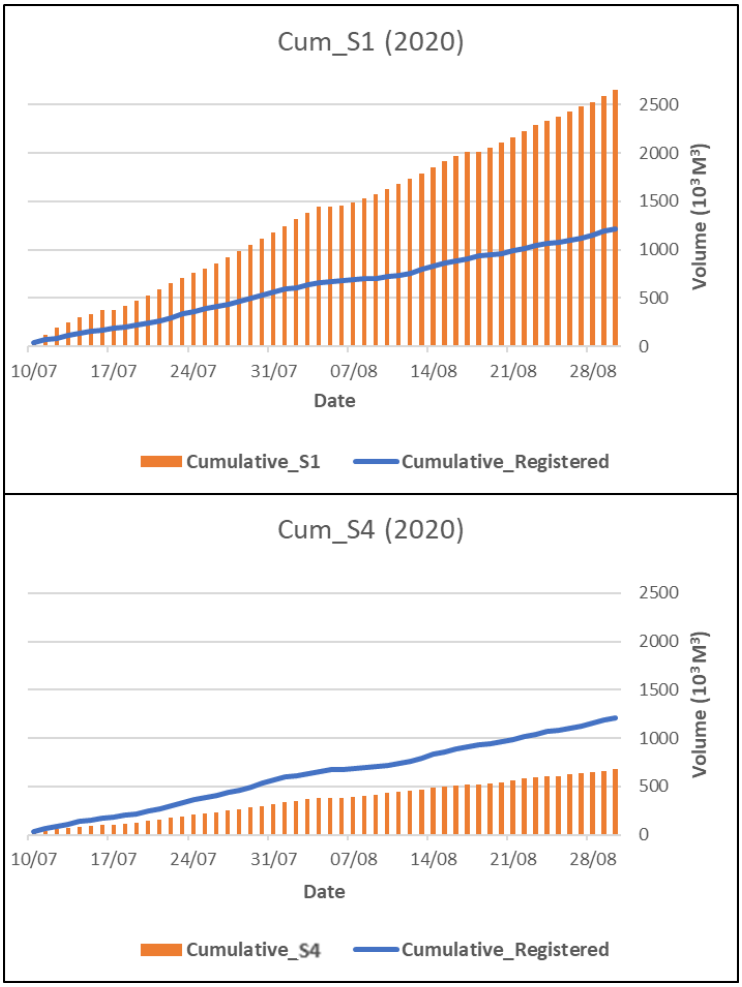

Fig. 32 - Cumulative pattern comparison for scenarios S1 and S4 between the estimated and registered irrigation volume for July and August 2020.

Turning our attention to scenarios S2 and S3, which are depicted in Fig. 33, we encountered a different situation. Scenario S2 displayed a slight overestimation of irrigation, albeit with a relatively minor cumulative discrepancy by the end of August 30th, 2020. In simpler terms, S2 predicted slightly more irrigation than what was observed, but the difference wasn't very significant. On the other hand, scenario S3 showed a much better agreement with the actual recorded irrigation data. This means that S3's predictions closely matched the real irrigation recorded throughout the entire period of interest.

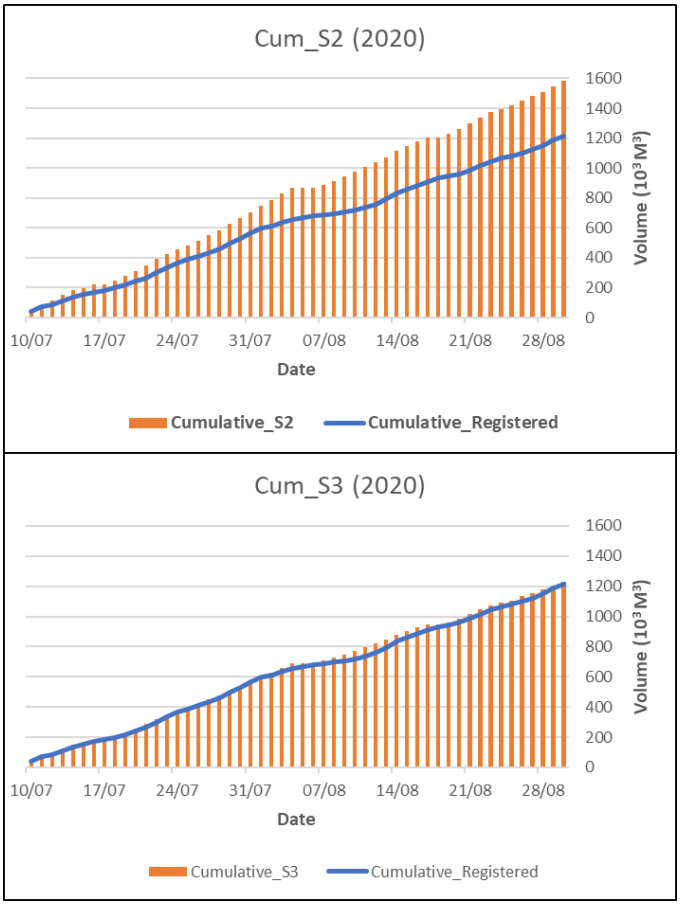

Fig. 33 - Cumulative pattern comparison for scenarios S2 and S3 between the estimated and registered irrigation volume for July and August 2020.

Now, let's transition to Scenarios S5, S6, and S7. It's important to note that these scenarios utilized the OPTRAM model, which incorporates leaf and soil resistances into its calculations. The primary objectives of the scenarios aimed to estimate cumulative ETa and irrigation requirements through two distinct approaches, namely the Penman-Monteith and Shuttleworth and Wallace methods.

When examining Scenarios S5 and S7, as illustrated in Fig. 34, it becomes evident that the cumulative estimated irrigation volumes were consistently higher than the cumulative actual recorded values. In simpler terms, both S5 and S7 tended to overestimate cumulative irrigation when compared to the recorded volumes data. It's

worth mentioning that in the case of scenario S6, the cumulative estimation of actual transpiration (Tp) from the canopy cover did not exhibit a significant overestimation, unlike the two modelled scenarios, S5 and S7.

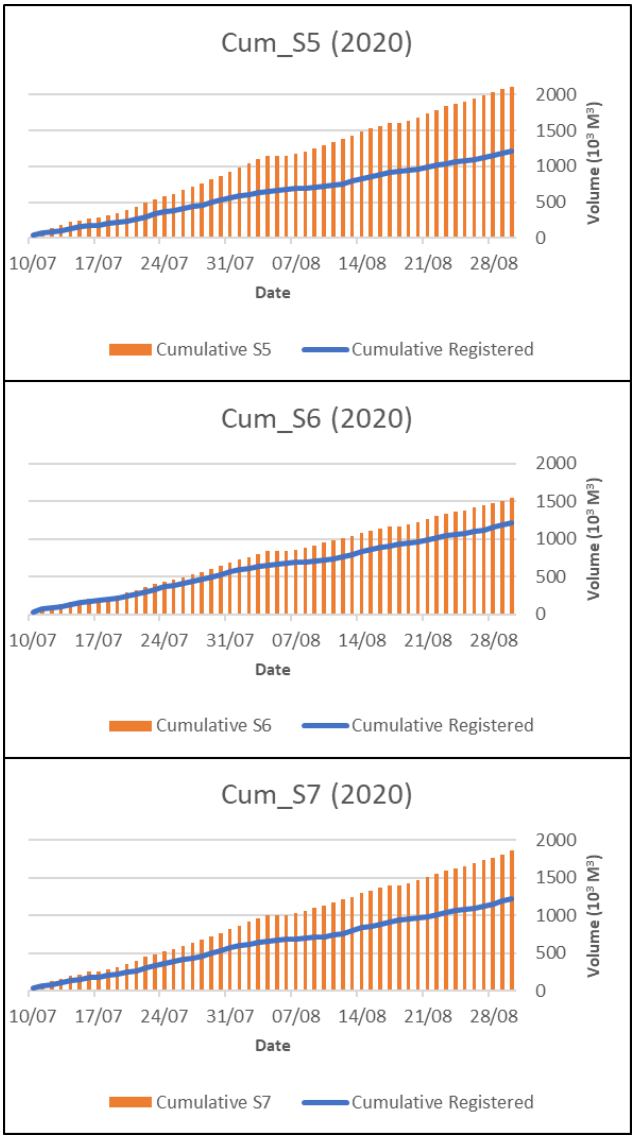

Fig. 34 - Cumulative pattern comparison for scenarios S5, S6 and S7 between the estimated and registered irrigation volume for July and August 2020.

5.6 Analytical evaluation different scenarios

In this analysis, we investigate into the performance of various irrigation volume scenarios, aiming to comprehend their accuracy on both a daily and aggregate five-day time scale. As illustrated before in the daily comparison, we extend our examination to encompass an aggregate five-day along the period comparison for the year 2020.

This temporal aggregation aims at reducing the error induces by the farmers' behaviour in applying irrigation, which may not be strictly linked to deterministic variables at the daily scale. There are several factors to consider such as the farm organisation, personnel and machinery availability and proper operation of irrigation distribution network. These factors may influence the decision of farmers on when apply irrigation, thus introducing a severe bias in the comparison with purely deterministic estimates as those obtained with the described methods.

To comprehensively assess the performance, there were employed a range of evaluation metrics, including root rean square error (RMSE), mean absolute error and (R^2). Furthermore, to gain a deeper insight into the comparative performance, it was utilized additional statistical measures such as Pearson correlation coefficients. Additionally, it was investigated the significance of differences between the irrigation volume scenarios and observed volumes through t-tests and KGE (Kling-Gupta Efficiency).

When scrutinizing the daily and five-days aggregated datasets for S1, S2, S3 and S4 as depicted in Table 12and Fig. 35, two scenarios, namely (S2) and (S3), emerge as noteworthy candidates for in-depth evaluation. In the context of daily data, S3 demonstrates superior performance compared to S2, boasting even lower values for key metrics such as RMSE at 8461.3 m^3/day, MAE at 6912.2 mm/day. Notably, the T-Test for S3 reveals a P-Value of 0.87, signifying that there is no substantial evidence to assert a significant distinction between the estimated and registered daily volumes. Concurrently, the (R^2) value of 0.236 indicates a less level of goodness of fit for S3, and KGE of 0.5 which consider reasonable performance scenario.

Similarly, when considering the aggregated five-day dataset in Table 12 and Fig. 36, S3 maintains its robust performance, characterized by a low RMSE of 16948

m^3/day, an MAE of 13223.93 m^3/day. Analogous to the findings in the daily data, the T-Test applied to S3 in the context of aggregated five-day data yields a P-Value of 0.86, indicating the absence of significant differences between the estimated and registered aggregated five-day volumes. Furthermore, the elevated R-squared value of 0.676 underscores a strong goodness of fit for S3, and KGE of 0.8 indicate high performance.

Conversely, when examining Scenario 2 (S2) in the context of aggregated five-day data, the T-Test returns a T-Test Statistic of P-Value of 0.031. The P-value exceeding the predefined significance level (alpha) of 0.01 implies the absence of a statistically significant difference between the estimated and registered aggregated five-day irrigation volumes. However, it is noteworthy that the (R^2) value remains robust at 0.68, affirming a higher degree of goodness of fit for S2, and KGE of 0.51 considered as a responsible performance.

Table 12 - Statistics metrics (S1, S2, S3 and S4) between registered and estimated irrigation volumes for a daily and aggregated five-days along July-August 2020.

		Daily				
Scenario	RMSE	MAE	R^2	T-test_pValue	Pearson	KGE
S1	28780.68	27150.50	0.26	2.87E-15	0.51	-0.53
S2	11995.68	10189.81	0.26	2.93E-04	0.51	0.35
S3	8461.32	6912.17	0.24	8.77E-01	0.49	0.49
S4	13126.75	11283.58	0.24	2.35E-12	0.49	0.19
		Five-day (Aggregated)				
Scenario	RMSE	MAE	R^2	T-test_pValue	Pearson	KGE
S1	130421.20	125621.86	0.70	1.98E-05	0.84	-0.65
S2	41448.82	36603.78	0.68	3.07E-02	0.82	0.49
S3	16948.70	13223.93	0.68	8.59E-01	0.82	0.80
S4	56220.58	53695.59	0.65	1.33E-04	0.81	0.30

Additionally, Pearson correlation coefficients computed for both scenarios indicate moderately positive linear relationships and strong monotonic relationships between the estimated and registered irrigation volumes. In summary, the statistical

analysis suggests that S3 emerges as the more favourable choice when considering these metrics, significance tests and KGE.

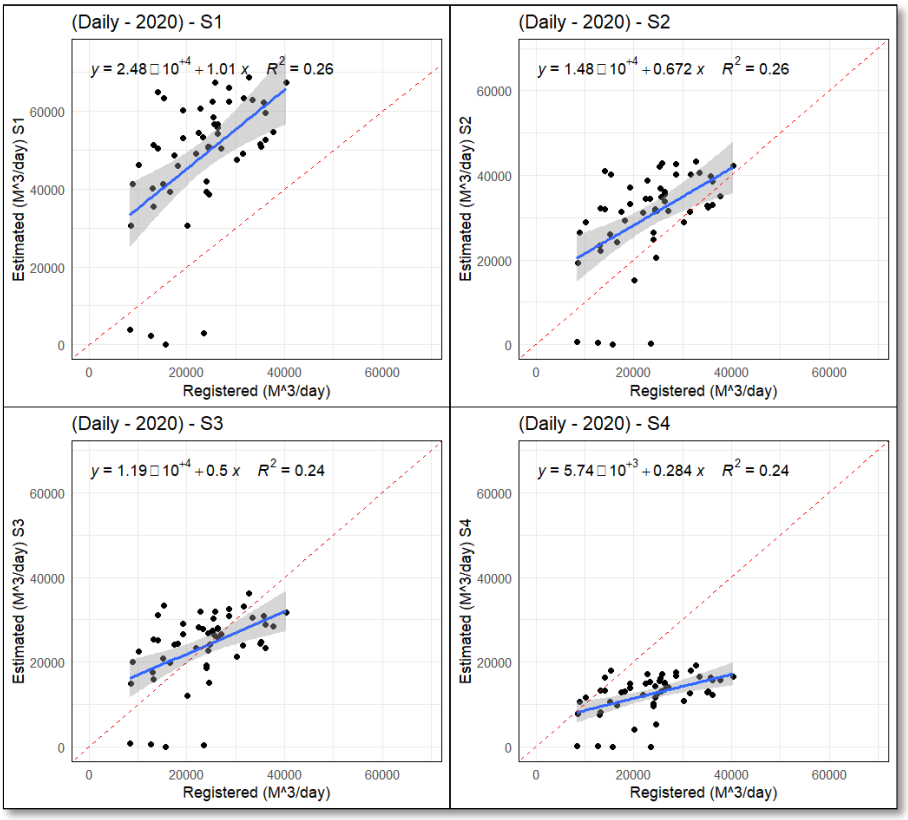

Fig. 35 - scatter plot daily comparison for scenarios S1, S2, S3 and S4 between the estimated and registered irrigation volume for July and August 2020.

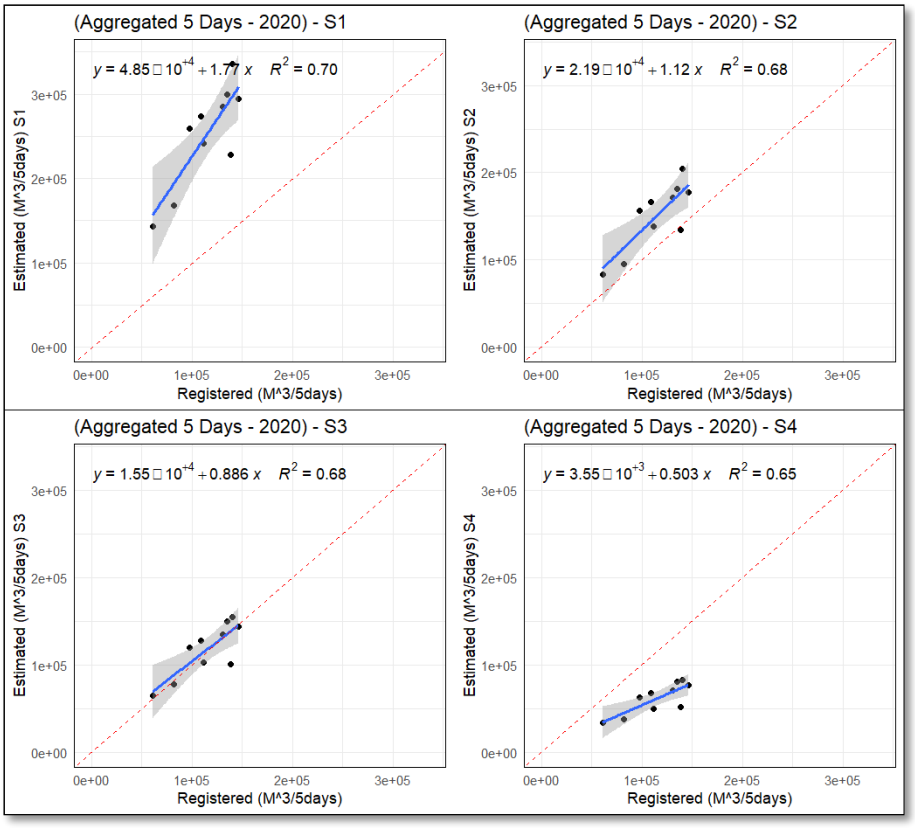

Fig. 36 - scatter plot aggregated 5-days comparison for scenarios S1, S2, S3 and S4 between the estimated and registered irrigation volume for July and August 2020.

In the context of scenarios S5, S6, and S7, as illustrated in Table 13, Fig. 36 and Fig.37, it's worth noting that Scenario S6 emerges as the superior choice in the daily comparison. S6 boasts RMSE of 11686 m^3/day, an MAE of 9774 m^3/day, and an (R^2) value of 0.25. The t-test for this scenario is statistically significant ($p = 0.00086$). However, in the aggregated five-day comparison, while scenario S6 maintains strong performance with an RMSE of 39903 m^3/5-days, an MAE of 35122 m^3/5-days, and an improved R-squared value of 0.6, it's important to note that the t-test does not reach statistical significance at the assumed alpha level of 0.01 ($p = 0.049$). The noteworthy observation from the analysis is the consistency of Pearson correlation coefficients,

both yielding positive values, indicating a favourable correlation between the scenarios and the observed data.

Table 13 – Statistics metrics (S5, S6 and S7) between registered and estimated irrigation volumes for a daily and aggregated five-days along July-August 2020.

		Daily				
Scenario	RMSE	MAE	R^2	T-test_pValue	Pearson	KGE
S5	21606.34	19924.65	0.26	1.76E-11	0.51	-0.16
S6	11686.68	9774.88	0.25	8.65E-04	0.5	0.35
S7	16332.66	14516.20	0.24	2.86E-08	0.49	0.14
		Five-day (Aggregated)				
Scenario	RMSE	MAE	R^2	T-test_pValue	Pearson	KGE
S5	93854.90	88188.00	0.61	2.94E-04	0.78	-0.13
S6	39903.15	35122.80	0.60	4.94E-02	0.78	0.48
S7	66887.24	61316.04	0.59	1.88E-03	0.77	0.21

It is notable that the coefficient of determination (R^2) displayed lower values in daily comparisons due to the common practice among farmers to schedule irrigation on days when rainfall occurs. The models used for estimating evapotranspiration and transpiration for various scenarios, as elucidated in chapter (4.7), required the incorporation of effective rainfall data to calculate irrigation water requirements. However, a significant improvement in correlation was observed for the selected scenarios, particularly S2, S3, and S6, which yielded superior results in daily volume estimations.

Furthermore, it is important to highlight that when aggregating data over five-day intervals during July and August 2020, notably, aggregating data over a five-day period has improved correlation and performance in the estimation scenarios, surpassing the difficulties encountered in capturing daily fluctuations in farmer behaviour. This effect may be further enhanced with an extended time frame.

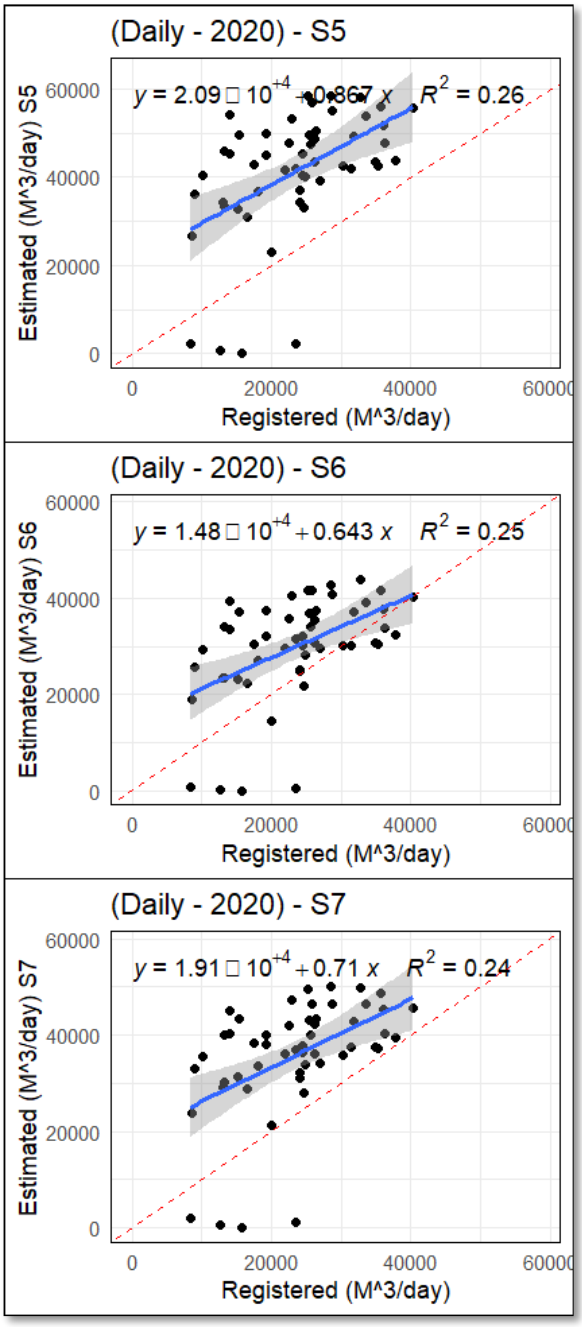

Fig. 37 – scatter plot daily comparison for scenarios S5, S6 and S7 between the estimated and registered irrigation volume for July and August 2020.

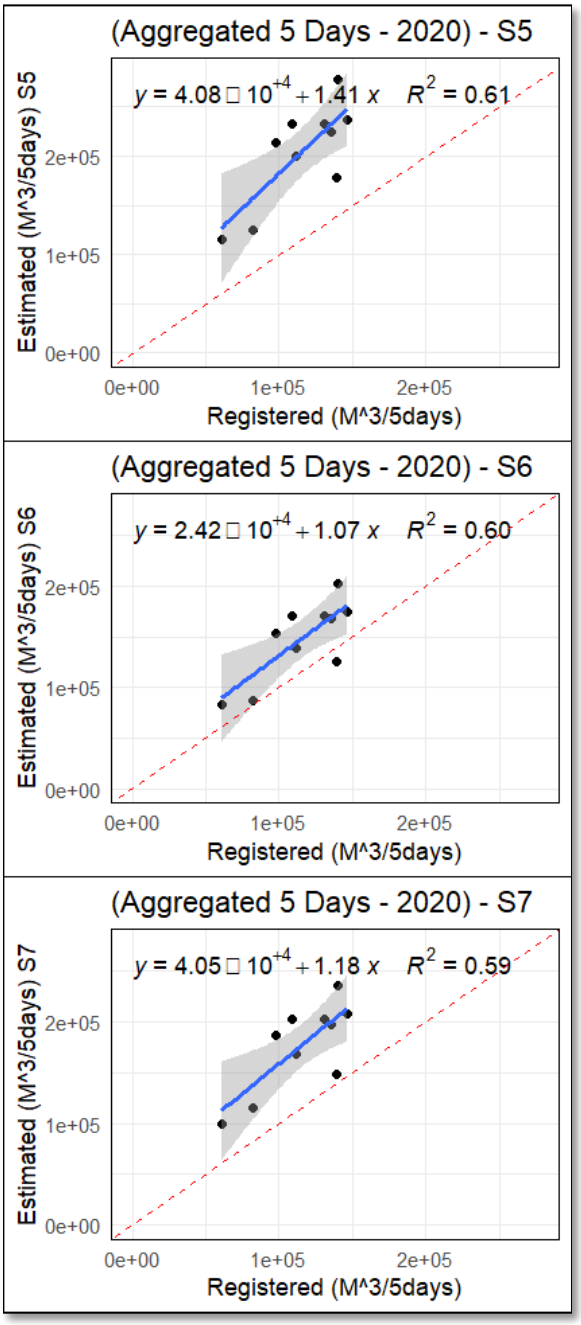

Fig. 38 - scatter plot aggregated 5-days comparison for scenarios S5, S6 and S7 between the estimated and registered irrigation volume for July and August 2020.

5.7 Interpretation scenarios result

The acquisition of irrigation data, encompassing parameters such as the spatial extent, temporal distribution, and quantification of irrigation water utilization, holds paramount significance within a multitude of scientific domains (Hu *et al.*, 2016; Chen *et al.*, 2018; Li, Jiang and Duan, 2020).

In the context of a statistical evaluation involving scenarios denoted as S1, S2, S3, and S4, on daily and aggregated five days, the Penman-Monteith (P-M) model exhibited commendable conformity with Scenario S3. This was particularly evident in the context of estimating canopy parameters, lineated in Table 5 and Table 6. This alignment facilitated certain assumptions regarding transpiration (Tp) in canopies exhibiting low vegetative density, where the intervention of soil evaporation substantially diminished when practical estimates of irrigation application were employed.

In the case of Scenario S2, a reasonable agreement was observed, marked by a reasonable efficiency when contrasted against the recorded irrigation volumes. This was achieved by presupposing a limited leaf resistance of 400 s/m, a value predominantly characteristic of vineyard crops within the study area. This underscored the criticality of managing product diversity for cultivators. It is noteworthy that agricultural practitioners typically contemplate the application and management of water stress in tree crops (perennial crops) as a means of augmenting product quality and augmenting financial returns. Consequently, the process of estimating Irrigation volumes for tree crops assumes a heightened level of complexity, as the primary aim of irrigation is to pre-empt water deficits that contravene the stipulated management objectives.

It is noteworthy that when applying the Ritchie equation (4.10) within scenario (S3) to compute transpiration and estimate irrigation volumes, it is imperative to recognize that this method does not yield precise irrigation volume estimations, given its reliance on empirical relationships. Nevertheless, for the study area in district N. 10, the Ritchie equation (4.10) may be appropriately applied to approximate irrigation requirements in line with local agricultural conditions and practices, especially since our prior knowledge about how farmers subject the crop to stress conditions was

limited. The assumption of minimal leaf resistance was made due to our lack of specific information regarding the implementation of deficit irrigation by local farmers.

This inherent uncertainty prompts an exploration of an innovative approach. OPTRAM offers a distinct advantage as it can adapt resistance parameters by leveraging the Shuttleworth and Wallace methods to estimate ETa and irrigation volumes. This approach represents a promising avenue for addressing the challenges posed by variable agricultural practices and delivering more precise estimates of irrigation needs within the study area.

Within Scenarios S5, S6, and S7, the OPTRAM model was deployed to modulate leaf and soil resistance. Subsequently, two modelling methodologies, namely P-M and the S-W approaches, were implemented. This strategy facilitated the computation of ETa and the estimation of irrigation volumes predicated on varying levels of leaf and soil resistance. The application of the OPTRAM model was notably featured within a Californian vineyard, where it was employed to ascertain evapotranspiration. The model integrated the equations of P-M and S-W with surface parameters and resistances derived from Sentinel-2 satellite data. The outcomes of this endeavour underscored a commendable level of precision, relative to measurements obtained via eddy covariance (D'Urso *et al.*, 2021).

Notably, amongst the aforementioned scenarios, Scenario S6 emerged as the most congruent with observed data, particularly when implementing the Shuttleworth and Wallace method. This method effectively regulated both plant transpiration and soil evaporation, thereby rendering it the optimal choice for scenarios typified by sparse vegetative canopies within the district. The estimation of irrigation requisites within this context was predicated upon transpiration, an approach necessitated by the utilization of drip irrigation, an efficient methodology that delivers water directly to the root zone of plants through a network of tubes, pipes, and emitters, facilitating careful water conservation.

The aforementioned overestimations witnessed within scenarios S2 and S6 may, in part, be ascribed to unauthorized water abstraction from privately owned wells

situated within the district, an occurrence extensively substantiated in preceding academic investigations (Levidow *et al.*, 2014; Coppola *et al.*, 2019).

Additionally, it was observed that farmers in the district persisted in irrigation activities during days characterized by precipitation, even in the presence of readily available on-demand pressurized irrigation systems, several rationale-based explanations may account for this behaviour.

On occasion, farmers were constrained from accessing irrigation resources during peak periods, typically in the months of July and August, prompting the adoption of a rotation irrigation regimen that necessitated their patience, despite the presence of precipitation. This conduct could be predicated upon the farmers' anticipation of inadequate precipitation. An additional contributing factor could be the spatial distribution of rainfall; notably, meteorological stations often registered rainfall, but this did not comprehensively cover the entirety of the district, a phenomenon commonly encountered in coastal areas of Mediterranean regions.

5.8 Evaluating flux tower validation models

The tabulated data in the Table 14 presents a comprehensive array of statistical metrics, derived from the utilization of P-M (Penman-Monteith) and S-W (Shuttleworth-Wallace) methodologies, both with and without OPTRAM integration, for the purpose of comparing the estimated evapotranspiration (ET) against registered eddy covariance measurements. This analysis encompasses a diurnal period spanning from March 19, 2022, to May 17, 2022, conducted within the GVC field. Accompanying scatter plots, as depicted in Fig. 39, delineate the uncertainty and variability in model-derived estimates through the graphical representation of standard error, subtly shaded in Gray. The breadth of this shaded region serves as a visual indicator: a narrower area signifies a more dependable model fit, while a broader span reflects heightened uncertainty in the predictive outputs, thereby conferring substantial visual insight into the quality and consistency of estimated ET concerning the observations.

Within this context, the performance metrics for the different methodologies become evident. The ET(P-M) model displays a lower Root Mean Square Error (RMSE)

of 0.69, a Mean Absolute Error (MAE) of 0.56, a negligible Mean Bias Error (MBE) of 0.01, and an R^2 coefficient of 0.83, indicating commendable performance. In contrast, ET predictions derived through the S-W method exhibit a marginally higher RMSE of 0.77 and MAE of 0.67, with a positive MBE of 0.46, while still maintaining a strong R^2 value of 0.84. Application of OPTRAM in conjunction with P-M leads to an elevated RMSE of 0.84, a MAE of 0.63, a negative MBE of -0.16, and an R^2 value of 0.7408. Similarly, ET estimation using ET (S-W) in tandem with OPTRAM results in an RMSE of 0.84, a MAE of 0.71, a positive MBE of 0.2, and an R^2 value of 0.73.

In summary, these scenarios illustrate the performance of different models or approaches in estimating daily evapotranspiration compared to eddy covariance measurements. P-M and S-W stand out as the most accurate, while ET (P-M and S-W with OPTRAM) are slightly less accurate but still provide meaningful estimations. The accuracy of using ET (P-M) can be explained by the fact that the crop canopy is covering uniformly the surface, thus adhering to the underlying "big leaf" assumption of P-M; in addition, the crop never met water stress conditions, due to the abundant irrigation, thus justifying the correctness of assumed value for the leaf resistance (minimum constant value 100 s/m); diversely, the Optram parameterisation and the resistance scheme may introduces some artifacts which affect the statistical indicators. On the basis of these results, the Shuttleworth and Wallace S-W would require an adjustment in the soil resistance scheme under conditions of full soil cover, in order to reach the same performance of P-M.

Table 14 – statistical analysis for eddy covariance validation

	RMSE_Daily	MAE_Daily	MBE	R^2
ET (P-M)	0.69	0.56	0.01	0.83
ET (S-W)	0.77	0.67	0.46	0.84
ET (P-M)_OPTRAM	0.84	0.63	-0.16	0.74
ET (S-W)_OPTRAM	0.84	0.71	0.2	0.73

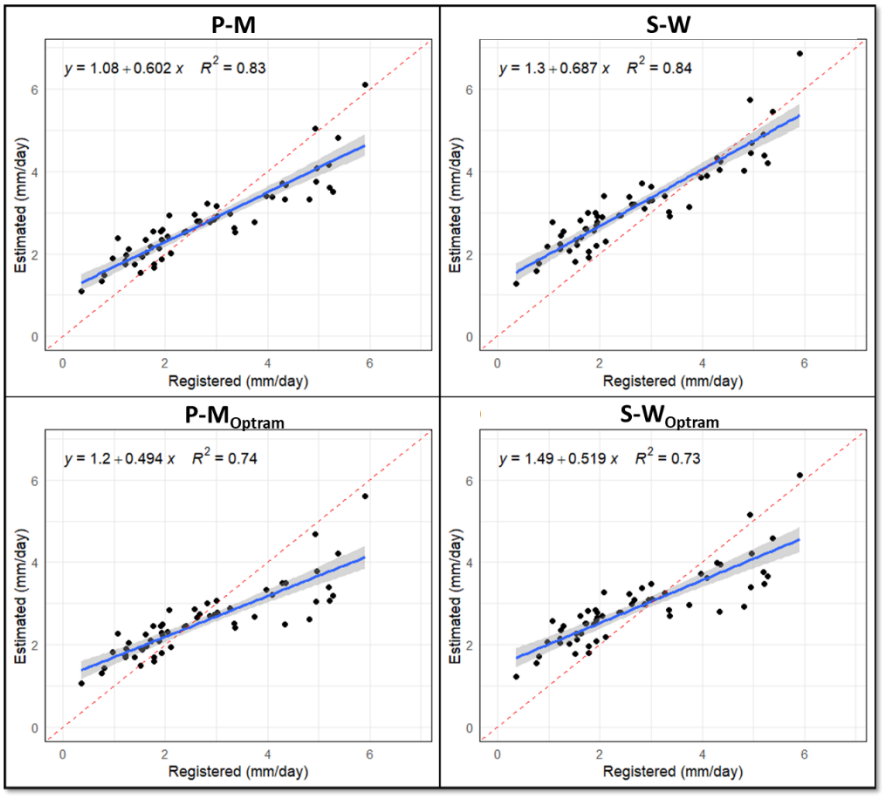

Fig. 39 - Scatter plot daily comparison between observed Eta flux tower and estimated ET from P-M, S-W, PM_{optram} and $S\text{-}W_{optram}$ for GVC field during period from March 19, 2022, to May 17, 2022.

Chapter 6: Conclusions:

This study conducted a comprehensive analysis based on Sentinel-2 satellite imagery for supporting irrigation management with two levels of information: i) actual extension of irrigated areas; ii) irrigation water requirements. To this end evapotranspiration (ET) and transpiration data were derived across various scenarios and to estimate irrigation volumes at a district scale. The investigation centered on the application of the Penman-Monteith (P-M) approach, which involved to assume a minimum and maximum constant leaf resistance value for perennial (tree) crops cultivated within the study area. The calibrated leaf resistance values were adjusted to align with the farmer's irrigation strategies. Notably, employing a constant leaf resistance value yielded a reasonable correlation when assessed over a period broader than daily comparisons.

Furthermore, the estimation of irrigation requirements through the OPTRAM model involved the dynamic modulation of leaf resistance, utilizing the foundational P-M Approach. In contrast, leaf and substrate resistance were ascertained employing the Shuttleworth and Wallace (S-W) approach in conjunction with Shortwave Infrared reflectance (SWIR) observations.

A key finding emerged, underscoring that the most effective means of estimating irrigation requirements in regions with sparse canopy coverage involves accounting for crop transpiration. These findings were validated by employing the OPTRAM model, which joined the Shuttleworth and Wallace methods to estimate actual irrigation requirements over expansive areas, particularly in situations where inter-row spaces between trees could potentially lead to overestimations and highlighting the irrigation mechanic existed which is drip irrigation.

Consequently, the consolidation of the Penman-Monteith and Shuttleworth and Wallace approaches applied within (GVC) field and compared against ET flux tower eddy covariance data demonstrated a strong agreement. These findings underscore the reliability and mutual compatibility of these models in the estimation of

evapotranspiration, thereby offering valuable insights for the advancement of agricultural practices and water resource management.

It's crucial to recognize that the results may vary when applied on a larger scale, depending on the diversity of crops, including both perennial and herbaceous varieties. While grapevines dominate as perennial crops, the situation diverges when comparing it to scenarios involving a uniform crop type. This divergence becomes apparent when assessing evapotranspiration (ET) on alfalfa in Australia using eddy covariance flux tower measurements. In such instances, the assumption is based on a single, homogeneous crop type. Consequently, the assessment of two testing methodologies, P-M and S-W, both with and without the incorporation of the OPTRAM model, revealed enhanced accuracy specifically under these conditions.

In conclusion, the implementation of a comprehensive strategy is essential for achieving enhanced agricultural outcomes and ensuring precise validation. This strategy begins with the establishment of in situ field monitoring systems to facilitate real-time data collection and analysis, providing valuable insights into farmers' irrigation practices. Overcoming the challenge of unreliable irrigation volume data is addressed through the calibration of canopy resistance, which is tailored to observed water stress conditions, significantly enhancing accuracy.

Moreover, it is vital to align water stress estimation with the socioeconomic context of farmers to meet their specific needs and constraints. Continuous refinement of irrigation techniques and the adoption of efficient irrigation management systems are imperative for promoting sustainable agricultural practices and optimizing resource utilization.

The incorporation of a decision support system that leverages field data, calibrated parameters, and water stress conditions empowers us to provide real-time recommendations, thereby fostering sustainable agriculture and responsible resource allocation. Collectively, these steps not only enable near-real-time monitoring but also contribute significantly to the overall development and growth of the agricultural sector.

Chapter 7: Acknowledgement

I express my gratitude for the unwavering support and contributions of numerous individuals and institutions that have been instrumental in bringing this work to fruition. Firstly, I extend my appreciation to the Polytechnic University of Bari for granting me a scholarship, enabling my dedicated three-year commitment to this research. I also acknowledge the hospitality and collaboration extended by the CIHEAM Bari institute and the University of Naples Federico II, where a significant portion of my PhD research transpired.

My deepest appreciation goes to my supervisors, Prof. Umberto Fratino and Prof. Nicola Lamaddalena, whose support, time, and dedication have been indispensable in guiding me through this academic journey. Their infectious enthusiasm for scientific inquiry has been a constant inspiration. I am genuinely grateful for their generosity and warm hospitality, which significantly enriched my experience in Italy. Additionally, I extend my thanks to the coordinator, Prof. Michele MOSSA, for aiding and streamlining procedures throughout my PhD.

I sincerely appreciate Prof. Guido D'urso for his kindness and hospitality during my internship at the Department of Agriculture at the University of Napoli Federico II in Naples, Italy. His assistance has been crucial to my thesis work, and he consistently made time for my inquiries and uncertainties.

My heartfelt gratitude extends to my colleague and friend, Dr. Oscar Belfiore, for his invaluable advice and steadfast scientific support. Oscar's enthusiastic approach to science has consistently inspired me, and I am genuinely thankful for his enduring guidance.

I also express my thanks to Prof. Francesco Vuolo, for his hospitality, excellent teaching, and engaging discussions at BOKU University in Vienna (Austria). Special appreciation to Prof. Giuseppe Ciraolo and Prof. Chiara Corbari for providing evaluations of my thesis.

I am grateful for the friendships formed during my time in Italy. Finally, profound thanks to my parents, brothers, and sister for their unwavering love and steadfast

support, which played a pivotal role in my decision to study abroad. Their guidance and encouragement have been invaluable throughout my PhD studies, and I deeply appreciate their enduring belief in my journey. A heartfelt thanks also to my wife for her boundless love and unwavering compassion, which have consistently been sources of strength and joy in my life.

References

Addabbo, P., Focareta, M., Marcuccio, S., Votto, C. and Ullo, S.L. (2016) 'Contribution of Sentinel-2 data for applications in vegetation monitoring', *Acta Imeko*, 5(2), pp. 44–54. Available at: https://doi.org/https://dx.doi.org/10.21014/acta_imeko.v5i2.352.

Alcamo, J., Dronin, N., Endejan, M., Golubev, G. and Kirilenko, A. (2007) 'A new assessment of climate change impacts on food production shortfalls and water availability in Russia', *Global Environmental Change*, 17(3–4), pp. 429–444.

Alexandratos, N. and Bruinsma, J. (2012) *World agriculture towards 2030/2050: the 2012 revision*. Available at: https://doi.org/10.22004/ag.econ.288998.

Allen, R.G., Howell, T.A., Pruitt, W.O., Walter, I.A. and Jensen, M.E. (1991) 'Lysimeters for evapotranspiration and environmental measurements', in. ASCE, pp. 456–456.

Allen, R.G., Pereira, L.S., Raes, D. and Smith, M. (1998) 'Crop evapotranspiration-Guidelines for computing crop water requirements-FAO Irrigation and drainage paper, 56', *Fao, Rome*, 300(9), p. D05109.

Allen, R.G., Tasumi, M. and Trezza, R. (2007) 'Satellite-based energy balance for mapping evapotranspiration with internalized calibration (METRIC)—Model', *Journal of irrigation and drainage engineering*, 133(4), pp. 380–394. Available at: https://doi.org/https://doi.org/10.1061/(ASCE)0733-9437(2007)133:4(380).

Altieri, S. (1995) 'Sinistra Ofanto irrigation scheme: management and maintenance problems', *Bonifica*, 1, p. 2.

Anderson, M.C., Allen, R.G., Morse, A. and Kustas, W.P. (2012) 'Use of Landsat thermal imagery in monitoring evapotranspiration and managing water resources', *Remote Sensing of Environment*, 122, pp. 50–65. Available at: https://doi.org/https://doi.org/10.1016/j.rse.2011.08.025.

Anderson, M.C., Norman, J.M., Diak, G.R., Kustas, W.P. and Mecikalski, J.R. (1997) 'A two-source time-integrated model for estimating surface fluxes using thermal infrared remote sensing', *Remote sensing of environment*, 60(2), pp. 195–216. Available at: https://doi.org/https://doi.org/10.1016/S0034-4257(96)00215-5.

Aplin, P. and Atkinson, P.M. (2004) 'Predicting missing field boundaries to increase per-field classification accuracy', *Photogrammetric Engineering & Remote Sensing*, 70(1), pp. 141–149.

Australian Bureau of Statistics (2023). Available at: https://www.abs.gov.au/ (Accessed: 19 July 2023).

Avissar, R. and Pielke, R.A. (1989) 'A parameterization of heterogeneous land surfaces for atmospheric numerical models and its impact on regional meteorology', *Monthly Weather Review*, 117(10), pp. 2113–2136. Available at: https://doi.org/https://doi.org/10.1175/1520-0493(1989)117<2113:APOHLS>2.0.CO;2.

Baret, F., Hagolle, O., Geiger, B., Bicheron, P., Miras, B., Huc, M., Berthelot, B., Niño, F., Weiss, M. and Samain, O. (2007) 'LAI, fAPAR and fCover CYCLOPES global products derived from VEGETATION: Part 1: Principles of the algorithm', *Remote sensing of environment*, 110(3), pp. 275–286. Available at: https://doi.org/https://doi.org/10.1016/j.rse.2007.02.018.

Bastiaanssen, W.G.M. (2000) 'SEBAL-based sensible and latent heat fluxes in the irrigated Gediz Basin, Turkey', *Journal of hydrology*, 229(1–2), pp. 87–100. Available at: https://doi.org/https://doi.org/10.1016/S0022-1694(99)00202-4.

Bastiaanssen, W.G.M., Menenti, M., Feddes, R.A. and Holtslag, A.A.M. (1998) 'A remote sensing surface energy balance algorithm for land (SEBAL). 1. Formulation', *Journal of hydrology*, 212, pp. 198–212. Available at: https://doi.org/https://doi.org/10.1016/S0022-1694(98)00253-4.

Belfiore, O.R., Castagna, A., Longo-Minnolo, G., Ippolito, M., Bavieri, A., Comegna, A. and D'Urso, G. (2023) 'Monitoring of Irrigation Water Use in Italy by Using IRRISAT Methodology: The INCIPIT Project', in S.M.C. Ferro, V., Giordano, G., Orlando, S., Vallone, M., Cascone, G., Porto (ed.) *AIIA 2022: Biosystems Engineering Towards the Green Deal. AIIA 2022. Lecture Notes in Civil Engineering*. Cham: Springer, pp. 41–49. Available at: https://doi.org/https://doi.org/10.1007/978-3-031-30329-6_4.

Bouwer, H. (2000) 'Integrated water management: emerging issues and challenges', *Agricultural water management*, 45(3), pp. 217–228. Available at: https://doi.org/https://doi.org/10.1016/S0378-3774(00)00092-5.

Braden, H. (1985) 'Ein energiehaushalts-und verdunstungsmodell for wasser und stoffhaushaltsuntersuchungen landwirtschaftlich genutzer einzugsgebiete', *Mittelungen Deutsche Bodenkundliche Geselschaft*, 42(S), pp. 294–299.

Bréda, N.J.J. (2003) 'Ground-based measurements of leaf area index: a review of methods, instruments and current controversies', *Journal of experimental botany*, 54(392), pp. 2403–2417. Available at: https://doi.org/https://doi.org/10.1093/jxb/erg263.

Brede, B., Verrelst, J., Gastellu-Etchegorry, J.-P., Clevers, J.G.P.W., Goudzwaard, L., den Ouden, J., Verbesselt, J. and Herold, M. (2020) 'Assessment of workflow feature selection on forest LAI prediction with sentinel-2A MSI, landsat 7 ETM+ and Landsat 8 OLI', *Remote Sensing*, 12(6), p. 915. Available at: https://doi.org/https://doi.org/10.3390/rs12060915.

Brombacher, J., de Oliveira Silva, I.R., Degen, J. and Pelgrum, H. (2022) 'A novel evapotranspiration based irrigation quantification method using the hydrological similar pixels algorithm', *Agricultural Water Management*, 267, p. 107602.

Brutsaert, W. (1982) *Evaporation into the Atmosphere Theory, History and Applications*. Springer Dordrecht. Available at: https://doi.org/https://doi.org/10.1007/978-94-017-1497-6.

Brutsaert, W. (2013) *Evaporation into the atmosphere: theory, history and applications*. Springer Science & Business Media.

Butler Jr, J.J., Whittemore, D.O., Wilson, B.B. and Bohling, G.C. (2018) 'Sustainability of aquifers supporting irrigated agriculture: A case study of the High Plains aquifer in Kansas', *Water International*, 43(6), pp. 815–828. Available at: https://doi.org/https://doi.org/10.1080/02508060.2018.1515566.

Calera, A., Campos, I., Osann, A., D'Urso, G. and Menenti, M. (2017) 'Remote sensing for crop water management: From ET modelling to services for the end users', *Sensors*, 17(5), p. 1104.

Campos-Taberner, M., García-Haro, F.J., Busetto, L., Ranghetti, L., Martínez, B., Gilabert, M.A., Camps-Valls, G., Camacho, F. and Boschetti, M. (2018) 'A critical comparison of remote sensing Leaf Area Index estimates over rice-cultivated areas: From Sentinel-2 and Landsat-7/8 to MODIS, GEOV1 and EUMETSAT polar system', *Remote Sensing*, 10(5), p. 763. Available at: https://doi.org/https://doi.org/10.3390/rs10050763.

CBC (1984) *Cinquant'anni di bonifica nel Tavoliere Consorzio di Bonifica per la Capitanata*. Bastogi Ed. Foggia, Italy.

Chen, Y., Lu, D., Luo, L., Pokhrel, Y., Deb, K., Huang, J. and Ran, Y. (2018) 'Detecting irrigation extent, frequency, and timing in a heterogeneous arid agricultural region using MODIS time series, Landsat imagery, and ancillary data', *Remote Sensing of Environment*, 204, pp. 197–211. Available at: https://doi.org/https://doi.org/10.1016/j.rse.2017.10.030.

Coppola, A., Dragonetti, G., Sengouga, A., Lamaddalena, N., Comegna, A., Basile, A., Noviello, N. and Nardella, L. (2019) 'Identifying optimal irrigation water needs at district scale by using a physically based agro-hydrological model', *Water*, 11(4), p. 841. Available at: https://doi.org/https://doi.org/10.3390/w11040841.

Cristina, S., Cordeiro, C., Lavender, S., Costa Goela, P., Icely, J. and Newton, A. (2016) 'MERIS phytoplankton time series products from the SW Iberian Peninsula (Sagres) using seasonal-trend decomposition based on loess', *Remote Sensing*, 8(6), p. 449. Available at: https://doi.org/https://doi.org/10.3390/rs8060449.

Culf, A.D., Foken, T. and Gash, J.H.C. (2004) 'The energy balance closure problem', in *Vegetation, Water, Humans and the Climate. Global Change — The IGBP*

Series. Berlin: Springer, pp. 159–166. Available at: https://doi.org/https://doi.org/10.1007/978-3-642-18948-7_13.

D'Urso, G. (2001) *Simulation and management of on-demand irrigation systems: a combined agrohydrological and remote sensing approach*. Wageningen University and Research.

D'Urso, G., Bolognesi, S.F., Kustas, W.P., Knipper, K.R., Anderson, M.C., Alsina, M.M., Hain, C.R., Alfieri, J.G., Prueger, J.H. and Gao, F. (2021) 'determining evapotranspiration by using combination equation models with sentinel-2 data and comparison with thermal-based energy balance in a California irrigated vineyard', *Remote Sensing*, 13(18), p. 3720. Available at: https://doi.org/https://doi.org/10.3390/rs13183720.

D'Urso, G. and Calera Belmonte, A. (2006) 'Operative approaches to determine crop water requirements from Earth Observation data: methodologies and applications', in *AIP conference proceedings*. American Institute of Physics, pp. 14–25. Available at: https://doi.org/https://doi.org/10.1063/1.2349323.

D'Urso, G. and Menenti, M. (1995) 'Mapping crop coefficients in irrigated areas from Landsat TM images', in *Remote Sensing for Agriculture, Forestry, and Natural Resources*. SPIE, pp. 41–47.

Dworak, T., Schmidt, G., De Stefano, L., Palacios, E. and Berglund, M. (2010) *Background paper to the conference: Application of EU water-related policies at farm level 28-29 September 2010*, *Report for the European Commission-DG Environment, Louvain-la-Neuve, Belgium*. Belgium.

Falanga Bolognesi, S., Pasolli, E., Belfiore, O.R., De Michele, C. and D'Urso, G. (2020) 'Harmonized landsat 8 and sentinel-2 time series data to detect irrigated areas: An application in Southern Italy', *Remote Sensing*, 12(8), p. 1275. Available at: https://doi.org/https://doi.org/10.3390/rs12081275.

FAO (2010a) *AQUASTAT - FAO's Global Information System on Water and Agriculture*. Available at: http://www.fao.org/nr/Water/aquastat/tables/WorldDataWithdrawal_eng.pdf (Accessed: 23 July 2023).

FAO (2010b) *Water Withdrawal by Sector*, *AQUASTAT - FAO's Global Information System on Water and Agriculture*. Available at: https://www.fao.org/aquastat/en/countries-and-basins/ (Accessed: 23 September 2023).

FAO (2017) *The future of food and agriculture – Trends and challenge*. Rome. Available at: https://www.fao.org/3/i6583e/i6583e.pdf.

Feddes, R.A., Kabat, P., Van Bakel, Pjt., Bronswijk, J.J.B. and Halbertsma, J. (1988) 'Modelling soil water dynamics in the unsaturated zone—state of the art',

Journal of hydrology, 100(1–3), pp. 69–111.

Feng, Z., Miao, Q., Shi, H., Feng, W., Li, X., Yan, J., Liu, M., Sun, W., Dai, L. and Liu, J. (2023) 'Simulation of water balance and irrigation strategy of typical sand-layered farmland in the Hetao Irrigation District, China', *Agricultural Water Management*, 280, p. 108236.

Foken, T. (2008) 'The energy balance closure problem: An overview', *Ecological Applications*, 18(6), pp. 1351–1367. Available at: https://doi.org/https://doi.org/10.1890/06-0922.1.

Foken, T. and Wichura, B. (1996) 'Tools for quality assessment of surface-based flux measurements', *Agricultural and forest meteorology*, 78(1–2), pp. 83–105. Available at: https://doi.org/https://doi.org/10.1016/0168-1923(95)02248-1.

Ganguly, S., Nemani, R.R., Zhang, G., Hashimoto, H., Milesi, C., Michaelis, A., Wang, W., Votava, P., Samanta, A. and Melton, F. (2012) 'Generating global leaf area index from Landsat: Algorithm formulation and demonstration', *Remote Sensing of Environment*, 122, pp. 185–202. Available at: https://doi.org/https://doi.org/10.1016/j.rse.2011.10.032.

Garrido-Rubio, J., Gonzalez-Piqueras, J., Campos, I., Osann, A., Gonzalez-Gomez, L. and Calera, A. (2020) 'Remote sensing–based soil water balance for irrigation water accounting at plot and water user association management scale', *Agricultural Water Management*, 238, p. 106236. Available at: https://doi.org/https://doi.org/10.1016/j.agwat.2020.106236.

Gatti, A. and Bertolini, A. (2013) 'Sentinel-2 products specification document', *Available online (accessed February 23, 2015) https://earth. esa. int/documents/247904/685211/Sentinel-2+ Products+ Specification+ Document* [Preprint].

Ghassemi, B., Immitzer, M., Atzberger, C. and Vuolo, F. (2022) 'Evaluation of Accuracy Enhancement in European-Wide Crop Type Mapping by Combining Optical and Microwave Time Series', *Land*, 11(9), p. 1397. Available at: https://doi.org/https://doi.org/10.3390/land11091397.

Giordano, R., D'Agostino, D., Apollonio, C., Lamaddalena, N. and Vurro, M. (2013) 'Bayesian belief network to support conflict analysis for groundwater protection: the case of the Apulia region', *Journal of environmental management*, 115, pp. 136–146. Available at: https://doi.org/https://doi.org/10.1016/j.jenvman.2012.11.011.

Giyanto, H. (2008) *Application of the k-means, k-medoid, gath geva clustering algorithm*. Tesis Tidak Terpublikasi. Yogyakarta: Universitas Gajah Mada.

Glenn, E.P., Huete, A.R., Nagler, P.L., Hirschboeck, K.K. and Brown, P. (2007) 'Integrating remote sensing and ground methods to estimate evapotranspiration', *Critical Reviews in Plant Sciences*, 26(3), pp. 139–168.

Gómez, C., White, J.C. and Wulder, M.A. (2016) 'Optical remotely sensed time series data for land cover classification: A review', *ISPRS Journal of photogrammetry and Remote Sensing*, 116, pp. 55–72. Available at: https://doi.org/https://doi.org/10.1016/j.isprsjprs.2016.03.008.

Gray, J. and Song, C. (2012) 'Mapping leaf area index using spatial, spectral, and temporal information from multiple sensors', *Remote Sensing of Environment*, 119, pp. 173–183. Available at: https://doi.org/https://doi.org/10.1016/j.rse.2011.12.016.

Günlü, A., Keleş, S., Ercanlı, İ. and Şenyurt, M. (2017) 'Estimation of leaf area index using WorldView-2 and Aster satellite image: a case study from Turkey', *Environmental monitoring and assessment*, 189, pp. 1–11. Available at: https://doi.org/https://doi.org/10.1007/s10661-017-6254-2.

Gutman, G. and Ignatov, A. (1998) 'The derivation of the green vegetation fraction from NOAA/AVHRR data for use in numerical weather prediction models', *International Journal of remote sensing*, 19(8), pp. 1533–1543. Available at: https://doi.org/DOI: 10.1080/014311698215333.

Haas, E.M., Bartholomé, E. and Combal, B. (2009) 'Time series analysis of optical remote sensing data for the mapping of temporary surface water bodies in sub-Saharan western Africa', *Journal of Hydrology*, 370(1–4), pp. 52–63. Available at: https://doi.org/https://doi.org/10.1016/j.jhydrol.2009.02.052.

Hu, X., Shi, L., Zeng, J., Yang, J., Zha, Y., Yao, Y. and Cao, G. (2016) 'Estimation of actual irrigation amount and its impact on groundwater depletion: A case study in the Hebei Plain, China', *Journal of Hydrology*, 543, pp. 433–449. Available at: https://doi.org/https://doi.org/10.1016/j.jhydrol.2016.10.020.

Huang, J., Gómez-Dans, J.L., Huang, H., Ma, H., Wu, Q., Lewis, P.E., Liang, S., Chen, Z., Xue, J.-H. and Wu, Y. (2019) 'Assimilation of remote sensing into crop growth models: Current status and perspectives', *Agricultural and forest meteorology*, 276–277, p. 107609. Available at: https://doi.org/https://doi.org/10.1016/j.agrformet.2019.06.008.

Huang, Y., Chen, Z., Tao, Y.U., Huang, X. and Gu, X. (2018) 'Agricultural remote sensing big data: Management and applications', *Journal of Integrative Agriculture*, 17(9), pp. 1915–1931. Available at: https://doi.org/https://doi.org/10.1016/S2095-3119(17)61859-8.

Ivits, E., Cherlet, M., Sommer, S. and Mehl, W. (2013) 'Addressing the complexity in non-linear evolution of vegetation phenological change with time-series of remote sensing images', *Ecological Indicators*, 26, pp. 49–60. Available at: https://doi.org/https://doi.org/10.1016/j.ecolind.2012.10.012.

Jackson, R.D., Moran, M.S., Gay, L.W. and Raymond, L.H. (1987) 'Evaluating evaporation from field crops using airborne radiometry and ground-based

meteorological data', *Irrigation Science*, 8, pp. 81–90.

Jacquemoud, S. and Baret, F. (1990) 'PROSPECT: A model of leaf optical properties spectra', *Remote sensing of environment*, 34(2), pp. 75–91. Available at: https://doi.org/https://doi.org/10.1016/0034-4257(90)90100-Z.

Jia, K., Liang, S., Gu, X., Baret, F., Wei, X., Wang, X., Yao, Y., Yang, L. and Li, Y. (2016) 'Fractional vegetation cover estimation algorithm for Chinese GF-1 wide field view data', *Remote sensing of Environment*, 177, pp. 184–191. Available at: https://doi.org/https://doi.org/10.1016/j.rse.2016.02.019.

Jia, K., Liang, S., Liu, S., Li, Y., Xiao, Z., Yao, Y., Jiang, B., Zhao, X., Wang, X. and Xu, S. (2015) 'Global land surface fractional vegetation cover estimation using general regression neural networks from MODIS surface reflectance', *IEEE Transactions on Geoscience and Remote Sensing*, 53(9), pp. 4787–4796. Available at: https://doi.org/10.1109/TGRS.2015.2409563.

Jiang, Z., Huete, A.R., Chen, J., Chen, Y., Li, J., Yan, G. and Zhang, X. (2006) 'Analysis of NDVI and scaled difference vegetation index retrievals of vegetation fraction', *Remote sensing of environment*, 101(3), pp. 366–378. Available at: https://doi.org/https://doi.org/10.1016/j.rse.2006.01.003.

Jiang, Z., Huete, A.R., Didan, K. and Miura, T. (2008) 'Development of a two-band enhanced vegetation index without a blue band', *Remote sensing of Environment*, 112(10), pp. 3833–3845. Available at: https://doi.org/https://doi.org/10.1016/j.rse.2008.06.006.

Jing, X., Yao, W.-Q., Wang, J.-H. and Song, X.-Y. (2011) 'A study on the relationship between dynamic change of vegetation coverage and precipitation in Beijing's mountainous areas during the last 20 years', *Mathematical and Computer Modelling*, 54(3–4), pp. 1079–1085. Available at: https://doi.org/https://doi.org/10.1016/j.mcm.2010.11.038.

Johansson, R.C. (2005) *Micro and macro-level approaches for assessing the value of irrigation water*. Washington, DC, USA: World Bank Publications.

Jury, W.A. and Vaux Jr, H.J. (2007) 'The emerging global water crisis: managing scarcity and conflict between water users', *Advances in agronomy*, 95, pp. 1–76. Available at: https://doi.org/https://doi.org/10.1016/S0065-2113(07)95001-4.

Jutz, S. and Milagro Perez, M.P. (2017) 'Copernicus space component: Status and evolution', in *EGU General Assembly Conference Abstracts*, p. 18668.

Kalma, J.D., McVicar, T.R. and McCabe, M.F. (2008) 'Estimating land surface evaporation: A review of methods using remotely sensed surface temperature data', *Surveys in Geophysics*, 29, pp. 421–469. Available at: https://doi.org/https://doi.org/10.1007/s10712-008-9037-z.

Kang, Y., Ozdogan, M., Gao, F., Anderson, M.C., White, W.A., Yang, Yun, Yang,

Yang and Erickson, T.A. (2021) 'A data-driven approach to estimate leaf area index for Landsat images over the contiguous US', *Remote Sensing of Environment*, 258, p. 112383. Available at: https://doi.org/https://doi.org/10.1016/j.rse.2021.112383.

Kelliher, F.M., Leuning, R., Raupach, M.R. and Schulze, E.-D. (1995) 'Maximum conductances for evaporation from global vegetation types', *Agricultural and Forest Meteorology*, 73(1–2), pp. 1–16. Available at: https://doi.org/https://doi.org/10.1016/0168-1923(94)02178-M.

Kennedy, R.E., Yang, Z. and Cohen, W.B. (2010) 'Detecting trends in forest disturbance and recovery using yearly Landsat time series: 1. LandTrendr—Temporal segmentation algorithms', *Remote Sensing of Environment*, 114(12), pp. 2897–2910. Available at: https://doi.org/https://doi.org/10.1016/j.rse.2010.07.008.

Keuchel, J., Naumann, S., Heiler, M. and Siegmund, A. (2003) 'Automatic land cover analysis for Tenerife by supervised classification using remotely sensed data', *Remote sensing of environment*, 86(4), pp. 530–541.

Keulen, H. van and Seligman, N.G. (1987) 'Simulation of water use, nitrogen nutrition and growth of a spring wheat crop', *(No Title)* [Preprint].

Khorasani, M., Ehteshami, M., Ghadimi, H. and Salari, M. (2016) 'Simulation and analysis of temporal changes of groundwater depth using time series modeling', *Modeling Earth Systems and Environment*, 2, pp. 1–10. Available at: https://doi.org/https://doi.org/10.1007/s40808-016-0164-0.

Körner, C. (1994) 'Leaf diffusive conductances in the major vegetation types of the globe', in M.M. Schulze, ED., Caldwell (ed.) *Ecophysiology of photosynthesis*. Springer, pp. 463–490. Available at: https://doi.org/https://doi.org/10.1007/978-3-642-79354-7_22.

Kottek, M., Grieser, J., Beck, C., Rudolf, B. and Rubel, F. (2006) 'World map of the Köppen-Geiger climate classification updated'.

Levidow, L., Zaccaria, D., Maia, R., Vivas, E., Todorovic, M. and Scardigno, A. (2014) 'Improving water-efficient irrigation: Prospects and difficulties of innovative practices', *Agricultural Water Management*, 146, pp. 84–94. Available at: https://doi.org/https://doi.org/10.1016/j.agwat.2014.07.012.

Li, F., Cao, R., Zhao, Y., Mu, D., Fu, C. and Ping, F. (2017) 'Remote sensing Penman–Monteith model to estimate catchment evapotranspiration considering the vegetation diversity', *Theoretical and Applied Climatology*, 127, pp. 111–121.

Li, X., Jiang, W. and Duan, D. (2020) 'Spatio-temporal analysis of irrigation water use coefficients in China', *Journal of environmental management*, 262, p. 110242. Available at: https://doi.org/https://doi.org/10.1016/j.jenvman.2020.110242.

Lockwood, S., Sarteel, M., Mugdal, S., Osann, A. and Calera, A. (2014) *Applying Earth observation to support the detection of non-authorised water*

abstractions, *Report for the European Commission, DG Environment, Bio by Deloitte, Universidad de Castilla-La Mancha*. Available at: https://circabc.europa.eu/sd/a/047979aa-052f-40ed-b177-100494dafef6/EO&IllegalAbstractions-.

Longo-Minnolo, G., Consoli, S., Vanella, D., Ramírez-Cuesta, J.M., Greimeister-Pfeil, I., Neuwirth, M. and Vuolo, F. (2022) 'A stand-alone remote sensing approach based on the use of the optical trapezoid model for detecting the irrigated areas', *Agricultural Water Management*, 274, p. 107975.

Lyu, H., Lu, H. and Mou, L. (2016) 'Learning a transferable change rule from a recurrent neural network for land cover change detection', *Remote Sensing*, 8(6), p. 506. Available at: https://doi.org/https://doi.org/10.3390/rs8060506.

Menenti, M., Bastiaanssen, W.G.M. and Van Eick, D. (1989) 'Determination of surface hemispherical reflectance with Thematic Mapper data', *Remote Sensing of Environment*, 28, pp. 327–337. Available at: https://doi.org/https://doi.org/10.1016/0034-4257(89)90124-7.

Meyer, L.H., Heurich, M., Beudert, B., Premier, J. and Pflugmacher, D. (2019) 'Comparison of Landsat-8 and Sentinel-2 data for estimation of leaf area index in temperate forests', *Remote Sensing*, 11(10), p. 1160. Available at: https://doi.org/https://doi.org/10.3390/rs11101160.

Mills, J., Dwyer, J., Ingram, J., Simpson, C.R., Oostindie, H., Primdahl, J., Bojesen, M., Powell, N. and Powell, S. (2009) *EU Environmental Regulations in Agriculture*, *Final Report to the Environment Agency. Countryside and Community Research Institute, UK*. Available at: https://www.researchgate.net/profile/Stina-Powell/publication/333324186_EU_environmental_regulations_in_agriculture_Final_Report_to_the_Environment_Agency_Countryside_and_Community_Research_Institute_UK/links/5ce79b4592851c4eabba3421/EU-environmental-regu.

Molden, D. (2013) *Water for food water for life: A comprehensive assessment of water management in agriculture*. International Water Management Institute, London,Earthscan, and Colombo: Routledge.

Möller, M., Alchanatis, V., Cohen, Y., Meron, M., Tsipris, J., Naor, A., Ostrovsky, V., Sprintsin, M. and Cohen, S. (2007) 'Use of thermal and visible imagery for estimating crop water status of irrigated grapevine', *Journal of experimental botany*, 58(4), pp. 827–838.

Monteith, J.L. (1965) 'Evaporation and environment', in *Symposia of the society for experimental biology*. Cambridge University Press (CUP) Cambridge, pp. 205–234.

Monteith, J.L. and Unsworth, M.H. (2008) 'Chapter 13: Steady state heat balance', *Principles of Environmental Physics, 3rd ed.; Academic Press: Burlington,*

VT, USA, pp. 250–255.

Moran, M.S., Inoue, Y. and Barnes, E.M. (1997) 'Opportunities and limitations for image-based remote sensing in precision crop management', *Remote sensing of Environment*, 61(3), pp. 319–346. Available at: https://doi.org/https://doi.org/10.1016/S0034-4257(97)00045-X.

Moreno-Pérez, M.F. and Roldán-Cañas, J. (2013) 'Assessment of irrigation water management in the Genil-Cabra (Córdoba, Spain) irrigation district using irrigation indicators', *Agricultural water management*, 120, pp. 98–106.

Moussa, R., Chahinian, N. and Bocquillon, C. (2007) 'Distributed hydrological modelling of a Mediterranean mountainous catchment–Model construction and multi-site validation', *Journal of Hydrology*, 337(1–2), pp. 35–51. Available at: https://doi.org/https://doi.org/10.1016/j.jhydrol.2007.01.028.

Myneni, R.B., Hall, F.G., Sellers, P.J. and Marshak, A.L. (1995) 'The interpretation of spectral vegetation indexes', *IEEE Transactions on Geoscience and remote Sensing*, 33(2), pp. 481–486.

Nellis, M.D., Price, K.P. and Rundquist, D. (2009) *Remote sensing of cropland agriculture*, *The SAGE handbook of remote sensing*. SAGE Publications Thousand Oaks, CA, USA.

Norman, J.M., Kustas, W.P. and Humes, K.S. (1995) 'Source approach for estimating soil and vegetation energy fluxes in observations of directional radiometric surface temperature', *Agricultural and Forest Meteorology*, 77(3–4), pp. 263–293. Available at: https://doi.org/https://doi.org/10.1016/0168-1923(95)02265-Y.

OECD (2015) *Drying Wells, Rising Stake: Towards Sustainable Agricultural Groundwater Use*, *OECD Studies on Water*. Paris, France: OECD Publishing.

Ortega-Farias, S., Carrasco, M., Olioso, A., Acevedo, C. and Poblete, C. (2007) 'Latent heat flux over Cabernet Sauvignon vineyard using the Shuttleworth and Wallace model', *Irrigation Science*, 25, pp. 161–170. Available at: https://doi.org/https://doi.org/10.1007/s00271-006-0047-7.

Ozdogan, M., Woodcock, C.E., Salvucci, G.D. and Demir, H. (2006) 'Changes in summer irrigated crop area and water use in Southeastern Turkey from 1993 to 2002: Implications for current and future water resources', *Water resources management*, 20, pp. 467–488. Available at: https://doi.org/https://doi.org/10.1007/s11269-006-3087-0.

Ozdogan, M., Yang, Y., Allez, G. and Cervantes, C. (2010) 'Remote sensing of irrigated agriculture: Opportunities and challenges', *Remote sensing*, 2(9), pp. 2274–2304.

Pachauri, R.K. and Reisinger, A. (2007) 'Climate change 2007: Synthesis report. Contribution of working groups I, II and III to the fourth assessment report of the

Intergovernmental Panel on Climate Change', *Climate Change 2007. Working Groups I, II and III to the Fourth Assessment*. Edited by IPCC, p. 104.

Pareeth, S., Karimi, P., Shafiei, M. and De Fraiture, C. (2019) 'Mapping agricultural landuse patterns from time series of Landsat 8 using random forest based hierarchial approach', *Remote Sensing*, 11(5), p. 601. Available at: https://doi.org/https://doi.org/10.3390/rs11050601.

Pasqualotto, N., D'Urso, G., Bolognesi, S.F., Belfiore, O.R., Van Wittenberghe, S., Delegido, J., Pezzola, A., Winschel, C. and Moreno, J. (2019) 'Retrieval of evapotranspiration from sentinel-2: Comparison of vegetation indices, semi-empirical models and SNAP biophysical processor approach', *Agronomy*, 9(10), p. 663. Available at: https://doi.org/https://doi.org/10.3390/agronomy9100663.

Perumal, K. and Bhaskaran, R. (2010) 'Supervised classification performance of multispectral images', *arXiv preprint arXiv:1002.4046* [Preprint].

Petitjean, F., Inglada, J. and Gancarski, P. (2014) 'Assessing the quality of temporal high-resolution classifications with low-resolution satellite image time series', *International Journal of Remote Sensing*, 35(7), pp. 2693–2712. Available at: https://doi.org/https://www.tandfonline.com/doi/full/10.1080/01431161.2014.883092?casa_token=ktVSnjqYOnwAAAAA%3AsQcqbSrqTlWM3o7iGyeJS9PoTnhyn0tBWdTwXKHlwYT_jUzvkjLxDbGcoeZOrW1nWzMaUwaJ3nE8#:~:text=https%3A//doi.org/10.1080/01431161.2014.883092.

Pinter Jr, P.J., Hatfield, J.L., Schepers, J.S., Barnes, E.M., Moran, M.S., Daughtry, C.S.T. and Upchurch, D.R. (2003) 'Remote sensing for crop management', *Photogrammetric Engineering & Remote Sensing*, 69(6), pp. 647–664. Available at: https://doi.org/https://doi.org/10.14358/PERS.69.6.647.

Portoghese, I., D'Agostino, D., Giordano, R., Scardigno, A., Apollonio, C. and Vurro, M. (2013) 'An integrated modelling tool to evaluate the acceptability of irrigation constraint measures for groundwater protection', *Environmental modelling & software*, 46, pp. 90–103. Available at: https://doi.org/https://doi.org/10.1016/j.envsoft.2013.03.001.

Portoghese, I., Vurro, M. and Lopez, A. (2015) 'Assessing the impacts of climate change on water resources: Experiences from the Mediterranean region', in M. (eds) Shrestha, S., Anal, A., Salam, P., van der Valk (ed.) *Managing Water Resources under Climate Uncertainty: Examples from Asia, Europe, Latin America, and Australia*. Cham: Springer, pp. 177–195. Available at: https://doi.org/https://doi.org/10.1007/978-3-319-10467-6_9.

Prueger, J.H., Hatfield, J.L., Parkin, T.B., Kustas, W.P., Hipps, L.E., Neale, C.M.U., MacPherson, J.I., Eichinger, W.E. and Cooper, D.I. (2005) 'Tower and aircraft eddy covariance measurements of water vapor, energy, and carbon dioxide fluxes

during SMACEX', *Journal of Hydrometeorology*, 6(6), pp. 954–960. Available at: https://doi.org/https://doi.org/10.1175/JHM457.1.

Raupach, M.R. (1994) 'Simplified expressions for vegetation roughness length and zero-plane displacement as functions of canopy height and area index', *Boundary-layer meteorology*, 71(1–2), pp. 211–216. Available at: https://doi.org/https://doi.org/10.1007/BF00709229.

Rembold, F., Meroni, M., Urbano, F., Royer, A., Atzberger, C., Lemoine, G., Eerens, H. and Haesen, D. (2015) 'Remote sensing time series analysis for crop monitoring with the SPIRITS software: new functionalities and use examples', *Frontiers in Environmental Science*, 3, p. 46. Available at: https://doi.org/https://doi.org/10.3389/fenvs.2015.00046.

Richards, J.A. and Richards, J.A. (2022) *Remote sensing digital image analysis*. Springer. Available at: https://doi.org/https://doi.org/10.1007/978-3-030-82327-6.

Ritchie, J.T. (1972) 'Model for predicting evaporation from a row crop with incomplete cover', *Water resources research*, 8(5), pp. 1204–1213.

Rosso, P., Nendel, C., Gilardi, N., Udroiu, C. and Chlebowski, F. (2022) 'Processing of remote sensing information to retrieve leaf area index in barley: a comparison of methods', *Precision Agriculture*, 23(4), pp. 1449–1472. Available at: https://doi.org/https://doi.org/10.1007/s11119-022-09893-4.

Sadeghi, M., Babaeian, E., Tuller, M. and Jones, S.B. (2017) 'The optical trapezoid model: A novel approach to remote sensing of soil moisture applied to Sentinel-2 and Landsat-8 observations', *Remote sensing of environment*, 198, pp. 52–68. Available at: https://doi.org/https://doi.org/10.1016/j.rse.2017.05.041.

Sadeghi, M., Jones, S.B. and Philpot, W.D. (2015) 'A linear physically-based model for remote sensing of soil moisture using short wave infrared bands', *Remote Sensing of Environment*, 164, pp. 66–76.

Shimabukuro, Y.E., Beuchle, R., Grecchi, R.C. and Achard, F. (2014) 'Assessment of forest degradation in Brazilian Amazon due to selective logging and fires using time series of fraction images derived from Landsat ETM+ images', *Remote sensing letters*, 5(9), pp. 773–782. Available at: https://doi.org/https://doi.org/10.1080/2150704X.2014.967880.

Shuttleworth, W.J. and Wallace, J.S. (1985) 'Evaporation from sparse crops-an energy combination theory', *Quarterly Journal of the Royal Meteorological Society*, 111(469), pp. 839–855.

Silvestro, P.C., Casa, R., Hanuš, J., Koetz, B., Rascher, U., Schuettemeyer, D., Siegmann, B., Skokovic, D., Sobrino, J. and Tudoroiu, M. (2021) 'Synergistic use of multispectral data and crop growth modelling for spatial and temporal

evapotranspiration estimations', *Remote Sensing*, 13(11), p. 2138. Available at: https://doi.org/https://doi.org/10.3390/rs13112138.

Soudani, K., François, C., Le Maire, G., Le Dantec, V. and Dufrêne, E. (2006) 'Comparative analysis of IKONOS, SPOT, and ETM+ data for leaf area index estimation in temperate coniferous and deciduous forest stands', *Remote sensing of environment*, 102(1–2), pp. 161–175. Available at: https://doi.org/https://doi.org/10.1016/j.rse.2006.02.004.

Su, Z. (2002) 'The Surface Energy Balance System (SEBS) for estimation of turbulent heat fluxes', *Hydrology and earth system sciences*, 6(1), pp. 85–100. Available at: https://doi.org/https://doi.org/10.5194/hess-6-85-2002.

Szeicz, G. and Long, I.F. (1969) 'Surface resistance of crop canopies', *Water Resources Research*, 5(3), pp. 622–633.

Teixeira, A.H. de C., Bastiaanssen, W.G.M. and Bassoi, L.H. (2007) 'Crop water parameters of irrigated wine and table grapes to support water productivity analysis in the Sao Francisco river basin, Brazil', *Agricultural water management*, 94(1–3), pp. 31–42. Available at: https://doi.org/https://doi.org/10.1016/j.agwat.2007.08.001.

Tian, J., Wang, L., Li, X., Gong, H., Shi, C., Zhong, R. and Liu, X. (2017) 'Comparison of UAV and WorldView-2 imagery for mapping leaf area index of mangrove forest', *International Journal of Applied Earth Observation and Geoinformation*, 61, pp. 22–31. Available at: https://doi.org/https://doi.org/10.1016/j.jag.2017.05.002.

Tou, J.T. and Gonzalez, R.C. (1974) 'Pattern recognition principles'.

Trimble, S.W. (1990) 'Geomorphic effects of vegetation cover and management: some time and space considerations in prediction of erosion and sediment yield.', in J.B. Thornes (ed.) *Vegetation and erosion. Processes and environments.* Chichester, UK: John Wiley and Sons Ltd., pp. 55–65.

Tulbure, M.G. and Broich, M. (2013) 'Spatiotemporal dynamic of surface water bodies using Landsat time-series data from 1999 to 2011', *ISPRS Journal of Photogrammetry and Remote Sensing*, 79, pp. 44–52. Available at: https://doi.org/https://doi.org/10.1016/j.isprsjprs.2013.01.010.

Verhoef, A., McNaughton, K.G. and Jacobs, A.F.G. (1997) 'A parameterization of momentum roughness length and displacement height for a wide range of canopy densities', *Hydrology and Earth System Sciences*, 1(1), pp. 81–91. Available at: https://doi.org/https://doi.org/10.5194/hess-1-81-1997, 1997.

Verhoef, W. (1984) 'Light scattering by leaf layers with application to canopy reflectance modeling: The SAIL model', *Remote sensing of environment*, 16(2), pp. 125–141. Available at: https://doi.org/https://doi.org/10.1016/0034-4257(84)90057-9.

Verrelst, J., Camps-Valls, G., Muñoz-Marí, J., Rivera, J.P., Veroustraete, F., Clevers, J.G.P.W. and Moreno, J. (2015) 'Optical remote sensing and the retrieval of terrestrial vegetation bio-geophysical properties–A review', *ISPRS Journal of Photogrammetry and Remote Sensing*, 108, pp. 273–290. Available at: https://doi.org/https://doi.org/10.1016/j.isprsjprs.2015.05.005.

Verstraeten, W.W., Veroustraete, F. and Feyen, J. (2008) 'Assessment of evapotranspiration and soil moisture content across different scales of observation', *Sensors*, 8(1), pp. 70–117. Available at: https://doi.org/https://doi.org/10.3390/s8010070.

Vuolo, F., D'Urso, G., De Michele, C., Bianchi, B. and Cutting, M. (2015) 'Satellite-based irrigation advisory services: A common tool for different experiences from Europe to Australia', *Agricultural water management*, 147, pp. 82–95. Available at: https://doi.org/https://doi.org/10.1016/j.agwat.2014.08.004.

Wakhidah, N. (2010) 'Clustering menggunakan k-means algorithm', *Jurnal Transformatika*, 8(1), pp. 33–39. Available at: https://doi.org/http://dx.doi.org/10.26623/transformatika.v8i1.45.

Wang, Q., Putri, N.A., Gan, Y. and Song, G. (2022) 'Combining both spectral and textural indices for alleviating saturation problem in forest LAI estimation using Sentinel-2 data', *Geocarto International*, 37(25), pp. 10511–10531. Available at: https://doi.org/https://doi.org/10.1080/10106049.2022.2037730.

Weiss, M., Baret, F. and Jay, S. (2020) 'S2ToolBox Level 2 products: LAI, FAPAR, FCOVER'.

Wilson, K., Goldstein, A., Falge, E., Aubinet, M., Baldocchi, D., Berbigier, P., Bernhofer, C., Ceulemans, R., Dolman, H. and Field, C. (2002) 'Energy balance closure at FLUXNET sites', *Agricultural and forest meteorology*, 113(1–4), pp. 223–243. Available at: https://doi.org/https://doi.org/10.1016/S0168-1923(02)00109-0.

Yang, Z., Shen, Y., Li, J., Jiang, H. and Zhao, L. (2021) 'Unsupervised monitoring of vegetation in a surface coal mining region based on NDVI time series', *Environmental Science and Pollution Research*, pp. 1–10.

Yebra, M., Van Dijk, A., Leuning, R., Huete, A. and Guerschman, J.P. (2013) 'Evaluation of optical remote sensing to estimate actual evapotranspiration and canopy conductance', *Remote Sensing of Environment*, 129, pp. 250–261. Available at: https://doi.org/https://doi.org/10.1016/j.rse.2012.11.004.

Zhang, S., Chen, H., Fu, Y., Niu, H., Yang, Y. and Zhang, B. (2019) 'Fractional vegetation cover estimation of different vegetation types in the Qaidam Basin', *Sustainability*, 11(3), p. 864. Available at: https://doi.org/https://doi.org/10.3390/su11030864.

Zhou, J., Yan Guo, R., Sun, M., Di, T.T., Wang, S., Zhai, J. and Zhao, Z. (2017)

‘The Effects of GLCM parameters on LAI estimation using texture values from Quickbird Satellite Imagery’, *Scientific Reports*, 7, pp. 1–12.

Curriculum

ALALI Qotada
Work: Via Ceglie 9, 70010 (Valenzano)
Email: qotada.alali@poliba.it **Phone:** (+39) 3282547935
Gender: Male **Date of birth:** 07/09/1990 **Nationality:** Syria
ABOUT ME: Qotada ALALI

EDUCATION AND TRAINING

BSc in Civil Engineering [10/2009 – 10/2015]
Faculty of Civil Engineering, Al Furat University. **Address:** Hasaka, Syria

Diploma in "Land and Water Resource Management / Irrigated Agriculture" [10/2017 – 06/2018]
Libera Università Mediterranea / CIHEAM Bari. **Address:** Via Ceglie 9, 70010, Valenzano (BA), Italy

MSc in "Land and Water Resource Management / Irrigated Agriculture" [11/2018 – 10/2019]
CIHEAM BARI. **Address:** Via Ceglie 9, 70010, Valenzano (BA), Italy

PhD in "Risk and Environmental, Territorial and Building Development" (ICAR/02) [11/2019 – Current]
Polytechnic University of Bari. **Address:** Via E. Orabona 4, 70125, Bari, Italy

LANGUAGE SKILLS

Mother tongue(s): Arabic, **Other language(s):**

English: **LISTENING** C2 **READING** C2 **WRITING** C2 **SPOKEN PRODUCTION** C2 **SPOKEN INTERACTION**C2

French: **LISTENING** A1 **READING** A1 **WRITING** A1 **SPOKEN PRODUCTION** A1 **SPOKEN INTERACTION**

Italian: LISTENING B2 READING B2 WRITING B1 SPOKEN PRODUCTION B1 SPOKEN INTERACTION B1

DIGITAL SKILLS

R Language and R Studio | Good familiarity with MATLAB, Simulink | GIS software: Arc GIS, QGIS | SNAP | AUTO CAD Civil | SAB | E-TABS | Hec-ras | SNAP | Internet, E-mail and social media | Microsoft Office (Microsoft) | Multivariate data analysis in R